2013

An *In Vitro* Study on the Non-Enzymatic Glycation of Melamine and Serum Albumin by Reducing Sugars

Weixi Liu
University of Rhode Island, weixi_liu@my.uri.edu

AN *IN VITRO* STUDY ON THE NON-ENZYMATIC GLYCATION OF MELAMINE AND SERUM ALBUMIN BY REDUCING SUGARS

BY

WEIXI LIU

A DISSERTATION SUBMITTED IN PARTIAL FULFILLMENT OF THE

REQUIREMENTS FOR THE DEGREE OF

DOCTOR OF PHILOSOPHY

IN

CHEMISTRY

UNIVERSITY OF RHODE ISLAND

2013

DOCTOR OF PHILOSOPHY DISSERTATION

OF

WEIXI LIU

APPROVED:

Dissertation Committee:

Major Professor: Joel A. Dain

Louis J. Kirschenbaum

Jay F. Sperry

Nasser H. Zawia

DEAN OF THE GRADUATE SCHOOL

UNIVERSITY OF RHODE ISLAND
2013

Abstract

Glycation is a non-enzymatic reaction with reactants including a reducing sugar and a free amino containing molecule such as protein, amino acids, DNA, RNA and lipids. In the initial phase of glycation, the carbonyl group of the reducing carbohydrate condenses with the free amino groups on the target biomolecule to form reversible glycosylamines, which are then converted to more stable Amadori products. Once formed, these Amadori products can with time undergo dehydration, cyclization, oxidation, and rearrangement to form a polymorphic group of compounds collectively referred to as Advanced Glycation Endproducts (AGEs). The accumulation of AGEs *in vivo* has been implicated as a major pathogenic process in diabetic complications including diabetic cataract formation, retinopathy and neurological diseases, as well as other health disorders, such as Alzheimer's disease (AD).

Chapter one reviewed the chemistry of glycation and the formation of AGEs in a mechanical perspective. The role of AGEs in the pathogenesis of diabetic nephropathy, diabetic neuropathy, diabetic retinopathy and Alzheimer's disease were considered. Here we also reviewed the potential inhibitors against glycation published to date, focusing on some novel potential AGE inhibitors such as zinc and gold nanoparticles.

The purpose of the study described in chapter two was to investigate the susceptibility of the amine groups of melamine to glycation by milk

sugars and sugar metabolites. Dairy products adulterated with melamine have been recently blamed for the death of at least several infants and the sickening of countless children in China. The presented study described the non-enzymatic glycation of melamine with milk sugar D-galactose and several sugar metabolites including methylglyoxal, glyoxal and DL-glyceraldehyde. The chemical structures of melamine AGEs were characterized by electrospray mass spectrometry. The factors influencing the rate and extent of melamine's glycation were also evaluated.

The third part of the dissertation described a study on anti-glycation effect of gold nanoparticles (GNPs). In this study we showed that certain sizes of spherical GNPs exhibit an inhibitory effect on the formation of AGEs when Bovine Serum Albumin (BSA) was glycated by D-ribose. A combination of UV spectrometry, HPLC and circular dichroism showed that only GNPs with size ranging from 2nm to 20nm inhibited the formation of BSA AGEs. The inhibition effect of GNPs was correlated to the overall surface area of nanoparticles in the solution. GNPs with higher surface areas were found to be better inhibitors of glycation, whereas those with low surface areas were less effective inhibitors. The inhibitory effect of GNPs on non-enzymatic glycation reactions may be due to the covalent bonding between gold atoms on the surface of GNP and ε amino groups of L-lysine residue on protein.

In chapter four, we evaluated the effect of UVC radiation on glycation of

Human Serum Albumin (HSA). In this study, we found that exposure to UVC radiation accelerated the glycation level of HSA and promoted the formation of AGEs, which may be stimulated by the generation of ROS by UVC radiation. A combination of several analytical methods including UV spectrometry, HPLC, and MALDI-TOF were used to evaluate the glycation level of HSA at 37 °C under neutral pH in the presence of D-glucose *in vitro*. This study warrants further investigation as there have been few reports on the correlation between the UVC radiation of proteins and their enhanced glycation by a reducing sugar.

ACKNOWLEDGMENTS

I would like to thank, gratefully and sincerely my major advisor Dr. Joel A. Dain for his guidance, patience, and most preciously, his hearty friendship during my doctoral study at University of Rhode Island. I honor him for perfect mentorship provided to me in pursuing my long-term career goals.

I would also like to thank Dr. Louis J. Kirschenbaum, Dr. Jay Sperry and Dr. Sze Yang for agreeing to serve on my thesis committee and for providing me with guidance during my Ph.D. study. I would like to thank Dr. Aftab Ahmed and Nathan Nous for providing instrumentation and patient instruction so I can fulfill my research.

I am thankful to all the members of the biochemistry research group in chemistry department, especially Champika and Sreekanth for giving me intellectual and emotional support during last four years. I would like to thank the faculty and staff in Department of Chemistry at University of Rhode Island, especially Dr. Menashi Cohenford and Dr. George Dombi for their innovative scientific discussion and help with writing the manuscripts. I also thank Dr. Leslie Frost in Department of Chemistry at Marshall University for providing me with guidance on mass spectrometry.

Finally, and most importantly, I thank my husband Joe, my dear parents and my grandmother for their constant support and encouragement so I complete this journey with a lot of joy.

Preface

This dissertation presents one review article and two scientific projects. All three manuscripts focus on the chemistry of glycation, a non-enzymatic reaction which plays an important role in the pathogenesis of diabetic complications including atherosclerosis, renal failure and cardiovascular disease. Chapter one reviews the mechanism and biological effects of glycation. Chapter two describes the glycation reaction of melamine with sugars found in milk and their metabolic products. Chapter three presents the study of gold nanoparticle's anti-glycation property when bovine serum albumin is glycated by D-ribose. Chapter four presents the study on enhancement effect of UVC radiation on the glycation level of HSA.

The dissertation is written in manuscript format. Manuscript two has been accepted by Bioorganic Chemistry in September 2012 and is expected to be published in the journal's latest issue. Manuscript one was prepared according to the format guidelines of Biochimica Biophysica Acta while manuscript three and manuscript four were prepared according to the format guidelines of Analytical Biochemistry.

Table of contents

Abstract……...ii

Acknowledgements……....v

Preface……vi

Table of contents……vii

List of Tables……x

List of Figures……...xi

Manuscript 1. A review of glycation：Mechanism, biological effects and novel inhibitors against the formation of advanced glycation endproducts 1

Abstract 2

1.1 Introduction 3

1.2 The chemistry of glycation 5

1.2.1. Initial stage: formation of Amadori products 5

1.2.2. Intermediate stage: formation of AGE precursors 6

1.2.3. Late stage: formation of AGEs 7

1.3 Biological effects of glycation 10

1.3.1 Physiological defense system against glycation 11

1.3.2 AGE mediated cell-signaling 12

1.3.3 AGE induced protein dysfunction 13

1.4 AGEs and diseases 15

1.4.1 AGEs and diabetic complications 15

1.4.2 AGEs and Alzheimer's Diseases 19

1.4.3 AGEs and aging 20

1.5 Inhibitors against AGE formation 21

1.6 Conclusion 24

Reference 26

List of figures 33

Manuscript 2. Non-Enzymatic Glycation of Melamine with Sugars and Sugar like Compounds 45

Abstract 46

2.1 Introduction 47

2.2 Materials and methods 49

2.2.1 Chemicals and supplies 49

2.2.2 Preparation of reaction mixtures 49

2.2.3 UV and fluorescence spectroscopy 51

2.2.4 High-performance liquid chromatography 51

2.2.5 Mass spectrometry 52

2.3 Results 53

2.4 Discussion 59

References 63

List of figures 68

List of tables 92

Manuscript 3. Inhibitory Effect of Gold Nanoparticles on the Glycation of Bovine Serum Albumin by D-Ribose 94

Abstract: 95

3.1 Introduction 96

3.2 Materials and methods 99

3.2.1. Chemicals and supplies 99

3.2.2. Preparation of reaction mixtures 99

3.2.3 UV and fluorescence spectroscopy 101

3.2.4 Circular dichroism 101
3.2.5 High-performance liquid chromatography 102
3.2.5 MALDI-TOF 103
3.3 Results 103
3.4 Discussion 110
Reference 114
List of figures 117
Tables 128
Manuscript 4. Ultraviolet C radiation enhances glycation of human serum albumin and the formation of CML in vitro 131
Abstract: 132
3.1 Introduction 134
3.2 Materials and methods 137
3.2.1. Chemicals and supplies 137
3.2.2. Preparation of reaction mixtures 137
3.2.3 UV spectroscopy 139
3.2.4 High-performance liquid chromatography 139
3.2.5 ELISA assay 140
3.2.5 MALDI-TOF 140
3.3 Results 141
3.4 Conclusion 147
Reference 151
List of figures 153
Tables 167

List of Tables

Table 2.1 UV readings of incubation mixtures containing melamine (2.5 mM) and different aldehydes (5 mM and 20 mM)..... 92

Table 2.2 Peak Retention Times and Percentages of AGE Band Areas Resulting from the Separation of Incubation Mixtures Containing Methylglyoxal, Glyoxal and DL-Glyceraldehyde with Melamine by HPLC .. 93

Table 3.1 Particle Size and Surface Area of 2nm, 5nm, 20nm Gold Colloid Water Solution in Experiment A and B 128

Table 3.2 HPLC Peak Areas of BSA AGEs generated under incubation condition with or without different sizes of GNP in experiment A 129

Table 3.3 Mass Shift of BSA glycated by D-ribose with or without the presence of GNP in experiment A..... 130

Table 4.1UV readings of reaction mixtures incubated in dark or under UVC radiation 167

Table 4.2HPLC peak areas of unglycated HSA and HSA AGEs generated withor wothout the exposure to UVC radiation 168

Table 4.3 Mass Shift of HSA glycated by D-glucose in dark or under the exposure of UVC radiation 169

LIST OF FIGURES

Figure 1.1 The initial stage of glycation resulting in the formation of a Schiff base and an Amadori product 33

Figure 1.2 *In vivo* sources of dicarbonyl glycation precursors which are responsible for the formation of AGEs and carbonyl stress. 34

Figure 1.3 Chemical structures of currently well-defined AGE dicarbonyl precursors (glyoxal, 3-deoxy-glucosone and methylglyoxal), and their interactions with glycated proteins 35

Figure 1.4 AGE crosslink structures formed under physiological condition which exhibit fluorescence absorbance 36

Figure 1.5 Chemical structures of some of the most important and well-studied non-crosslinking AGEs including pyrraline, 1-carboxyalkyl lysine and imidazolone A and B 37

Figure 1.6 Pathways for the formation of N^{ε}-carboxymethyl lysine *in vivo*. 38

Figure 1.7 Intracellular accumulation of AGEs damages target cells through receptor-mediated pathway 39

Figure 1.8 Structures of reactive oxygen species (ROS) 40

Figure 1.9 Pathways for the generation of ROS which lead to oxidative stress 41

Figure 1.10 Schematic of *in vivo* glycation reactions and common targets for AGE inhibition in the pathways 42

Figure 1.11 Structures of some synthetic anti-glycation agents which act as

dicarbonyl compound scavengers 43

Figure 1.12 Structures of some typical AGE breakers which reduce the damage of glycation 44

Figure 2.1 Chemical structure of melamine. 68

Figure 2.2a Time course UV spectral profiles of reaction mixtures containing 150 mM milk sugar with 1 mM of melamine for 2 hours 69

Figure 2.2b Time course fluorescence spectral profiles of reaction mixture containing 150 mM milk sugar with 1mM melamine at 80 °C for 2 hours ... 70

Figure 2.3 HPLC elution profile of melamine (1 mM) after 1 hour of incubation at 80 °C with 150 mM D-galactose, D-glucose and lactose 71

Figure 2.4 HPLC elution profile of melamine with D-galactose in phosphate buffer incubted for 1 hour at 90 °C, 70 °C, and 40 °C 72

Figure 2.5 UV absorbance profiles of incubation mixtures containing varied amounts of methylglyoxal, glyoxal and DL-glyceraldehyde with set concentration of melamine 73

Figure 2.6 HPLC elution profiles of melamine with methylglyoxal, glyoxal and DL-glyceraldehyde after 30 days incubation at 37 °C 74

Figure 2.7 The order of reactivity of DL-glyceraldehyde, methylglyoxal, glyoxal with melamine 76

Figure 2.8 Mass spectral analysis of solutions of melamine incubated with methylglyoxal for 30 days 77

Figure 2.9 CID mass spectra of mass spectrum profile for melamine

incubated with methylglyoxal for 30 days recorded on the $(M+H)^+$ ion..... 78

Figure 2.10 Mass spectral analysis of solutions of melamine incubated with glyoxal for 30 days. 80

Figure 2.11 CID mass spectra of mass spectrum profile for melamine incubated with glyoxal for 30 days recorded on the $(M+H)^+$ ion 81

Figure 2.12 Mass spectral analysis of solutions of melamine incubated with DL-glyceraldehyde for 30 days..... 83

Figure 2.13 CID mass spectra of mass spectrum profile for melamine incubated with DL-glyceraldehyde for 30 days..... 84

Figure 2.14 Mass spectral analysis of solutions of melamine incubated with D-galactose for 30 days 86

Figure 2.15 ID mass spectra of mass spectrum profile for melamine incubated with D-galactose for 30 days recorded on the $(M+H)^+$ ion. 87

Figure 2.16 Elucidation of structures consistent with mass spectrometric data for products formed in incubation mixtures containing melamine with methyglyoxal, glyoxal, DL-glyceraldehyde, and D-galactose. 89

Figure 2.17 Postulated pathway for the formation of melamine AGEs with methylglyoxal 90

Figure 2.18 UV absorbance profiles of incubation mixtures of melamine with set concentration of methylglyoxal in phosphate buffer under different pHs 91

Figure 3.1 UV absorbance spectrum of reaction mixtures in A..... 117

Figure 3.2 UV absorbance spectrum of reaction mixtures in B..... 118

Figure 3.3 CD profiles of reaction mixtures in experiment A after 21 days incubation. 119

Figure 3.4 CD profiles of reaction mixtures in experiment B after 21 days of incubation 120

Figure 3.5 HPLC-UV elution profile for reactions in experiment A..... 121

Figure 3.6 HPLC-fluorescence elution profile for reaction mixtures in experiment A 122

Figure 3.7 MALDI-TOF profile of reaction mixture containing 35 mg/ml BSA incubated in dark at 37 °C for 21 days 123

Figure 3.8 MALDI-TOF profile of reaction mixture containing 35 mg/ml BSA glycated by 20 mM D-ribose in dark at 37 °C for 21 days. 124

Figure 3.9 MALDI-TOF profile of reaction mixture containing 35 mg/ml BSA glycated by 20 mM D-ribose at the presence of 2 nm GNP 125

Figure 3.10 MALDI-TOF profile of reaction mixture containing 35 mg/ml BSA glycated by 20 mM D-ribose at the presence of 5 nm GNP 126

Figure 3.11 MALDI-TOF profile of reaction mixture containing 35 mg/ml BSA glycated by 20 mM D-ribose at the presence of 20 nm GNP 127

Figure 4.1 HPLC-UV elution profile of 35 mg/ml HSA alone in 0.1 M phosphate buffer, pH 7.2 serving as blank solution..... 153

Figure 4.2 HPLC elution profile of control reaction mixture containing 35 mg/ml HSA and 20 mM D-glucose incubated for 2 days in experiment A 154

Figure 4.3 HPLC-UV elution profile of experimental reaction mixture containing 35 mg/ml HSA and 20 mM D-glucose incubated for 2 days in experiment A 154

Figure 4.4 HPLC elution profile of control reaction mixture containing 35 mg/ml HSA incubated for 7 days in experiment A 155

Figure 4.5 PLC-UV elution profile of experimental reaction mixture containing 35 mg/ml HSA incubated for 7 days in experiment A..... 155

Figure 4.6 PLC-UV elution profile of control reaction mixture containing 35 mg/ml HSA and 20 mM D-glucose in experiment B. 156

Figure 4.7 PLC-UV elution profile of experimental reaction mixture containing 35 mg/ml HSA and 20 mM D-glucose in experiment B. 156

Figure 4.8 Modified HPLC-UV elution profile for spectrum shown in figure 6. 157

Figure 4.9 Modified HPLC-UV elution profile for spectrum shown in figure 7. 157

Figure 4.10 Comparison of the production of CML in each reaction mixture in experiment A with incubation times of 0, 2 and 7 days..... 158

Figure 4.11 Comparison of the production of CML in each reaction mixture in experiment B with incubation times of 12, 24 and 48 hours 159

Figure 4.12 MALDI-TOF profile of reaction mixtures containing 35 mg/ml HSA incubated in dark at 37 °C for 7 days..... 160

Figure 4.13 MALDI-TOF profile of reaction mixtures containing 35 mg/ml

HSA and 20 mM D-glucose incubated in dark at 37 °C for 2 days (experiment A)..... 161

Figure 4.14 MALDI-TOF profile of reaction mixtures containing 35 mg/ml HSA and 20 mM D-glucose incubated under UVC radiation at 37 °C for 2 days (experiment A)..... 162

Figure 4.15 MALDI-TOF profile of reaction mixtures containing 35 mg/ml HSA and 20 mM D-glucose incubated in dark at 37 °C for 7 days (experiment A)..... 163

Figure 4.16 MALDI-TOF profile of reaction mixtures containing 35 mg/ml HSA and 20 mM D-glucose incubated under UVC radiation at 37 °C for 7 days (experiment A)..... 164

Figure 4.17 MALDI-TOF profile of reaction mixtures containing 35 mg/ml untreated HSA and 20 mM D-glucose (experiment B)..... 165

Figure 4.18 MALDI-TOF profile of reaction mixtures containing 35 mg/ml UVC pre-treated HSA and 20 mM D-glucose (experiment B)..... 166

Manuscript 1

Prepared for Biochimica Biophysica Acta
Anticipated submission date: February 2013

A review of glycation：Mechanism, biological effects and novel inhibitors against the formation of advanced glycation endproducts

Weixi Liu [1], Champika Seneviratne [2], Sreekanth Suravajjala [3], Joel A. Dain [*]

Department of Chemistry, University of Rhode Island, Kingston, RI 02881

*Corresponding author: Phone: + 1-401-874-5942; fax: + 1-401-874-5072
E-mail address: jdain@chm.uri.edu

Abstract

Glycation is a non-enzymatic reaction between reducing sugars and amino groups in proteins, nucleic acids and lipids. The final products of this reaction are a polymorphic group of compounds collectively referred to as Advanced Glycation Endproducts (AGEs). The gradual built-up of AGEs in body tissues plays an important role in the pathogenesis of diabetic complications including atherosclerosis, renal failure and cardiovascular disease. Recent studies suggest that AGEs selectively bound to AGE receptors found in several cell types, many of which are affected by diabetes. The interaction of AGEs to these receptors triggers the release of pro-inflammatory molecules and free radicals, inducing oxidative cellular dysfunction. The intracellular uptake of AGEs also alters cell signaling and gene expression that contribute towards the pathology of diabetic complications. This article reviews the chemistry of glycation and the formation of AGEs in a mechanical perspective. The role of AGEs in the pathogenesis of diabetic nephropathy, diabetic neuropathy, diabetic retinopathy and Alzheimer's disease are considered. Here we also review the potential inhibitors against glycation published to date, focusing on some novel potential AGE inhibitors such as zinc and gold nanoparticles.

Key words: glycation; AGEs; diabetes; ROS

1.1 Introduction

The Non-enzymatic reaction between the carbonyl group of a reducing sugar and the amino containing molecule such as protein, peptide or amino acid was first studied under defined conditions by Louis Camille Maillard in 1912. Ever since its description in early 1900s, the Maillard reaction has continued to be a topic of research interest. For researchers in nutrition science, harnessing the Maillard reaction has allowed for controlling food flavor, food aroma, food coloring, and food texture. In addition to its benefits, the Maillard reaction occurring during food processing also results in the loss of protein quality and the formation of harmful compounds with mutagenic, carcinogenic and genotoxic properties (1-3).

During the 1970s and 1980s, researchers in clinical medicine realized that this process also occurs slowly *in vivo*. Subsequently, Maillard reaction *in vivo* was termed glycation, distinguished from enzymatic glycosylation. The final products of this reaction are a polymorphic group of compounds collectively referred to as Advanced Glycation Endproducts (AGEs). The gradual built-up of AGEs in body tissues plays an important role in the pathogenesis of diabetic complications including atherosclerosis, renal failure and cardiovascular disease. Glycation is also found to be related to other health disorders such as Alzheimer Diseases (AD) and normal aging (4-6).

Intracellular hyperglycemia can induce the formation of glucose-derived

dicarbonyl molecules such as glyoxal, methylglyoxal and 3-deoxyglucosone. These intracellular dicarbonyls, also called AGE precursors, are much more reactive comparing to D-glucose due to their lack of cyclic structure and comparatively smaller size. AGE precursors glycate with amino groups of both intracellular and extracellular proteins at a much faster rate than D-glucose, leading the accumulation of AGEs. These AGEs specifically binds to a certain groups of cell surface receptors (RAGEs), inducing receptor-mediated production of reactive oxygen species (ROS), finally resulting in oxidative cellular dysfunction (3, 7). AGEs such as glyoxal lysine dimer (GOLD) and methylglyoxal lysine dimer (MOLD) are responsible for protein crosslinking on longest-lived extracellular proteins such as collagen and elastin. Such proteins provide strength and flexibility to tissues, and do not get recycle very often. Glycation and crosslinking gradually change the property and function of these proteins, reduce their flexibility and elasticity, and increase their stiffness as well. This process has been implicated as strong contributors to many progressive diseases of aging, including vascular diseases, stiffness of joints, arthritis and kidney failure (4-6).

Both synthetic compounds and natural products have been found to be inhibitors against the formation of AGEs. These glycation inhibitors are proposed to block the formation of intermediate Amadori products, or break the crosslinking of proteins. Their classification and corresponding inhibition mechanism will be discussed later in this article.

1.2 The chemistry of glycation

Glycation is a non-enzymatic browning reaction that involves a series of steps with the reactants typically including a reducing sugar and a free amino containing molecule. The progress of the reaction includes three distinguishable phases: the initial stage, the intermediate stage and the late stage. In the initial phase of glycation, the carbonyl group of a reducing carbohydrate condenses with the free amino group on a protein or other amino containing molecule to form reversible glycosylamine, which is then converted to more stable Amadori products. Under appropriate condition, these Amadori products could degrade to more reactive dicarbonyls such as methylglyoxal, glyoxal and glyceraldehyde. These intermediates are responsible for most of the AGE formation due to their high reactivity. In the late stage of glycation, the Amadori product itself could with time undergo dehydration, cyclization, oxidation, and rearrangement to form AGEs. Meanwhile, the AGE precursors formed from the intermediate stage of glycation such as methylglyoxal will in turn interact with protein or other amino containing molecules to produce AGEs at a much higher reaction rate comparing to reducing sugars.

1.2.1. Initial stage: formation of Amadori products

In the initial phase of glycation, the nitrogen atom of a terminal α-amino group or of the ε-amino group on lysine or arginine residue covalently condenses with the carbonyl group of a reducing sugar by nucleophilic

attack. The product of this reaction contains an unstable aldimine structure named Schiff base. The formation of Schiff base is reversible due to the unstable property of aldimine functional group. Schiff base intermediate can then undergo Amadori rearrangement to produce a relatively stable ketosamine structure, referred to as Amadori product (See figure 1). Formation of Amadori product from Schiff base is much faster than the reversed reaction so Amadori adducts tend to accumulation on proteins. This process is thought to be facilitated by localized acid-base catalysis if there is a histidine or lysine side chain about 5 Å from the target amino residue (8).

1.2.2. Intermediate stage: formation of AGE precursors

AGE precursors are formed *in vivo* via two major pathways: 1) the fragmentation of Amadori products or Schiff base, and 2) the metabolic degradation of D-glucose. The physiologically relevant D-glucose is one of the least reactive reducing sugars in protein glycation (9). Under physiological condition, over 90% of D-glucose is in cyclic confirmation which cannot be a target of the nucleophilic attack by a primary amino group. However, other sugars and dicarbonyl compounds, many of which are found intracellular such as glyoxal (Gly), 3-deoxyglucosone (3-DG) and methylglyoxal (MG) participate in glycation at a proportionally faster rate (10, 11). Gly is formed from several reactions such as the oxidative fragmentation of Schiff base via the Namiki pathway (12, 13), glucose

auto-oxidation catalyzed by metal (Wolff pathway) or lipid peroxidation via the Acetol pathway (14, 15). 3-DG is produced from non-oxidative fragmentation and hydrolysis of Amadori product. 3-DG also forms from fructose-3-phosphate, an intermediate of the Polyol pathway in which glucose is reduced to sorbitol by aldose reductase. Further degradation of 3-DG generates methylglyoxal and glyceraldehyde (GA) by retro-aldol condensation (16, 17). Methylglyoxal is found to be one of the most reactive glycation agents, and could react with different amino acids including lysine and arginine to generate dicarbonyl-derived AGEs. MG could also alter the secondary structure of a protein, resulting in the loss of its function (18, 19). A summary of the sources of these reactive carbonyl species are shown in figure 2.

The increase in the concentration of reactive carbonyl compounds from glycoxidation, lipoxidation or the degradation of Schiff base/Amadori adducts will lead to carbonyl stress (20, 21), a situation that aggravates the modification of proteins and prompts the formation of AGEs. Figure 3 is a list of chemical structures of currently well-defined AGE dicarbonyl precursors and their interactions with glycated proteins.

1.2.3. Late stage: formation of AGEs

AGEs are a group of heterogeneous compounds including fluorescent crosslinking structures such as pentosidine, non-fluorescent crosslinking substances such as glyoxal lysine dimer (GOLD) or methylglyoxal lysine

dimer (MOLD), and non-fluorescent, non-crosslinking compounds such as N^{ε}-carboxymethyl lysine (CML). AGEs are produced both *in vitro* and *in vivo* via several pathways, including direct degradation of Amadori products or Schiff base, protein modification by dicarbonyl compounds and reactions between Amadori products and AGE precursors.

One of the major consequences of protein being modified by active dicarbonyl glycation agents is the formation of protein cross-links, a situation that is related to several diabetic complications. Reactions of dicarbonyl compounds with lysine and arginine residue or with Amadori intermediate are involved in the formation of many AGE crosslinking structures which exhibit fluorescence absorbance (Figure 4). Among these compounds, pentosidine from the glycation of ribose has been determined in many tissues such as lens proteins and skin collagens (22). Pentosidine can also be formed from several more reactive carbohydrate intermediates including 3-DG and fructose. It has been recently proposed as an index for evaluating tissue damage under glycation condition (23).

Although fluorescent crosslinking AGEs are important biomarkers of hyperglycemia condition due to their easy of detection, these structures are account for only a small portion of protein crosslinks which is about 1% in physiological condition (24). On the other hand, non-fluorescent crosslinking AGEs are the major contribution to *in vivo* protein-protein crosslinks. A group of most well defined crosslinking structures are imidazolium

crosslinks including glyoxal-derived AGE glyoxal-lysine dimer (GOLD) and methylglyoxal-derived AGE methylglyoxal-lysine dimer (MOLD) (25, 26). Both of these structures are found in human lens protein and human serum. (27-29). Glyoxal and methylglyoxal could irreversibly modify the ε-amino group of lysine residues in protein under physiological condition to form these imidazolium compounds which are responsible for protein crosslinking.

The third class of AGEs is non-fluorescent, non-crosslinking structures, which act as biological receptor ligands to initiate cellular signaling and induce tissue oxidation stress. These compounds could also perform as precursor of protein crosslinks. The chemical structures of some of the most important and well-studied non-crosslinking AGEs including pyrraline, 1-carboxyalkyl lysine and imidazolone A and B are shown in figure 5.

3-DG rapidly reacts with lysine residues of a protein to form pyrraline. Though pyrraline itself is not a crosslink structure, it may cause crosslinks between proteins when its aldehyde group forms a Schiff base with another amino group, resulting in lysine-lysine or lysine-arginine crosslinking in *vivo.* Imidazolone is derived from reaction of dicarbonyl compounds with the guanidino group of an arginine residue.

AGEs such as N^{ε}-carboxymethyl lysine (CML) and N^{ε}-carboxymethyl lysine (CEL) with a carboxyalkyl group attached to the ε-amino group of an amino acid are found *in vivo.* CML is known as one of the most well

characterized AGEs which is used as a biomarker for long-term protein damage in diabetes and oxidative tissue abnormality. CML can be produced through different pathways including glycation and oxidation reactions (22, 30, 31), resulting in its wide distribution in a variety of tissues such as serum, skin collagen and kidney.

CML is produced through four major pathways shown in figure 6: 1) oxidative cleavage of Amadori product 2) Schiff base degradation through Namiki pathway (32); 3) oxidation of ascorbic acid (33) and 4) autoxidation glycosylation with lysine and glyoxal (32). The oxidative degradation of Amadori adducts is thought as the major source of CML formation (25, 34). Under physiological condition, CML is found to be produced mainly from fructoselysine, an Amadori intermediate derived from fructose and lysine. The Schiff base can undergo degradation via Namiki pathway to form active carbonyl compounds such as glyoxal and its corresponding imine analog, which are responsible for the formation of CML. The other CML precursor formed via Namiki pathway is aminoaldehyde. Aminoaldehyde could oxidize to CML by any of the oxygen reactive species present in the glycation system, or by oxygen under metal catalysis. Other sources of CML formation include the oxidation of ascorbic acid derived from glucose and direct condensation of glyoxal with the ε-amino group of lysine residues in proteins.

1.3. Biological effects of glycation

Non-enzymatic glycation has been thought to play an important role in the pathogenesis of diabetic complications including cataract formation, renal failure and cardiovascular disease. Glycation is also approved to be related to other health disorders such as Alzheimer's disease (AD), atherosclerosis and normal aging. Most of the effects of glycation which lead to chronic complications are due to AGE accumulation on long-lived proteins such as collagen and lens crystallins. In the meantime, glycation can induce the formation of reactive oxidation species (ROS), causing oxidation stress and tissue damage (35, 36).

1.3.1 Physiological defense system against glycation

There are several defense systems occurring physiologically against the deleterious effects of AGE, including enzymes such as aldose reductase，which inhibit the formation of AGE precursors or antioxidants such as glutathione which reduce the production of reactive oxidative species. Aldose reductase is a NADPH-dependent enzyme that catalyzes the degradation of dicarbonyl AGE intermediates including MG and 3-DG (37-39). Most recently, fructoselysine, an Amadori intermediate derived from fructose and lysine, was found to be phosphorylated by human fructosamine-3-kinase (FN3K) and spontaneously degradation afterwards (40). The glyoxalase system catalyzes the conversion of methylglyoxal to D-lactic acid by glyoxalase I and glyoxalase II. This system is present in the cytosol and mitochondria of cells and has a wide distribution in living

organisms (41, 42). Another natural common defense mechanism is glutathione (GSH) system. GSH is an antioxidant, preventing oxidative damage to tissues caused by reactive oxidative species such as peroxides and free radicals, whose formations are prompted by glycation. GSH also facilitated the rearrangement of methylglyoxal to D-lactate in the glyoxalase pathway (43).

1.3.2 AGE mediated cell-signaling

Intracellular accumulation of AGEs damages target cells through receptor-mediated pathway, in which the glycated plasma proteins bind to AGE receptors on the cell surface, inducing cell signaling and oxidation stress (see figure 7). Several AGE binding proteins have been identified such as RAGE, the AGE receptor complex (AGE-RG) and macrophage scavenger receptor (44-46), many of which play a critical part in the pathology associated with AGE related complications.

In endothelial cell system, plasma proteins modified by AGEs act as ligands to AGE receptors found on the surface of the cell. This process activates intracellular transducers and leads to the changes in gene expression. A rise in the expression of pro-inflammatory and pro-coagulatory molecules was found in endothelial cell when it was exposed to high glucose (47-50). RAGE is a member of the immunoglobulin receptor family. Pro-inflammatory NF-κB pathway is thought to be one of the major targets of RAGE. The activation of the pathway is related to several

inflammatory diseases in diabetes. In addition, NF-κB in turn elevates RAGE expression, establishing a positive feed-back cycle. In summary, the intracellular accumulation of AGE results in the increase of RAGE ligands, activating NF-κB pathway and lead to chronic inflammation.

Additionally, AGE receptors are found on the surface of macrophage and mesangial cell. Binding of AGE ligands to the receptor induces the formation of reactive oxygen species (ROS) including peroxyl, superoxide anions, hydroxyl radicals and hydrogen peroxides (structures seen in figure 8). As discussed previously in this article, the abnormal excess of ROS under hyperglycemia conditions originate from several mechanisms including the degradation of glycation intermediates, the by-production of carbonyl AGE precursors, and cellular oxidant stress triggered by RAGE. The abnormal accumulation of ROS caused by hyperglycemia is known to mediate the progression of several chronic complications due to the impaired antioxidant defense system. Such situation is defined as oxidative stress. Pathways for the generation of ROS which lead to oxidative stress are summarized in figure 9. The rise in the oxidant level in a living organism can cause damage to various cell components and triggers the activation of certain cell signaling pathways, resulting in pathological changes in gene expression.

1.3.3 AGE induced protein dysfunction

Several intracellular proteins modified by glycation are found to have

altered activities and stabilities. One example is serum albumin, the most abundant protein in blood plasma which exhibits a broad range of physiological functions such as catalytic activities. Serum albumin can catalyze the hydrolysis of esters, showing an esterase-like activity. However, its enzymatic activity is impaired drastically when the protein is glycated by methylglyoxal. Since a lysine residue of the protein has been suggested as the catalytic center, the loss of the protein's esterase activity is thought to be related to the modification of this lysine residue by glycation agents (51). Another example of dysfunctional AGE modified protein is proteases, a class of enzymes which degrade polypeptides. The catalyze sites of this enzymes include cysteine and histidine, both of which can be glycated by methylglyoxal, resulting in the loss of enzymes' activity (52).

AGE formation does not only alter the activity of intracellular proteins, but affect the functional properties of important molecules on extracellular matrix such as various types of collagens. Collagen is the main components of connective tissue, responsible for skin elasticity, blood vessel strength and tissue regeneration. This type of proteins has a comparatively long biological half-life and is exposed to extracellular glucose whose level is considerably higher than that inside the cell. Collagen can react with other collagen molecules through protein crosslinking by some typical AGE structures including methylglyoxal lysine dimer (MOLD) and glyoxal lysine dimer (GOLD). Such crosslinking structures can be gradually built up during

normal aging and are accumulated much faster under hyperglycemia condition. As a result, the formation of MOLD and GOLD plays a critical role in the pathologenesis of vascular stiffening and atherosclerotic lesions (17).

1.4 AGEs and diseases

The accumulation of AGEs has been implicated as strong contributors to many progressive diseases including diabetic complications, aging and Alzheimer's disease. AGEs play a role in the pathogenesis of such health disorders through three major mechanisms: 1) AGE modified plasma proteins could bind to AGE receptors on the surface of the cell, activate cell signaling and lead to the production of ROS and inflammatory factors; 2) intracellular proteins, specifically catalytic proteins, could lose their function and stability if the activate site is glycated by AGE precursors; 3) proteins on the extracellular matrix such as collagen could crosslink with other matrix components, leading to the loss in their function.

1.4.1 AGEs and diabetic complications

1.4.1.1 Diabetic nephropathy

Diabetic kidney disease is one of the major microvascular complications of diabetes. The hyperglycemia related mechanisms of diabetic nephropathy can be explained in three pathways. First, by binding to signaling cell surface receptors, AGEs can activate protein kinase C (PKC) which plays a center role in the pathogenesis of diabetic nephropathy. Second, binding of AGEs to their receptors can increase the expression of

several transcription factors and enhance the formation of ROS. Third, the intracellular AGEs also initiate cell signaling events which alter the expression of extracellular matrix proteins including type I and type IV collagens. Meanwhile, AGEs can form crosslinking structures with collagens, causing altered cell adhesiveness and capillary permeability.

PKC is an intracellular signaling kinase which can be activated by the binding of AGEs with RAGE. The activation of PKC will lead to endothelial dysfunction resulting in altered blood flow and capillary permeability. PKC can also induce the generation of pro-inflammatory factors such as NF-κB and lead to local tissue inflammatory (53, 54). Hyperglycemia condition promotes the generation of ROS during or after the formation of AGEs. There is considerate *in vitro* study suggesting the involvement of ROS in the pathogenesis of renal injury. The generation of ROS is coupling with the biological alteration of tubular cells with loss of epithelial cell adhesion (55). Moreover, the balance of nitroso-redox can be disturbed by the formation of ROS when the radicals inactive relaxing nitric oxide and cause hypertension. Besides the activation of PKC and the up-modulation of ROS, the accumulation of AGEs causes the increased synthesis of extracellular matrix and decreased expression of its degrading enzymes, leading to the polymerization and expansion of extracellular matrix proteins (56-58).

1.4.1.2 Diabetic neuropathy

The symptoms of diabetic neuropathy often develop slowly over years,

including the loss of sensation, nausea, deep pain in legs and feet. The pathology can be characterized by progressive nerve fiber lose caused by long-term high blood sugar level in diabetes. The precise mechanisms underlying diabetic neuropathy is unclear, however most recent study suggests that the loss in nerve fiber can be caused by multiple pathways including the enhanced polyol pathway under hyperglycemia condition, the increased protein modification by AGEs and the up-regulated oxidation stress.

In polyol pathway, glucose is degraded to sorbitol by aldose reductase. This process can be up-regulated under hyperglycemia condition, causing increased consumption of NADPH and reduced formation of glutathione. The impaired synthesis of glutathione will then cause vascular insufficiency and degeneration of nerve fibers (59). The activation of polyol pathway also suppresses the activity of protein kinase C, and eventually elicits reduced nerve blood flow and decreased nerve conduction (60). Meanwhile, the binding of AGEs to their receptors has been found to induce oxidative stress, result in over expression of pro-inflammatory genes, and exaggerate neurological dysfunction, including altered pain sensation. The AGE-RAGE interaction can also activate the formation of extracellular matrix proteins. AGEs in terns covalently bond to these proteins to form crosslink structures, and lead to the development of vascular abnormalities, such as thickening of capillary basement membrane.

1.4.1.3 Diabetic retinopathy

Many *in vitro* and *in vivo* studies showed that AGEs play a significant pathogenic part in diabetic retinopathy, when the retinal microvascular becomes dysfunctional progressively, resulting in damage to the retina of the eye (61). The accumulation of AGEs is proposed to participate in the progression of the disease via three pathways. First, the binding of AGEs to their receptors induce the formation of vascular basement membrane proteins. These proteins are then cross-linked by certain species of AGEs, resulting in basement membrane thickening and the breakdown of the inner blood-retinal barrier (62, 63). Second, AGEs-RAGE binding inappropriately initializes intracellular signaling, cause abnormal expression of transducers or growth factors, which result in the failure of endothelial cells. Third, retinal vascular endothelia cells show disturbed nitric oxide expression when exposed to high concentration of AGEs, which may be a cause of capillary closure and retinal ischemia.

Besides diabetic retinopathy, the cataract formation is another major complication developing gradually in diabetes disorder. Under hyperglycemia condition, there is an increased production of highly reactive dicarbonyl compounds such as methylglyoxal and glyoxal. These molecules not only act as AGE precursors but also cause AGE crosslinks and protein aggregations on crystallins, leading to the formation of cataract (64-66). Other study suggests that oxidation stress, which is upgraded by glycation,

can promote the formation of cataract as well.

1.4.2 AGEs and Alzheimer's Diseases

Alzheimer's disease (AD) is an age-related chronic complication which severely affects patients' memory and behavior in their late life. The causes of such disease include early stage triggering events and late stage inflammation and neurodegeneration. Several studies suggest that the formation of AGEs plays an important role in the pathogenesis of AD.

The deposition of β-Amyloid (Aβ) in the cerebral cortex is one of the major pathological features of AD. Aβ peptides contain 39 to 43 amino acid residues and are found overproduced in AD brains. These peptides are thought to be one of the most important contributors to neurodegeneration (67, 68). Solid evidence revealed that extensive protein crosslinking and the increased production of ROS, inflammatory factors and reactive dicarbonyl compounds are responsible for AD characteristics including the Aβ deposit (69). Meanwhile, all the above mentioned chemical processes are related to glycation and AGEs, whose formation is found to be accelerated in AD.

It has been suggested that the accumulation of AGEs is involved in the pathogenesis of AD through two major mechanisms including AGE-RAGE interaction and protein-Aβ crosslinking. As described in the previous chapter, AGE modified proteins can interact with cell surface receptors such as RAGE, and trigger a serial of cellular signaling pathways. Besides AGEs, Aβ is found to be another ligand of RAGE. The interactions of AGEs and Aβ

with RAGE elicit the production of ROS and pro-inflammatory factors. The generation of these molecules will then cause oxidative stress and inflammatory, subsequently leading to neuronal dysfunction. The accumulation of AGEs is also responsible for protein-Aβ crosslinks, a major cause to neurodegeneration in AD. Such binding down-regulates the expression of genes involved in Aβ clearance, resulting in Aβ accumulation.

1.4.3 AGEs and aging

Hyperglycemia is shown to be correlated to several age-related diseases and the controlling of such condition prolonged life span in experimental animals. Hyperglycemia induces the formation of AGEs when protein is glycated by reducing sugars or active dicarbonyl compounds. AGEs up-regulate oxidative stress and inflammation, cause crosslinks on long lived protein such as extracellular matrix and vascular basement membrane, and reduce the clearance of harmful protein aggregations. Thus AGEs play a significant role in the pathogenesis of several diseases across different organ systems, many of which are age-related. AGEs interact with their receptors and trigger the induction of ROS and pre-inflammatory factors. AGEs and AGE receptors are found in different cell types including smooth muscle cells, endothelium and mono nuclear cells. Such wide distribution of these compounds causes the chronic damage to virtually every tissue in the body. Meanwhile, AGEs elicit protein cross-links and affect most on tissues composed with long-lived proteins such as skin,

skeletal muscle, heart, arteries and lens. AGE-mediated protein crosslinking in connective tissues causes the loss in their elasticity and flexibility, resulting in skin aging, hypertension and cataract formation.

1.5 Inhibitors against AGE formation

Since non-enzymatic glycation of proteins is a major contributor to the pathology of diabetes and other diseases including AD, the inhibitors to prevent the formation of AGEs have been extensively investigated and a number of potential AGE inhibitors have been proposed over years. A schematic of *in vivo* glycation reactions is shown in figure 10. On this scheme are also common targets for AGE inhibition which are labeled by circled letters from A to F. Type A and type B inhibitors prevent the formation of Amadori product at the initial stage of glycation by competing with glycation agents (type A) or reacting with reducing sugars (type B) (70-72). Other types of inhibitors (type C1 and C2) disturb glycation mechanisms such as Wolff pathway and Namiki pathway, enhance antioxidant activity, and reduce the production of dicarbonyl AGE precursors. Type D drugs interact with reactive dicarbonyl compounds such as methylglyoxal and glyoxal, preventing their binding to protein (73, 74). Comparing to class D, class E compounds directly act on Amadori adducts, and trap it from further modification (75). Instead of preventing AGE formation, drugs in F group reduce AGE toxicity by breaking protein-AGE cross-linking. There are also numbers of novel AGE inhibitors such as zinc and nanoparticles, whose

inhibition mechanisms are still under investigation.

1.5.1. Carbonyl compounds scavengers

The first and most well-known synthetic glycation inhibitor is aminoguanidine (AG) (76), whose structure can be found in figure 11. Aminoguanidine prevents the formation of AGEs by reacting with reactive dicarbonyl compounds such as methylglyoxal and glyoxal, hindering the late stage of glycation. Several *in vivo* studies demonstrated that AG retarded the development of several diabetes related complications including renal failure and cataract formation (77). Unfortunately, AG showed considerable toxicity to human body during clinical trial, thus structural modification on the compound is required to reduce its toxicity. Pyridoxamine (PM), one of the vitamin B complexes, is another potent carbonyl scavenger which showed better inhibitory effect on reducing the glycation level in bovine serum albumin model (78). PM inhibits the formation of AGEs not only by trapping the reactive dicarbonyl AGE precursors, but by blocking the oxidative degradation of the Amadori intermediates as well, preventing it from further modification by reducing sugars (79).

1.5.2 AGE breakers

Cell tissue constantly exposed to AGEs tent to lose its function due to protein crosslinking. Recently, a few AGE breakers have been discovered to combat deleterious protein cross-links. Their structures are shown in figure 12. This class of anti-glycation agents provides a potential new therapeutic

approach especially for diabetic cardiovascular disease. Patients who received alagebrium chloride (ALT-711), one of the most well studied AGE breakers, showed significant reduction in arterial pulse pressure (80). Another prototypic protein cross-link breaker is *N*-phenacylthiazolium bromide (PTB). PTB reacts with AGE-induced protein aggregates and covalently cleaves protein crosslinking structures (81).

1.5.3 Dietary antioxidant

A dietary antioxidant is considered to be relatively safe for human consumption comparing to above mentioned synthetic compounds. The accumulation of AGEs induces the formation of ROS, leading to cell dysfunction and tissue damage. Dietary antioxidants are substances found in food that decrease the damage of ROS, and restore physiological function in humans. Vitamin C and vitamin E, for instance, both prevented the formation of AGEs in experimental models. Treatment of diabetic rats with these antioxidants resulted in a reduced plasma lipid peroxidation level. The study also showed that vitamin E has a potent to restore nerve system by reversing nerve conduction velocity deficits (82).

1.5.4 Novel AGE inhibitors

Besides synthetic anti-glycation agents and traditional dietary substances which reduce the damage of ROS, some novel AGE inhibitors have also been proposed recently, including zinc and gold nanoparticles (GNP). In a recent *in vitro* study, human serum albumin treated with different

concentrations of zinc showed lower glycation level comparing to control experiment, suggesting that zinc inhibited the formation of AGEs. In this study, a combination of analytical methods was used to evaluate the level of protein glycation. Moreover, the treatment of zinc not only reduced the formation of glycation products, but also retained protein's secondary structure, an observation which was confirmed by circular dichroism. Zinc was proposed to inhibit glycation by binding to the reactive sites on the protein and preventing sugar's non-enzymatic condensation with these sites (83). GNP is another substance which showed anti-glycation activity as well as satisfying bio compatibility. In one study, spherical gold nanoparticles (GNPs) with a diameter of 2 nm showed an inhibition effect on the formation of AGEs when human serum albumin was glycated with DL-glyceraldehyde. The inhibitory effect of GNPs on non-enzymatic glycation reactions may be due to the covalent bonding between gold atoms on the surface of GNP and ε amino groups of L-lysine residue on protein. As GNP is highly biocompatible and water soluble, an insight of its anti-glycation effect and its inhibition mechanism on the formation of AGEs might lead to a novel therapeutic application of GNP on reducing AGE related complications (84).

1.6. Conclusion

In conclusion, glycation is a non-enzymatic reaction with reactants including a reducing sugar and a free amino containing molecule such as

protein, amino acids, DNA, RNA and lipids. In the initial phase of glycation, the carbonyl group of the reducing carbohydrate condenses with the free amino groups on the target biomolecule to form reversible glycosylamines, which are then converted to more stable Amadori products. Once formed, these Amadori products can with time undergo dehydration, cyclization, oxidation, and rearrangement to form a polymorphic group of compounds collectively referred to as Advanced Glycation Endproducts (AGEs). The accumulation of AGEs *in vivo* has been implicated as a major pathogenic process in diabetic complications including diabetic cataract formation, retinopathy and neurological diseases, as well as other health disorders, such as aging and Alzheimer's disease (AD).

AGEs play a role in the pathogenesis of such health disorders through different yet complicated cellular mechanisms including ligand induced cell signaling which causes oxidative stress and inflammation; protein dysfunction due to modification on the active site by glycation; and protein crosslink which leads to its denaturation. The inhibitors to prevent the formation of AGEs have been extensively investigated based on these pathways. The most promising glycation inhibitors include amino-guanidine and pyridoxamine which trap the active dicarbonyl molecules and prevent the formation of AGEs. Some novel anti-glycation substances such as zinc and gold nanoparticles have also been proposed recently.

Reference:

1. Yaylayan, V.A.; Machiels, D.; Istasse, L.J. Agric. Food Chem., 2003, 51, 3358.
2. Monti, S.M.; Ritieni, A.; Sacchi, R.; Skog, K.; Borgen, E.; Fogliano, V. J. Agric. Food Chem., 2001, 49, 3969.
3. Persson, E.; Graziani, G.; Ferracane, R.; Fogliano, V.; Skog, K. Food Chem. Toxicol., 2003, 41, 1587.
4. Furth, A.J. Br. J Biomed. Sci., 1997, 54, 192.
5. Ulrich, P.; Cerami, A. Recent Prog. Horm. Res., 2001, 56, 1.
6. Thornalley, P.J. Int. Rev. Neurobiol., 2002, 50, 37.
7. Kato, T.; Harashima, T.; Moriya, N.; Kikugawa, K.; Hiramoto, K. Carcinogenesis, 1996, 17, 2469.
8. Acosta, J.; Hettinga, J.; Fluckiger, R.; Krumrei, N.; Goldfine, A.; Angarita, L.; Halperin, J. Proc. Nat. Acad. Sci. U.S.A. 2000, 91, 5450.
9. Bunn, H.F.; Gabbay, K.H.; Gallop, P.M. Science, 1978, 200, 21.
10. Li, Y.; Cohenford, M.A.; Dutta, U.; Dain, J.A. Anal. Bioanal. Chem., 2008, 390, 679.
11. Li, Y.; Dutta, U.; Cohenford, M.A.; Dain, J.A. Bioorganic Chemistry, 2007, 35, 417.
12. Glomb, M.A.; Monnier, V.M. J. Biol. Chem., 1995, 276, 10017.
13. Dyer, D.G.; Dunn, J.A.; Thorpe, S.R.; Bailie, K.E.; Lyons, T.J.; McCance, D.R.; Baynes, J.W. J. Clin. Invest., 1993, 91 , 2463.

14. Wolff, S.P.; Dean, R.T. Biochem. J., 1987, 245, 243.
15. Wolff, S.P.; Jiang, Z.Y.; Hunt, J.V. Free Radical Biol. Med., 1991, 10, 339.
16. Martins, S.I.; Marcelis, A.T.; Boekel, M.A. Carbohydr. Res., 2003, 338, 1651.
17. Thornalley, P.J.; Langborg, A.; Minhas, H.S. Biochem. J., 1999, 344, 109.
18. Shinohara, M.; Thornalley, P.J.; Giardino, I.; Beisswenger, P.; Thorpe, S.R.; Onorato J.; Brownlee M. J. Clin. Invest., 1998, 101, 1142.
19. Meade, S.J.; Miller A.G.; Gerrard, J.A. Bioorg. Med. Chem., 2003, 11, 853.
20. Miyata, T.; Ypersele de Strihou, C.; Kurokawa K.; Baynes, J.W. Kidney Int., 1999, 55, 389.
21. Miyata, T. Bull. Mem. Acad. R. Med. Belg., 2002, 157, 189.
22. Sell, D.R.; Monnier, V.M. J. Clin. Invest., 1990, 85, 380.
23. Sell, D.R.; Nagaraj, R.H.; Grandhee, S.K.; Odetti, P.; Lapolla, A.; Fogarty J.; Monnier, V.M. Diabetes Metab. Rev., 1991, 7, 239.
24. Dyer, D.G.; Blackledge, J.A.; Thorpe S.R.; Baynes, J.W. J. Biol. Chem., 1991, 266, 11654.
25. Glomb, M.A.; Monnier, V.M. J. Biol. Chem., 1995, 276, 10017.
26. Wolff, S.P.; Dean, R.T. Biochem. J., 1987, 245, 243.
27. Chellan, P.; Nagaraj, R.H. Arch. Biochem. Biophys., 1999, 368, 98.
28. Brinkmann, E.; Degenhardt, T.P.; Thorpe, S.R.; Baynes, J.W. J. Biol.

Chem. , 1998, 273, 18714.

29. Nagaraj, R.H.; Shipanova, I.N.; Faust, F.M. J. Biol. Chem., 1996, 271, 19338.
30. Dunn, J.A.; McCance, D.R.; Thorpe, S.R.; Lyons, T.J.; Baynes, J.W. Biochemistry, 1991, 30, 1205.
31. Vrdoljak, A.; Trescec, A.; Benko, B.; Hecimovic, D.; Simic, M. Clin. Chim. Acta, 2004, 345, 105
32. Wells-Knecht, K.J.; Zyzak, D.V.; Litchfield, J.E.; Thorpe, S.R.; Baynes, J.W. Biochemistry, 1995, 34, 3702.
33. Dunn, J.A.; Ahmed, M.U.; Murtiashaw, M.H.; Richardson, J.M.; Walla, M.D.; Thorpe, S.R.; Baynes, J.W. Biochemistry, 1990, 29, 10964.
34. Ahmed, M.U.; Thorpe, S.R.; Baynes, J.W. J. Biol. Chem., 1986, 261, 4889.
35. Baynes, J.W.; Thorpe, S.R. Diabetes, 1999, 48, 1.
36. Miyata, T.; Ishikawa, N.; Ypersele de Strihou, C. Clin. Chem. Lab. Med., 2003, 41, 1150.
37. Boel, E.; Selmer, J.; Flodgaard, H.J.; Jensen, T. J. Diabetes Complicat., 1995, 9, 104.
38. Suzuki, K.; Koh, Y.H.; Mizuno, H.; Hamaoka, R.; Taniguchi, N. J. Biochem., 1998, 123, 353.
39. Vander Jagt D.L.; Hassebrook R.K.; Hunsaker, L.A.; Brown, W.M.; Royer, R.E. Chem. Biol. Interact., 2001, 130–132, 549.

40. Szwergold, B.S.; Howell, S.; Beisswenger, P.J. Diabetes, 2001, 50, 2139.
41. Thornalley, P.J. Biochem. J., 1990, 269, 1.
42. Thornalley, P.J. Chem. Biol. Interact., 1998, 111, 137.
43. Westwood, M. E.; Thornalley, P.J. J. Protein Chem., 1995, 14, 359.
44. Schmidt, A.M.; Hori, O.; Brett, J. Arterioscler. Thromb., 1994, 4, 1521.
45. Li, Y.M.; Mitsuhashi, T.; Wojciehowicz, D. Proc. Natl. Acad. Sci., 1996, 93, 11047.
46. Stitt, A.W.; He, C.J.; Vlassara, H. Biochem. Biophys. Res. Comm., 1999, 256, 549.
47. Vlassara, H. Science, 1988, 240, 1546.
48. Kirstein, M.; Aston, C.; Hintz, R.; Vlassara, H.J.; Clin. Invest., 1992, 90, 439.
49. Skolnik, E.Y. J. Exp. Med., 1991, 174, 931.
50. Doi, T. Proc. Natl. Acad. Sci., 1992, 89, 2873.
51. Ahmed, N.; Thornalley, P.J. Ann. NY Acad. Sci., 2005, 1043, 260.
52. Zeng, J.; Davies, M.J. Chem. Res. Toxicol., 2005, 18, 1232.
53. Li., J.; Gobe, G. Nephrology, 2006, 11, 428.
54. Inoguchi, T.; Sonta, T.; Tsubouchi, H.; Etoh, T.; Kakimoto, M.; Sonoda, N.; Sato, N.; Sekiguchi, N.; Kobayashi, K.; Sumimoto, H.; Utsumi, H.; Nawata. H. J. Am. Soc. Nephrol., 2003, 14, S227.
55. Phillips, A.O. Curr. Diab. Rep., 2003, 3, 491.

56. Brownlee, M. Nature, 2000, 414, 813.

57. Schena, F.P.; Gesualdo, L. J. Am. Soc. Nephrol., 2005, 16, S30.

58. Tan, A.l.; Forbes, J.M.; Cooper, M.E. Semin. Nephrol., 2007, 27, 130.

59. Hirai, A.; Yasuda, H.; Joko, M.; Maeda, T.; Kikkawa, R. J. Neurol. Sci., 2000, 172, 55.

60. Yagihashi, S.; Yamagishi, S.I.; Wada, R.; Baba, M.; Hohman, T.C.; Yabe-Nishimura, C. Brain, 2001, 124, 2448.

61. Archer, D.B. Eye, 1999, 13, 497.

62. Stitt, A.W.; Li, Y.M.; Gardiner, T.A. Am. J. Pathol., 1997, 150, 523.

63. Clements, R.S. Jr.; Robison, W.G. Jr.; Cohen, M.P. J. Diabetes Comp., 1998, 12, 28.

64. Bron, A.J.; Vrensen, G.F.; Koretz, J. Intern. J Ophthol., 2000, 214, 86.

65. Farrukh, A.S.; Sharkey, E.; Creighton, D. Exp. Eye. Res., 2000, 70, 369.

66. Chellan, P.; Nagaraj, R.H.; Arch. Biochem. Biophys., 1999, 368, 98.

67. Behl, C.; Davis, J.B.; Lesley, R.; Schubert, D. Cell, 1994, 77, 817.

68. Toth, C.; Martinez, J.; Zochodne, D.W. Curr. Mol. Med., 2007, 7, 766.

69. Münch, G.; Thome, J.; Foley, P.; Schinzel, R.; Riederer, P. Brain Res. Rev., 1997, 23, 134.

70. Reiser, K. M. Proc. Soc. Exp. Biol. Med., 1998, 218, 23.

71. Harding, J.J. Adv. Protein Chem., 1985, 37, 247.

72. Hirsch, J.; Petrakova, E.; Feather, M.S.; Barnes, C.L. Carbohydr. Res., 1995, 267, 17.

73. Hirsch, J.; Petrakova, E.; Feather, M.S. Carbohydr. Res. 1992, 232, 125.
74. Vinson, J. A.; Howard, T.B. J. Nutr. Biochem., 1996, 7, 659.
75. Hud, E.; Cohen, M.P. Clin. Chim. Acta., 1989, 185, 157.
76. Brownlee, M.; Vlassara, H.; Kooney, A.; Ulrich, P.; Cerami, A. Science, 1986, 232, 1629.
77. Brownlee, M Diabetes, 1994, 43, 836.
78. Voziyan, P.A.; Metz, T.O.; Baynes, J.W.; Hudson, B.G J. Biol. Chem., 2002, 277, 3397.
79. Voziyan, P.A.; Hudson, B.G. Cell Mol Life Sci, 2005, 62, 1671.
80. Kass, D.A.; Shapiro, E.P.; Kawaguchi, M.; Capriotti, A.R.; Scuteri, A.; DeGroof, R.C.; Lakatta, E.G. Circulation, 2001, 104, 1464.
81. Vasan, S.; Zhang, X.; Kapurniotu, A.; Bernhagen, J.; Teichberg, S.; Basgen, J.; Wagle, D.; Shih, D.; Terlecky, I.; Bucala, R.; Cerami, A.; Egan J.; Ulrich, P. Nature, 1996, 382, 275.
82. Cameron, N.E.; Cotter, M.A. Diabet. Med., 1993, 10, 593.
83. Seneviratne, C.; Dombi, G.W.; Liu W.; Dain, J.A. J. Inorg. Biochem., 2011, 105, 1548.
84. Seneviratne, C.; Narayanan, R.; Liu W.; Dain, J.A. Biochem. Biophys. Res. Commun., 2012, 422, 447.
85. Rahbar, S.; Figarola, J.L. Arch. Biochem. Biophys., 2003, 419, 63.
86. Basta, G.; Schmidt A.M.; Caterina, R.D. Cardiovasc. Res., 2004, 63, 582.

87. Khalifah, R.G.; Baynes, J.W.; Hudson, B.G. Biochem. Biophys. Res. Commun., 1999, 257, 251.

88. Peng, X.; Ma, J.; Chen, F.; Wang, M. Food Func., 2011, 2, 289.

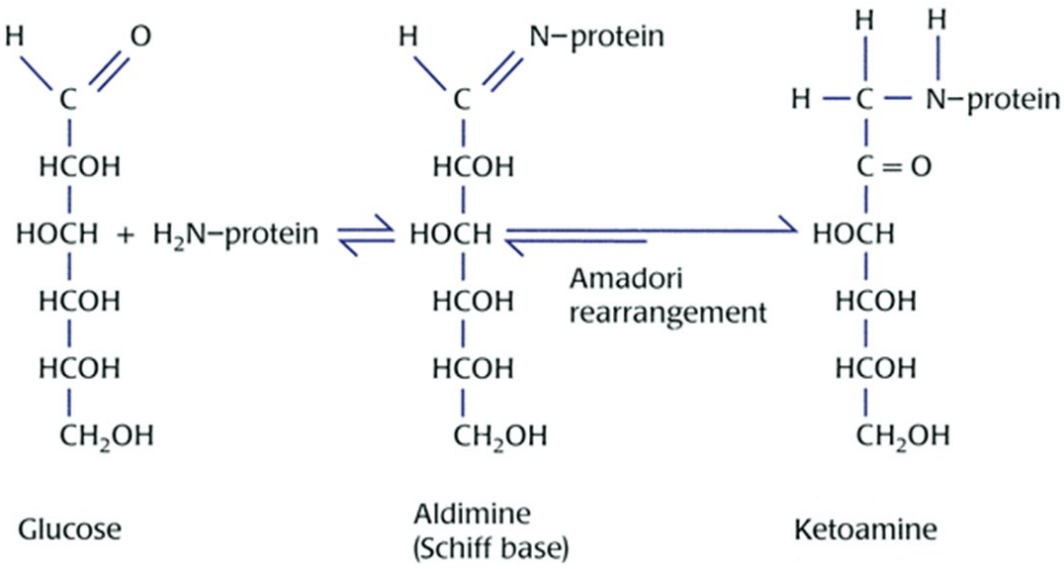

Figure 1. The initial stage of glycation resulting in the formation of a Schiff base and an Amadori product.

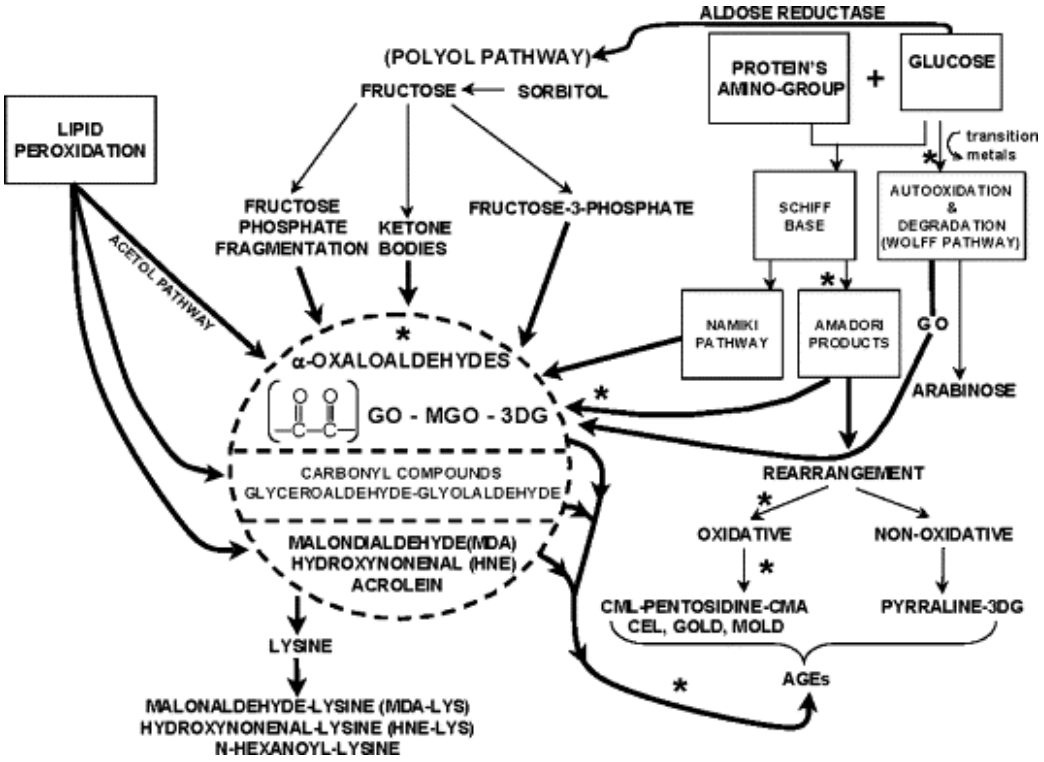

Figure 2. *In vivo* sources of dicarbonyl glycation precursors which are responsible for the formation of AGEs and carbonyl stress (85).

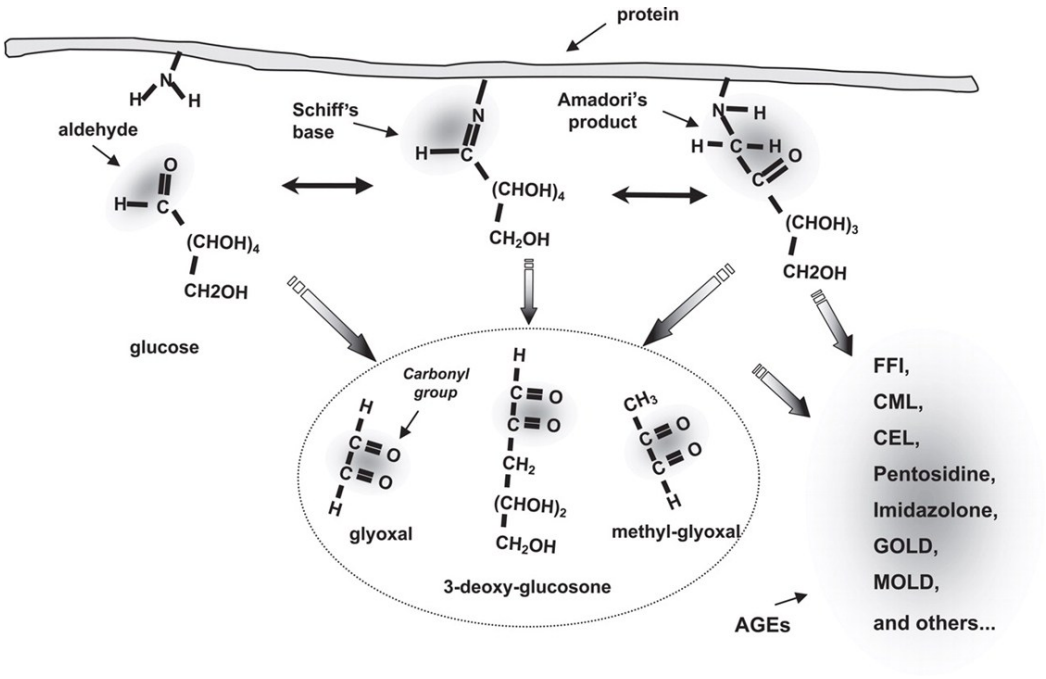

Figure 3. Chemical structures of currently well-defined AGE dicarbonyl precursors (glyoxal, 3-deoxy-glucosone and methylglyoxal), and their interactions with glycated proteins (86).

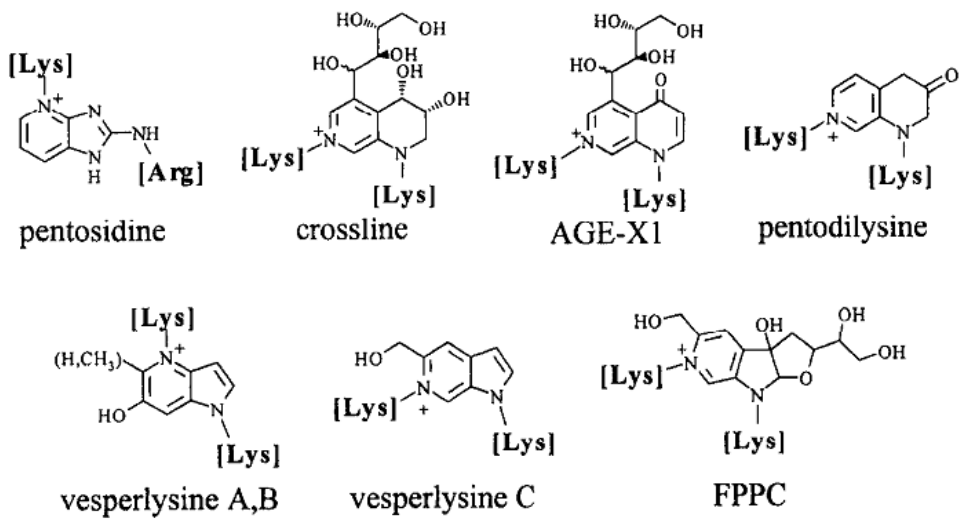

Figure 4. AGE crosslink structures formed under physiological condition which exhibit fluorescence absorbance. [Lys] indicates to lysine residue and [Arg] indicates to arginine (5).

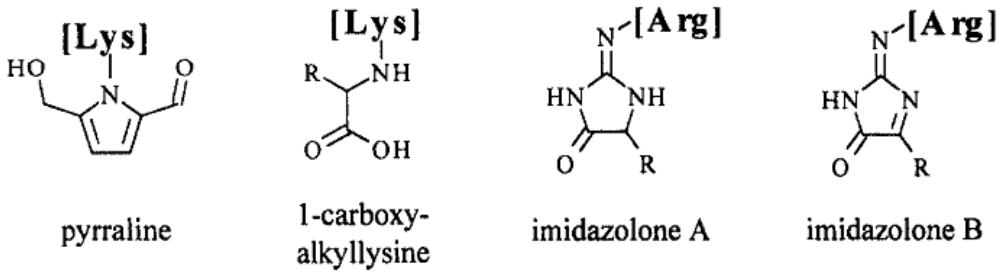

Figure 5. Chemical structures of some of the most important and well-studied non-crosslinking AGEs including pyrraline, 1-carboxyalkyl lysine and imidazolone A and B. [Lys] indicates to lysine residue and [Arg] indicates to arginine (5).

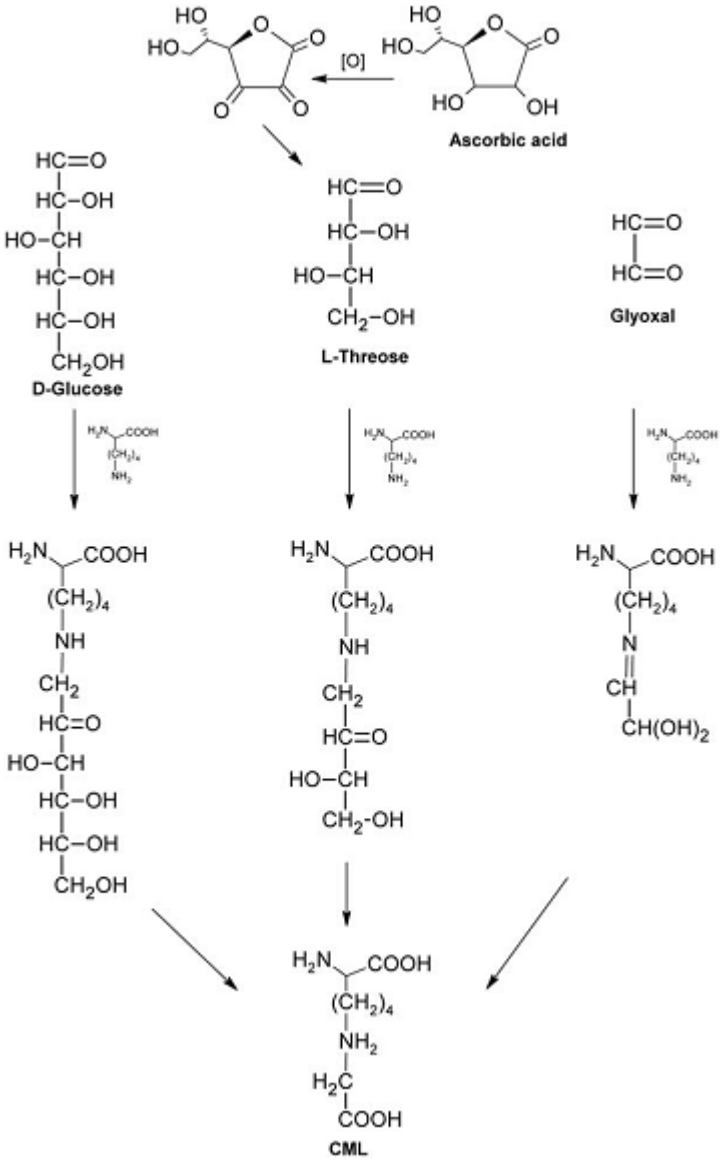

Figure 6. Pathways for the formation of N^{ε}-carboxymethyl lysine *in vivo* (87).

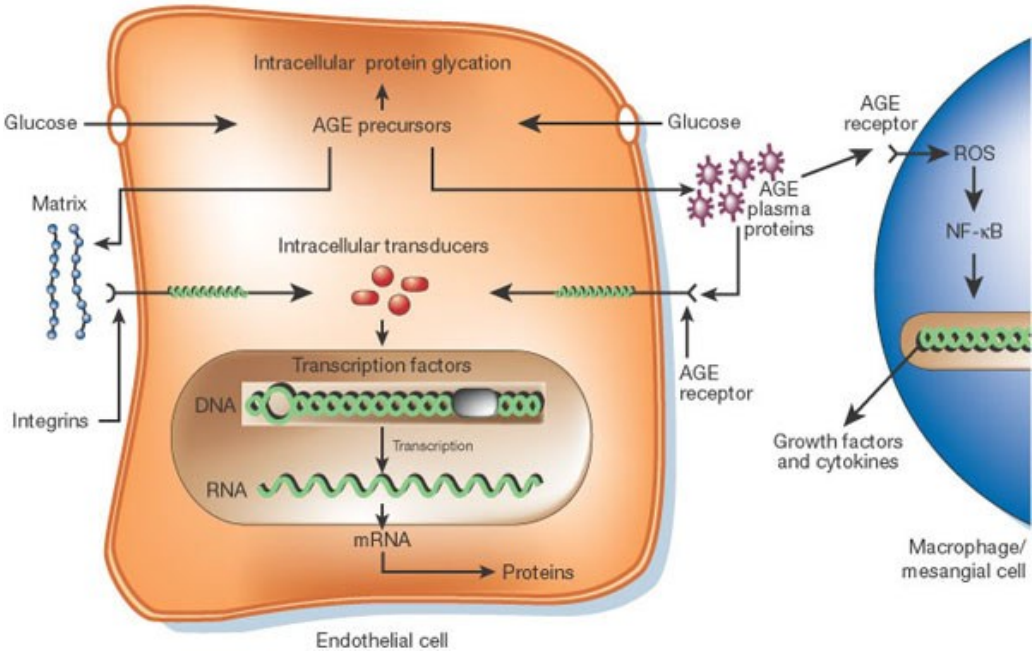

Figure 7. Intracellular accumulation of AGEs damages target cells through receptor-mediated pathway, in which the glycated plasma proteins bind to AGE receptors on cell surface, inducing cell signaling and oxidation stress (56).

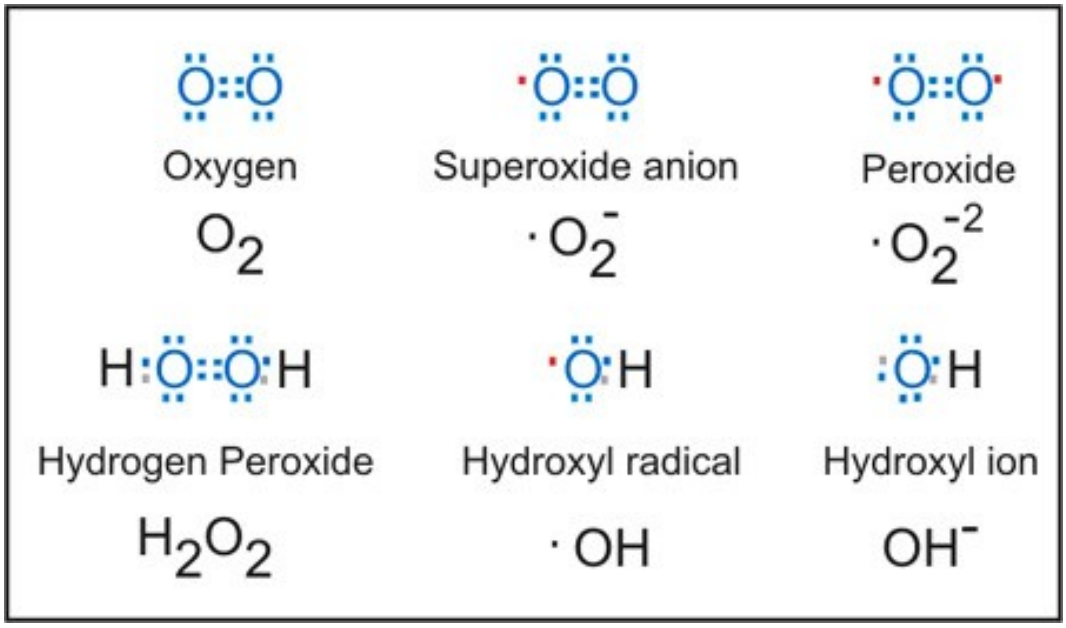

Figure 8. Structures of reactive oxygen species (ROS).

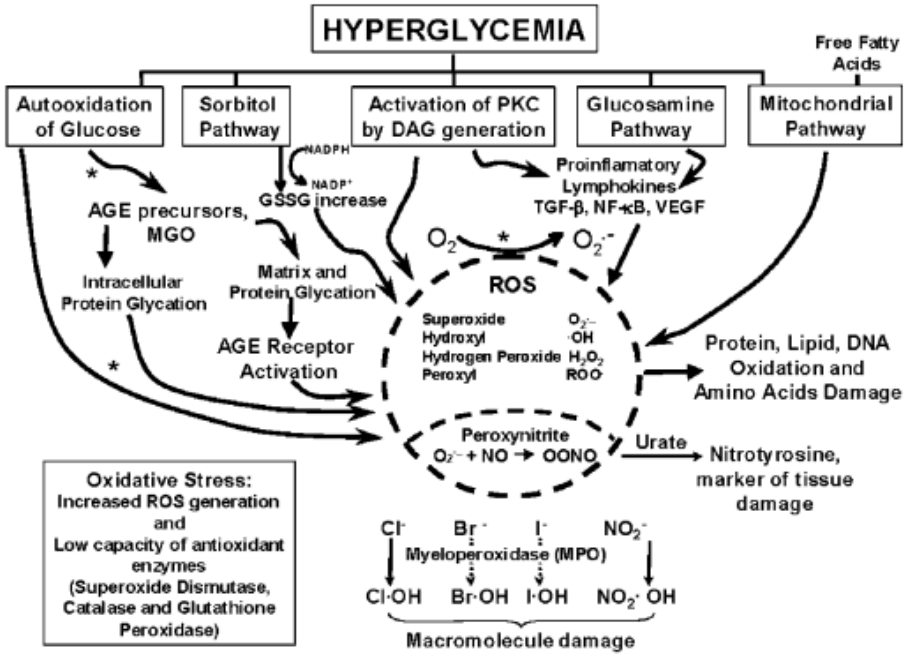

Figure 9. Pathways for the generation of ROS which lead to oxidative stress (85).

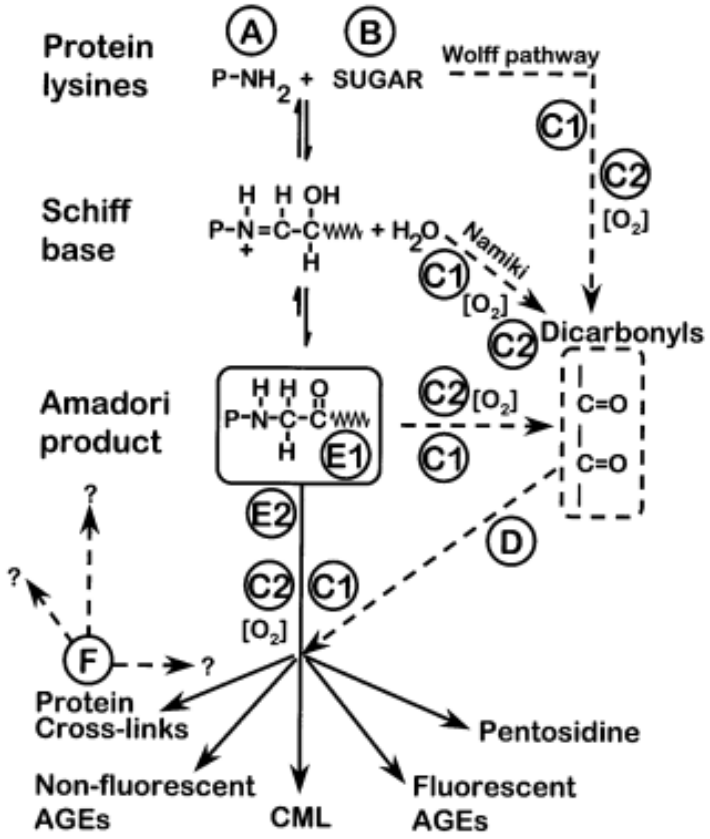

Figure 10. Schematic of *in vivo* glycation reactions and common targets for AGE inhibition in the pathways (87).

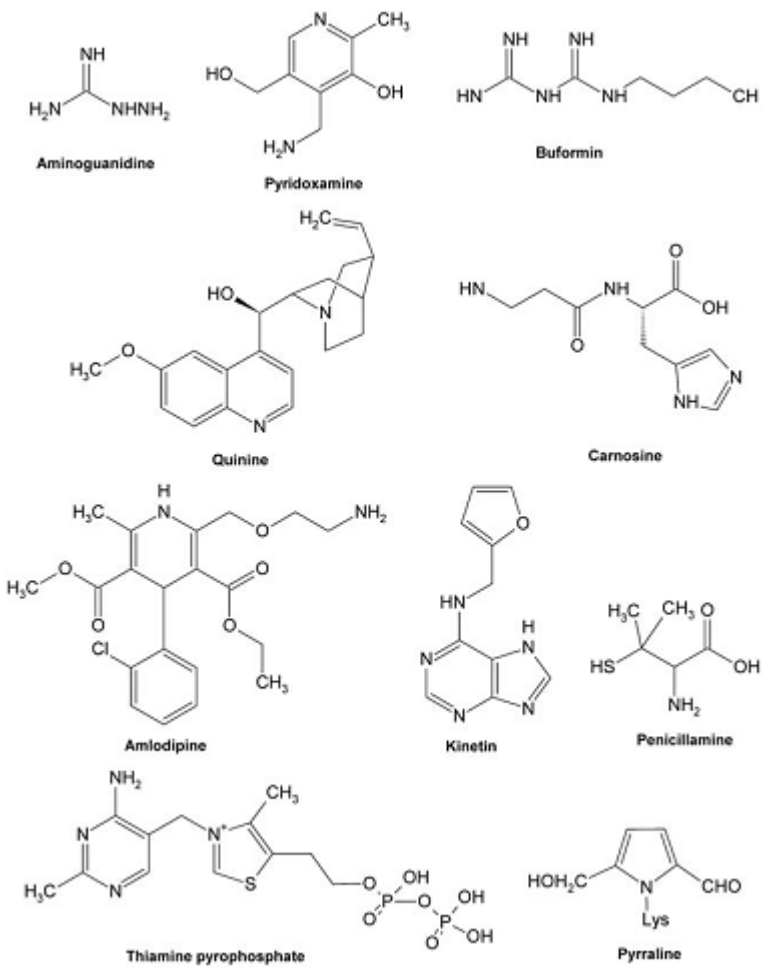

Figure 11. Structures of some synthetic anti-glycation agents which act as dicarbonyl compound scavengers (88).

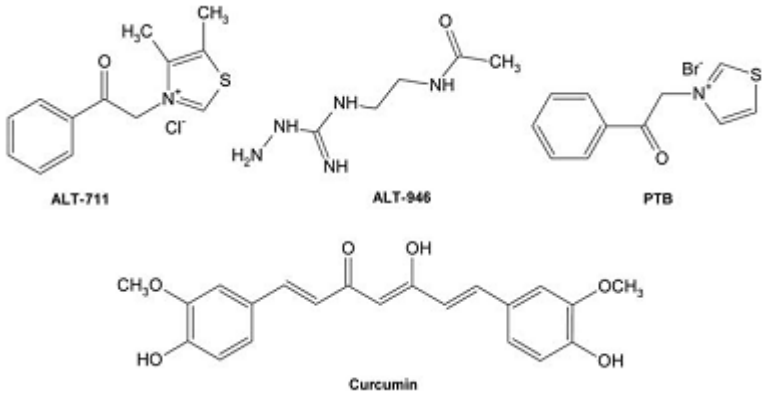

Figure 12. Structures of some typical AGE breakers which reduce the damage of glycation (88).

Manuscript 2

Accepted by Bioorganic Chemistry in September, 2012

Non-Enzymatic Glycation of Melamine with Sugars and Sugar like Compounds

Weixi Liu [1], Menashi A. Cohenford [2], Leslie Frost [3], Champika Seneviratne [1], Joel A. Dain [1*]

[1] Department of Chemistry, University of RI, Kingston, RI 02881
[2] Department of Integrated Science and Technology, Marshall University, Huntington, WV 25755
[3] Department of Chemistry, Marshall University, Huntington, WV 25755

E-mail address: wliu@chm.uri.edu (Weixi Liu).
E-mail address: cohenford@marshall.edu (Menashi A. Cohenford).
E-mail address: frost@marshall.edu (Frost Leslie)
E-mail address: pseneviratne@chm.uri.edu (Champika Seneviratne)
*Corresponding author: Phone: + 1-401-874-5942; fax: + 1-401-874-5072
E-mail address: jdain@chm.uri.edu (Joel A. Dain).

Abstract

Melamine (1,3,5-triazine-2,4,6-triamine) is employed in the manufacture of plastics, laminates and glues, yet, it has been found sometimes added illegally to dairy products to artificially inflate foods' protein content. In 2008, dairy products adulterated with melamine were blamed for the death of several infants in China, a situation that forced Beijing to introduce stricter food safety measures. The objectives of this study were threefold: 1) to investigate, using UV and fluorescence spectrometry, the susceptibility of the amine groups of melamine to glycation with D-galactose, D-glucose and lactose, sugars commonly found in milk, 2) to study the rate and extent of melamine's glycation with methylglyoxal, glyoxal and DL-glyceraldehyde, three highly reactive metabolites of D-galactose, D-glucose and lactose, and 3) to characterize, using HPLC and mass spectrometry, the Advanced Glycation Endproducts (AGEs) of melamine with sugars found commonly in milk and their metabolites. Incubation of D-galactose, D-glucose and lactose with melamine revealed that D-galactose was the most potent glycator of melamine, followed by D-glucose, then lactose. Methylglyoxal, glyoxal, and DL-glyceraldehyde glycated melamine more extensively than D-galactose, with each yielding a broader range of AGEs. The nonenzymatic modification of melamine by sugars and sugar-like

compounds warrants further investigation, as this process may influence melamine's toxicity *in vivo*.

Keywords: melamine; glycation; D-galactose; methylglyoxal; AGEs

1.0. Introduction

In 2008, many dairy products in China were found to be adulterated with the chemical melamine, a situation that contributed to the death and hospitalization of children and a massive recall of many food products (1 - 5). The adulteration of food products with melamine unfortunately continues to this day in China, despite the government's ongoing efforts to halt this practice.

Melamine is an organic base with a 1,3,5-triazine backbone. That is essentially a trimer of cyanamide with three amino groups attached to its hexagonal structure (see figure 1). The three amino groups suggest that melamine should be a target for nonenzymatic glycation by the Maillard reaction.

The Maillard reaction is a non-enzymatic browning reaction that involves a series of steps with the reactants typically including a reducing sugar and a protein. In the initial phase of the Maillard reaction, the carbonyl group of the reducing carbohydrate condenses with the free amino groups on the protein to form reversible glycosylamines, which are then converted to more stable

Amadori products. Once formed, these Amadori products can with time undergo dehydration, cyclization, oxidation, and rearrangement to form a polymorphic group of compounds collectively referred to as Advanced Glycation Endproducts (AGEs) (6 - 8).

Ever since its description in 1912, the Maillard reaction has continued to be a topic of research interest. One reason for this focus on the Maillard reaction is that it cuts across several disciplines with nutrition science and medicine serving as examples. For researchers in nutrition science, harnessing the Maillard reaction has allowed for control of food flavor, food aroma, food coloring, and food texture (9 - 10). For researchers in clinical medicine exploring the Maillard reaction has meant gaining a deeper insight into the biochemistry of diabetes and its chronic complications including renal failure, cataract formation and atherosclerosis (11 - 13).

Studies in our laboratory and those of others have shown that AGEs can form both in vitro and in vivo, and that besides proteins can involve other free amino containing molecules such as DNA, RNA, lipids, amino acids and amino sugars (14 - 17). The objectives of this study were three fold: first, to determine if melamine can be glycated by by D-galactose, D-glucose and lactose, three sugars that are present in milk; second, to compare the glycation levels of melamine with D-galactose, D-glucose and lactose; third, to determine if melamine can nonenzymatically react with methylglyoxal,

glyoxal and DL-glyceraldehyde, three highly reactive metabolic products of D-galactose, D-glucose and lactose (15; 18 - 21).

In this report, we show that melamine is susceptible to glycation by D-galactose and demonstrate the ability of melamine to form AGEs. We also describe the nonenzymatic glycation of melamine with methylglyoxal, glyoxal, and DL-glyceraldehyde, the three more reactive metabolites of milk sugars. Emphasis is also placed on the characterization of the AGEs of melamine by HPLC, UV, fluorescence and mass spectrometry.

2 Materials and methods

2.1 Chemicals and supplies

Analytical grade D-galactose, D-glucose, lactose, glyoxal, methylglyoxal, DL-glyceraldehyde and melamine were purchased from Sigma Chemical Co. (St. Louis, MO). Disposable UV-transparent cuvettes (12.5 mm X12.5 mm X 36 mm) and HPLC analytical grade solvents were obtained from Thermo Fisher Scientific (Rockford, IL). Reverse phase HPLC columns containing C_8 silica resins were obtained from Agilent Technologies (Chelmsford, MA) with all other HPLC supplies from Phenomenex (Torrance, CA).

2.2 Preparation of reaction mixtures

2.2.1 *Reaction of lactose, D-glucose and D-galactose (milk sugars) with melamine:* Stock solutions of melamine (5 mM) and sugar (300 mM) were prepared in 0.1 M phosphate buffer, pH 6.7. Final incubation mixtures included variable amounts of melamine (0.2, 1, or 2.5 mM) with a set concentration of D-glucose, D-galactose or lactose (150 mM). Blanks included melamine alone (0.2, 1 or 2.5 mM) or sugar alone (lactose, D-glucose or D-galactose) each at a final concentration of 150 mM. Freshly mixed sugars with melamine served as the control solutions. All reaction mixtures and blanks were incubated in the dark in a shaking water bath for 2 hours at variable temperatures (40 °C, 50 °C, 60 °C, 70 °C, 80 °C and 90 °C). After incubation, samples were placed at -20 °C until analyzed.

2.2.2 *Reaction of methylglyoxal, glyoxal and DL-glyceraldehyde with melamine:* Unless otherwise indicated, all reactions were conducted in 0.2 M phosphate buffer, pH 7.2, containing 0.02% sodium azide. Stock solutions of melamine (5 mM), methyglyoxal (40 mM), glyoxal (40 mM) and DL-glyceraldehyde (40 mM) were prepared by separately dissolving each in the 0.2 M phosphate buffer. Final incubation mixtures included variable amounts of methylglyoxal, glyoxal or DL-glyceraldehyde (5 or 20 mM) with different concentrations of melamine (0.2, 1, or 2.5 mM). Blank solutions included methylglyoxal, glyoxal or glyceraldehyde alone (5 mM or 20

mM), or melamine alone (0.2 mM, 1 mM or 2.5 mM). Controls included non-incubated freshly mixed solutions of each aldehyde (methylglyoxal, glyoxal or DL-glyceraldehyde) with melamine. All reaction mixtures and blank solutions were incubated in the dark at 37 °C in a shaking water bath for 30 days. After incubation, samples were placed at -20 °C until analyzed.

2.3 UV and fluorescence spectroscopy

UV readings were obtained at a wavelength of 240 nm with an UltroSpec 2100 instrument (Biochrom Ltd, Cambridge, UK). Fluorescence measurements were made at respective excitation and emission wavelengths of 260 nm and 380 nm using a Spectra Max M2 spectrometer (Molecular Devices, Sunnyvale, CA). All readings were obtained in thermostatically controlled cuvettes that were maintained at 25±1 °C. The above excitation and emission wavelengths were determined optimal for detecting melamine AGEs.

2.4 High-performance liquid chromatography

Each HPLC run was performed in triplicate using a Hitachi system (San Jose, CA, USA) equipped with a low-pressure gradient pump (L-2130), a four-channel degasser, a sequential auto sampler (L-2200), and a high sensitivity diode-array detector (190–800 nm) (L-2455). AGE species were

separated on a C_8 reverse phase HPLC column (5 µm×4.6 mm×150 mm) and monitored at 240 nm. Mobile phase consisted of a 92% solution of 10 mM citrate heptane sulfonate buffer, pH 3.0 and 8% acetonitrile. An isocratic condition was applied for 15 min at a constant flow rate of 1.00 ml min^{-1}. Prior to HPLC analysis, all solvents were filtered with a 0.45 µm membrane (Millipore, Billerica, MA, USA), degassed for 15 min, and centrifuged.

2.5 Mass spectrometry

Mass spectrometry studies were performed on a ThermoFinnigan LCQ mass spectrometer (ThermoScientific, Waltham, MA) equipped with an electrospray ionization source and a quadrupole ion trap mass analyzer. Samples were diluted into a solvent consisting of 50/50 (v/v) 0.1% acetic acid in water/acetonitrile and directly infused into the electrospray source using a capillary syringe pump at a flow rate of 3 µL min^{-1}. Nitrogen was used as the sheath gas (setting at 60), and ultrapure helium was used as the collision gas. The ion spray voltage was set as 4.5 kV and the capillary temperature was 210 °C. The mass spectrometer was set to function in the positive ion mode with parameters optimized during direct infusion of caffeine standards with solvent. Samples were analyzed by MS and tandem mass spectrometry (CID fragmentation with Helium) favoring isolation and fragmentation of singly charged ions. The ESI/MS system was operated

with the Xcalibur software (version 2.0, ThermoFinnigan), with the same software used also for data analysis.

3 Results

Figure 2a and 2b show the time course of melamine's glycation with D-glucose, D-galactose and D-lactose under temperature and pH conditions employed in the manufacture of powdered milk products. The amounts of D-glucose, D-galactose and lactose were adjusted to actual concentrations of the sugars in unprocessed milk and lactose free milk formulas [22]. At pH 6.7 and 80 °C for 120 min, D-glucose and D-lactose were found to be poor glycators of melamine yielding UV and fluorescence spectral profiles that were nearly superimposable. Under equivalent incubation conditions, mixtures of D-galactose and melamine yielded higher fluorescence readings demonstrating that relative to D-glucose and D-lactose, D-galactose was a more effective glycator of melamine. As expected, the blank solutions and controls yielded no changes in their fluorescence, confirming that for glycation to occur, both sugar and melamine had to be in the same reaction mixture and incubated over time.

The pronounced reactivity of D-galactose relative to D-glucose may be explained by the enhanced general instability of the hemiacetal ring of D-galactose, which in solution renders the molecule more prone to an open-chain configuration [23, 24]. Thus, with a higher percentage of the

sugar existing in an open ring structure than D-glucose, D-galactose becomes more vulnerable to nucleophilic attack by the amino groups on melamine [23, 24]. This phenomenon may also explain galactose's higher reactivity than D-lactose since as a disaccharide, lactose contains D-glucose at it reducing end.

Figures 3A, 3B and 3C display the respective HPLC elution profiles of mixtures of melamine incubated with D-galactose, D-glucose and lactose at 80 °C for 1 hour. Figure 3D shows the HPLC elution profiles of solutions containing melamine alone (blank), and melamine freshly added to D-galactose, D-glucose or D-lactose (controls). Melamine alone eluted as one prominent peak with a retention time (R_t) of 7.40 min. Each of the control mixtures yielded an elution profile identical to the blank, showing one peak coincident to where melamine eluted (R_t 7.40 min).

The HPLC chromatograms in figures 3A to 3D revealed two important things: 1) that glycation was a time dependent process requiring the presence of both melamine and sugar, and 2) that D-galactose was a more potent glycator of melamine than D-glucose and D-lactose, a finding consistent with the fluorescence data in figure 2. Incubation mixtures of D-galactose with melamine yielded three distinct AGE products by HPLC. Of the bands corresponding to the AGE products, one eluted with a retention time of 3.85 min, one at 4.49 min and one at 5.08 min (figure 3A). A fourth band appearing at a retention time of 7.40 min corresponded to the

fraction of melamine that did not condense with D-galactose. Integration of the band areas revealed that with D-galactose as the glycating sugar 32.1% of melamine was nonenzymatically modified; i.e., in contrast to 12.3% with D-glucose and 6.3% with D-lactose. Other results revealed that reducing the incubation temperatures, reduced the extent glycation of melamine and the number of AGEs of melamine in the reaction mixtures. Figures 4A, 4B and 4C exemplify this behavior with D-galactose as the model glycating agent.

Tables I displays the changes in UV absorption readings of incubation mixtures of melamine with methylglyoxal, glyoxal and DL-glyceraldehyde (hereon referred to as “aldehydes”) at 37 °C covering different time intervals. Increasing incubation time enhanced the AGE formation of melamine with the highest levels of glycation achieved when aldehyde concentrations were adjusted to 20 mM. A close scrutiny of the table confirmed the earlier observations that the extent glycation of melamine was a time dependent process relatable to the chemistry and concentration of the aldehydes in the incubation mixtures. Increases in the aldehyde concentrations prompted AGE formation, with methylglyoxal yielding the highest UV absorbing products followed by glyoxal then DL-glyceraldehyde (figures 5a and 5b). Increases in melamine concentration in the presence of set amounts of the various aldehydes also promoted AGE formation, demonstrating that the rate of glycation reaction was dependent on both the concentrations of melamine and the various aldehydes (data not shown). Using variable

amounts of melamine in the incubation mixtures had no effect on the intensity order of the glycated compounds that were formed with methylglyoxal and DL-glyceraldehyde, once again, producing AGEs with the highest and lowest UV intensities, respectively.

Table II and figures 6A, B and C show the HPLC retention times of the various AGEs of melamine with methylglyoxal, glyoxal and DL-glyceraldehyde at 37 °C over 30 days. Included in Table II is also the number of AGE products and their percent amount relative to the total AGEs in each incubation mixture over time. The band eluting at retention time 7.4 min was assigned to nonglycated melamine; an observation based on the HPLC elution profiles of both the blank and control solutions (figure 6D). Analysis of the data in Table II showed that with methylglyoxal there were more AGE products formed than with glyoxal and DL-glyceraldehyde, with DL-glyceraldehyde yielding the lowest number of AGEs. A further evaluation of the results in Table II revealed that glyoxal was the most active glycator of melamine followed by methyglyoxal then DL-glyceraldehyde (figure 7).

Figures 8 shows the mass spectral profiles of 2.5 mM melamine incubated with 20 mM methylglyoxal at 37 °C for 30 days. Mass spectral analysis of melamine alone yielded one primary peak located at m/z 127 (data not shown). In reaction tubes containing melamine and methylglyoxal, the main product ions were at m/z 199, 271, and 343. The product with m/z 199

corresponded to the addition of one methylglyoxal monomer (∆ m/z 72) to melamine, whereas those with m/z 271 and 343 corresponded to the condensation of two and three monomers.

Figure 9a-c show the CID mass spectrum for methylglyoxal's primary product ion at m/z 199 (figure 9a), 271(figure 9b) and 343 (figure 9b) with the main fragmentation pattern revealing a loss in water (-18 Da) and a loss in CO (-28 Da). The absence of a peak at m/z 155 indicated that no carboxylic acid functional group was present. This conclusion was further supported by the absence of a peak at m/z 197 after repeated analysis of the sample in the negative ion mode. The product ion at m/z 199 appears to contain a hemiaminal structure without loss of water forming a Schiff base at pH 7.2.

For the reaction with 20 mM glyoxal (figure 10), a prominent peak at m/z 185 was observed. This ion corresponded to the addition of one glyoxal monomer (Δ m/z 58) to melamine. Figure 11a shows the CID mass spectrum for glyoxal product ion at m/z 185 with the main fragmentation pattern, again, showing a loss in water (-18 Da), and a loss in CO (-28 Da). This suggests that the reaction of melamine with glyoxal was similar to that of methylglyoxal in forming a hemiaminal structure.

In contrast to glyoxal and methylglyoxal, glyceraldehyde condensed with melamine through a Schiff base/Amadori reaction, forming a product ion at

m/z 199 (figure 12). The mass spectrometric profile of D-galactose with melamine was more difficult to interpret (figure 14); however, the product ion at m/z 289 suggested the occurrence of Schiff base formation between the anomeric carbon of D-galactose with one of the amino groups of melamine. This result was confirmed by CID fragmentation of the product ion at 289 (figure 15a). The additional ions indicated that more than one D-galactose monomer could have condensed with melamine with the latter then rearranging to yield multiple products.

Figures 16A thru 10D display the proposed structures consistent with the mass spectral data for the primary products formed in incubation mixtures containing melamine with methylglyoxal, glyoxal, DL-glyceraldehyde and D-galactose. A detailed analysis of the predominant product ions generated from the reaction of melamine with methylglyoxal (figure 8) leads to the postulated mechanism pathway for the formation of AGEs seen in Figure 17. It should be noted that a portion of the signal for ion at m/z 181 in the mass spectrum (figure 8) could be arising from the dehydration of the ion at m/z 199 in the electrospray source.

Other findings revealed that increases in pH promoted melamine AGEs with D-galactose and methylglyoxal (figure 18). This effect of pH on the glycation of melamine was not surprising since increases in pH have been shown to promote Schiff base formation (15 - 16).

4 Discussion

Melamine is a chemical that has been employed in the manufacture of adhesives, laminates, plastics, floor tiles, kitchenware, and commercial filters. Yet, it has been also used as an additive to artificially boost a food's protein content, creating a lucrative market for edibles believed to be of nutritious value. The deliberate adulteration of foods with melamine would not have surfaced, if it wasn't for the recent events of 2007 and 2008. In 2007, there was an outbreak of acute renal failure in cats and dogs in the United States that resulted in the death of hundreds of animals across the country (25). Investigations into the etiology of the outbreak traced the problem to gluten, an ingredient in pet foods exported from China found contaminated with 'scrap melamine' (26 - 27). 'Scrap melamine' is a byproduct of melamine industry that in addition to melamine contains variable amounts of cyanuric acid including different oxytriazines (28). Melamine alone has been shown to cause no or little toxicity in animals (29 - 30); however, when combined with cyanuric acid, the two chemicals can trigger the formation of kidney stones which ultimately leads to renal failure (29 - 31).

In 2008, the melamine crisis expanded from a pet problem to a human problem when 'scrap melamine' was discovered in infant's formulas, powdered milk and other dairy products; blamed for the sickening of

countless children and the death of at least several infants in China (1; 3; 32). The melamine contamination was also found in non-dairy food products made in China such as candies, egg products and non-dairy creamers, some of which have been exported to other countries (29; 31 - 32). The deliberate adulteration of edibles with melamine caused an unprecedented hysteria throughout China forcing Beijing to adopt stricter food safety regulations and to step up inspection of its dairy industry. The crisis of 2008 also triggered urgency for new standards to be set for tolerable daily levels of melamine. For instance, in the US, the FDA has now set the limit from 0.63mg to 0.063 mg per kg of body mass, whereas in Europe the limit now stands at 0.2 mg (2; 29; 31).

Melamine is rich in nitrogen and contains three amino groups which form part of its hexagonal structure (figure1). These amino groups make melamine a target for glycation as we have shown here in this study. Our work with melamine revealed four important findings. First, it demonstrated that melamine can non-enzymatically react with sugars most abundant in milk and their metabolites. Second, it revealed that glycated products of melamine can with time form AGEs that could be readily resolvable by HPLC. Third, the observation was made that not all sugars and aldoses reacted at the same rate and extent with melamine and that increased temperatures and pH accelerated AGE formation. Lastly, mass spectrometric data revealed that glycation of melamine occurred via the

Amadori pathway yielding different AGE products with methylglyoxal, glyoxal, DL-glyceraldehyde and D-galactose.

At present, there is little information on the long term toxicity of melamine and human consumption, and there is practically no data on the toxicity of glycated melamine in vivo. The high reactivity of melamine with milk sugar metabolites suggests that the immediate and long term toxicity of melamine may not only be related to its interactions with cyanuric acid, but may be caused also by its Maillard products.

Acknowledgment

This research was made possible by the use of Research and Bioinformatics Core Facilities supported jointly by NCRR/NIH Grant # P20 RR016457 and the Network institutions.

References:

1. N. Guan, Q. Fan, J. Ding, Y. Zhao, J. Lu, Y. Ai, G. Xu, S. Zhu, C. Yao, L. Jiang, J. Miao, H. Zhang, D. Zhao, X. Liu, Y. Yao, Melamine-contaminated powdered formula and urolithiasis in young children, N. Engl. J. Med. 360 (2009) 1067-1074.

2. M. Rambla-Alegre, J. Peris-Vicente, S. Marco-Peiró, B. Beltrán-Martinavarro, J. Esteve-Romero, Development of an analytical methodology to quantify melamine in milk using micellar liquid chromatography and validation according to EU Regulation 2002/654/EC, Talanta 81 (2010) 894–900.

3. L. Zhang, L. Wu, Y. Wang, A. Liu, C. Zou, Z. Zhao, Melamine-contaminated milk products induced urinary tract calculi in children, World J. Pediatr. 5 (2009) 31–35.

4. G. Huang, Z. Ouyang, R.G. Cooks, High-throughput trace melamine analysis in complex mixtures, Chem. Comm. 5 (2009) 556.

5. J.R. Ingelfinger, Melamine and the global implications of food contamination, N. Engl. J. Med. 359 (2008) 2745-2748.

6. J. DeGroot, The AGE of the matrix: chemistry, consequence and cure, Curr. Opin. Pharmacol. 4 (2004) 301-305.

7. C.I. Neglia, H.J. Cohen, A.R. Garber, P.D. Ellis, S.R. Thorpe, J.W. Baynes, 13C NMR investigation of nonenzymatic glucosylationof protein: Model studies using RNase A, J. Biol. Chem. 258 (1983) 14279-14283.

8. A.J. Furth, Glycated proteins in diabetes, Br. J. Biomed. Sci. 54 (1997) 192–200.

9. J.A. Gerrard, The Maillard reaction in food – challenges ahead, Trends Food Sci. Technol. 17 (2006) 324–330.

10. S.Lertsiri, R.Maungma, A. Assavanig, A. Bhumiratana, Roles of the Maillard reaction in browning during moromi process of Thai soy sauce, J. Food Process. Preserv. 25 (2001) 149–162.

11. J. Uribarri, M. Peppa, W. Cai, T. Goldberg, M. Lu, C. He, H. Vlassara, Restriction of dietary glycotoxins reduces excessive advanced glycation end products in renal failure patients, J. Am. Soc. Nephrol. 14 (2003) 728-731.

12. P. Ulrich, A. Cerami, Protein glycation, diabetes, and aging, Recent Prog. Horm. Res. 56 (2001) 1-21.

13. P.J. Thornalley, Measurement of protein glycation, glycated peptides, and glycation free adducts, Periton. Dialysis Int. 25 (2005) 522-533.

14. U. Dutta, M.A. Cohenford, M. Guha, J.A. Dain, In vitro nonenzymatic glycation of DNA nucleobases: an evaluation of advanced glycation end

products under alkaline pH, Anal. Bioanal. Chem. 386 (2006) 1633–1640.

15. Y. Li, M.A. Cohenford, U. Dutta, J.A. Dain, The structural modification of DNA nucleosides by nonenzymatic glycation: an in vitro study based on the reactions of glyoxal and methylglyoxal with 2'-deoxyguanosine, Anal. Bioanal. Chem. 390 (2008) 679–688.

16. Y. Li, U. Dutta, M.A. Cohenford, J.A. Dain, Nonenzymatic glycation of guanosine 5'-triphosphate by glyceraldehyde: An in vitro study of AGE formation, Bioorg. Chem. 35 (2007) 417–429.

17. X. Fan, J. Zhang, M. Theves, C. Strauch, I. Nemet, X. Liu, J. Qian, F.J. Giblin, V.M. Monnier, Mechanism of lysine oxidation in human lens crystallins during aging and in diabetes, J. Biol. Chem. 284 (2009) 34618-34627.

18. P.F.G. De Sa, J.M. Treubig Jr, P.R. Brown, J.A. Dain, The use of capillary electrophoresis to monitor Maillard reaction products (MRP) by glyceraldehydes and the epsilon amino group of lysine, Food Chem. 72 (2001) 379–384.

19. U. Dutta, M.A. Cohenford, J.A. Dain, Nonenzymatic glycation of DNA nucleosides with reducing sugars, Anal. Biochem. 345 (2005) 171–180.

20. M.P. Kalapos, Methylglyoxal and glucose metabolism: a historical perspective and future avenues for research, Drug Metabol. Drug Interact. 23 (2008) 69-91.

21. P.J. Thornalley, Glycation in diabetic neuropathy: characteristics, consequences, causes, and therapeutic options, Int. Rev. Neurobiol. 50 (2002) 37-57.

22. V. Rajendran, J. Irudayaraj, Detection of glucose, galactose, and gactose in milk with a microdialysis-coupled flow injection amperometric sensor, J. Dairy Science 85 (2002) 1357–1361.

23. L.D. Hayward, S.J. Angyal, Circular-dichroism of reducing sugars .1. symmetry rule for circular-dichroism of reducing sugars, and proportion of carbonyl forms in aqueous-solutions thereof, Carbohydr. Res. 53 (1977) 13-20.

24. R.B. Kelly, A relationship between the conformations of cyclohexane derivatives and their physical properties, Can. J. Chem. 35 (1957) 149-158.

25. R. L. M. Dobson, S. Motlagh, M. Quijano, R.T. Cambron, T.R. Baker, A.M. Pullen, B.T. Regg, A.S. Bigalow-Kern, T. Vennard, A. Fix, R. Reimschuessel, G. Overmann, Y. Shan, G.P. Daston, Identification and characterization of toxicity of contaminants in pet, Toxicol. Sci. 106 (2008) 251–262.

26. M. Lin, L. He, J. Awika, L. Yang, D.R. Ledoux, H. Li, A. Mustapha, Detection of melamine in gluten, chicken feed, and processed foods using surface enhanced Raman spectroscopy and HPLC, J. Food Sci. 73 (2008) T129–T134.

27. Pet Food Industry Association, What's behind the pet food scandal? Food Rev. 34 (2007) 44.

28. K. Burns, Events leading to the major recall of pet foods, J. Am. Vet. Med. Assoc. 230 (2007) 1600-20.

29. C.M.E. Gossner, J. Schlundt, P.B. Embarek, S. Hird, D. Lo-Fo-Wong, J.J.O. Beltran, Keng Ngee Teoh, A. Tritscher, The melamine incident: implications for international food and feed safety, Environ. Health Perspect. 117 (2009) 1803–1808.

30. H.D. Heck, R.W. Tyl, The induction of bladder stones by terephthalic acid, dimethyl terephthalate, and melamine (2,4,6-triamino-s-triazine) and its relevance to risk assessment, Regul. Toxicol. Pharmacol. 5 (1985) 294–313.

31. Y. Tyan, M. Yang, S. Jong, C. Wang, J. Shiea, Melamine contamination, Anal. Bioanal. Chem. 395 (2009) 729–735.

32. Anon, Lessons from the Chinese melamine milk catastrophe, Int. Food Hyg. 19 (2008) 5, 7.

List of figures:

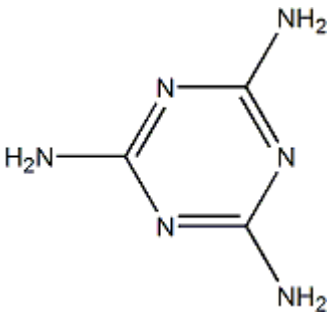

Figure 1. Chemical structure of melamine (1,3,5-triazine-2,4,6-triamine).

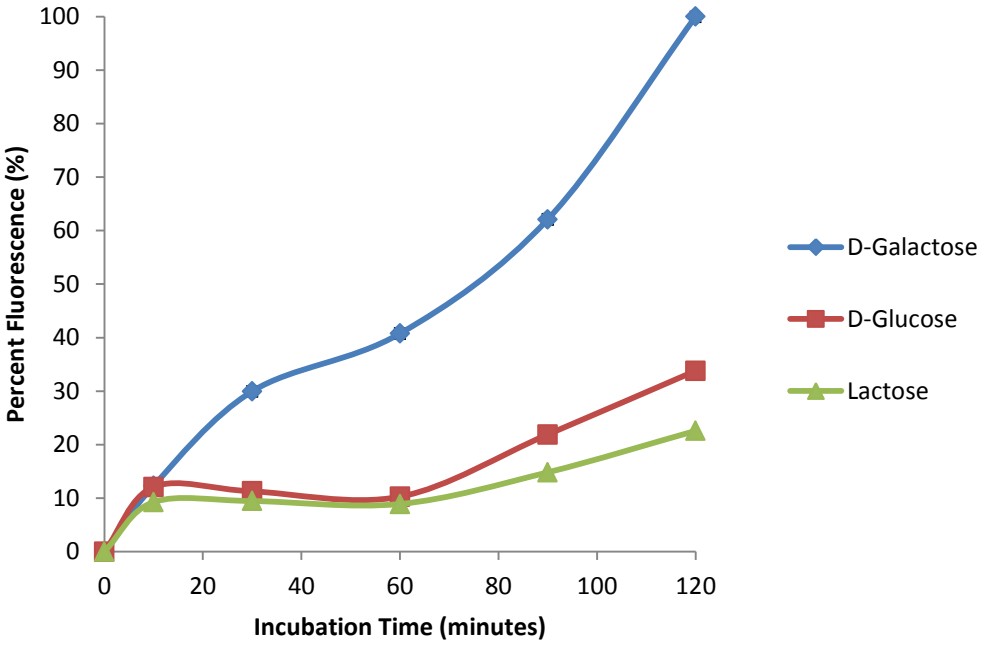

Figure 2a. Time course UV spectral profiles of reaction mixtures containing 150 mM milk sugar (D-galactose, D-glucose or) lactose with 1 mM of melamine at 80 °C for 2 hours. Blank solutions were incubated under identical conditions as above and included either sugar (150 mM) alone, or melamine alone (1 mM). All points represent the average of triplicate measurements. Every reading was compared with the highest reading set at 100%. Excitation and emission wavelengths were set at 260 nm and 380 nm, respectively.

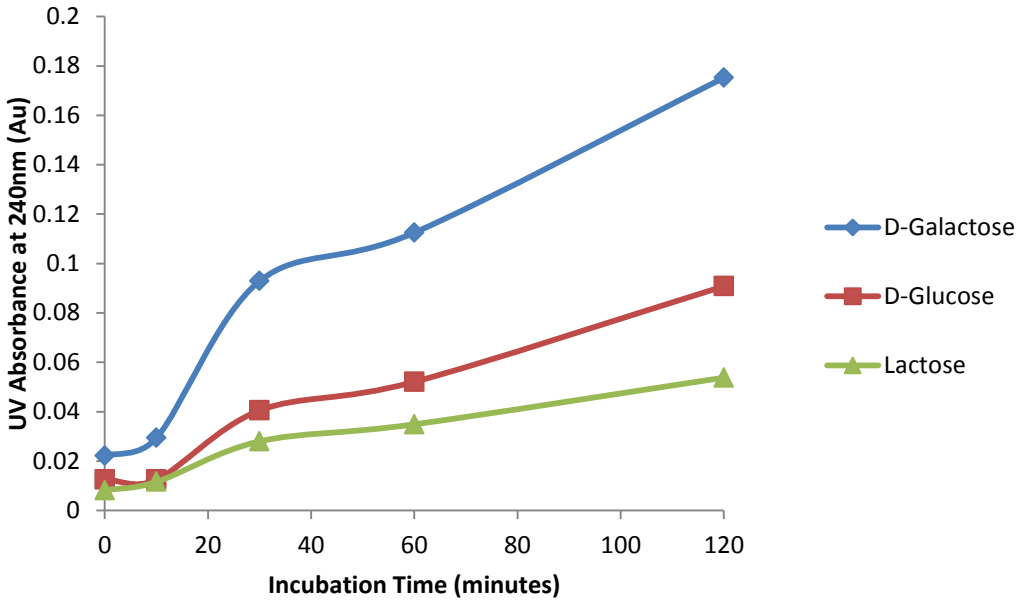

Figure 2b. Time course fluorescence spectral profiles of reaction mixture containing 150 mM milk sugar (D-galactose, D-glucose or lactose) with 1mM melamine at 80 °C for 2 hours. Blank solutions were incubated under identical conditions as above and included either sugar (150 mM) alone, or melamine alone (1 mM). All points represent the average of triplicate measurements. Every reading was compared with the highest reading set at 100%. Excitation and emission wavelengths were set at 260 nm and 380 nm, respectively.

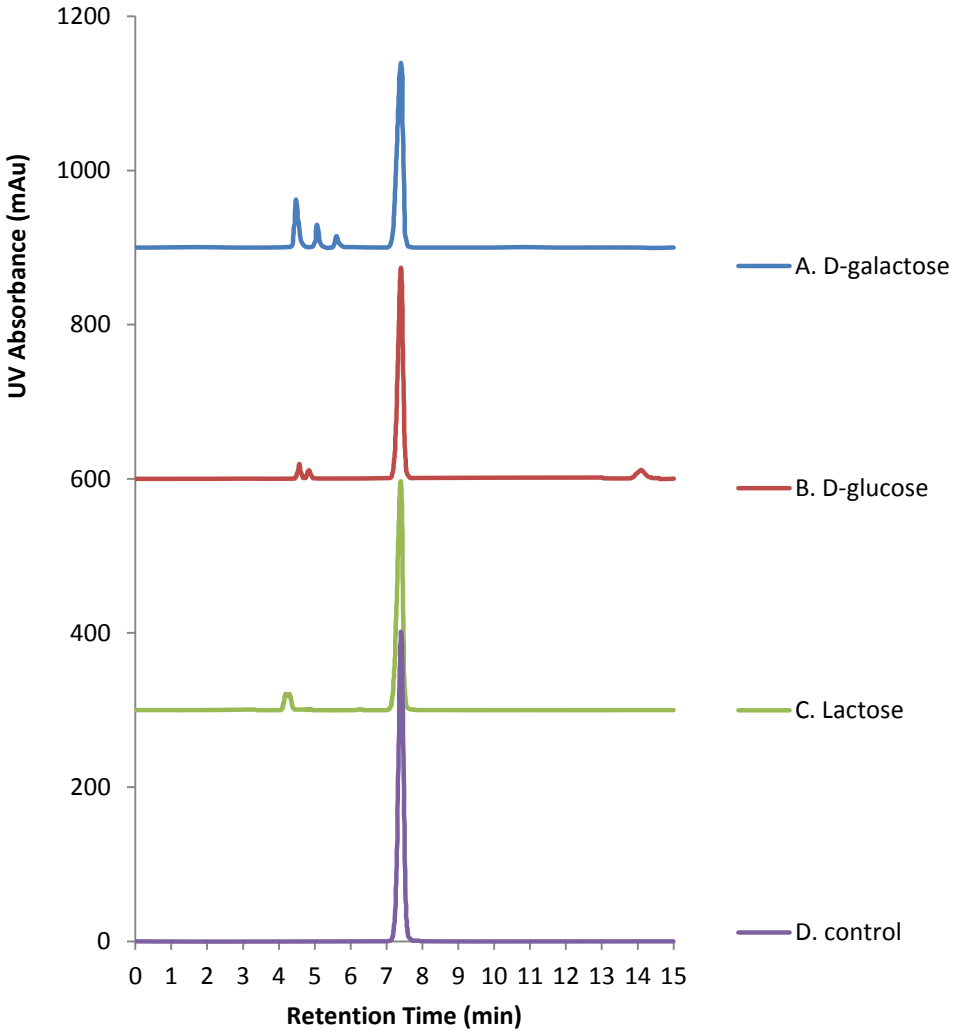

Figure 3. HPLC elution profile of melamine (1 mM) after 1 hour of incubation at 80 °C with 150 mM D-galactose (A), D-glucose (B) and lactose (C). Control reaction mixtures contained freshly mixed solutions of sugar with melamine (D). Repeat chromatographic studies by HPLC revealed no significant difference in the elution profiles and the retention times of the different AGEs.

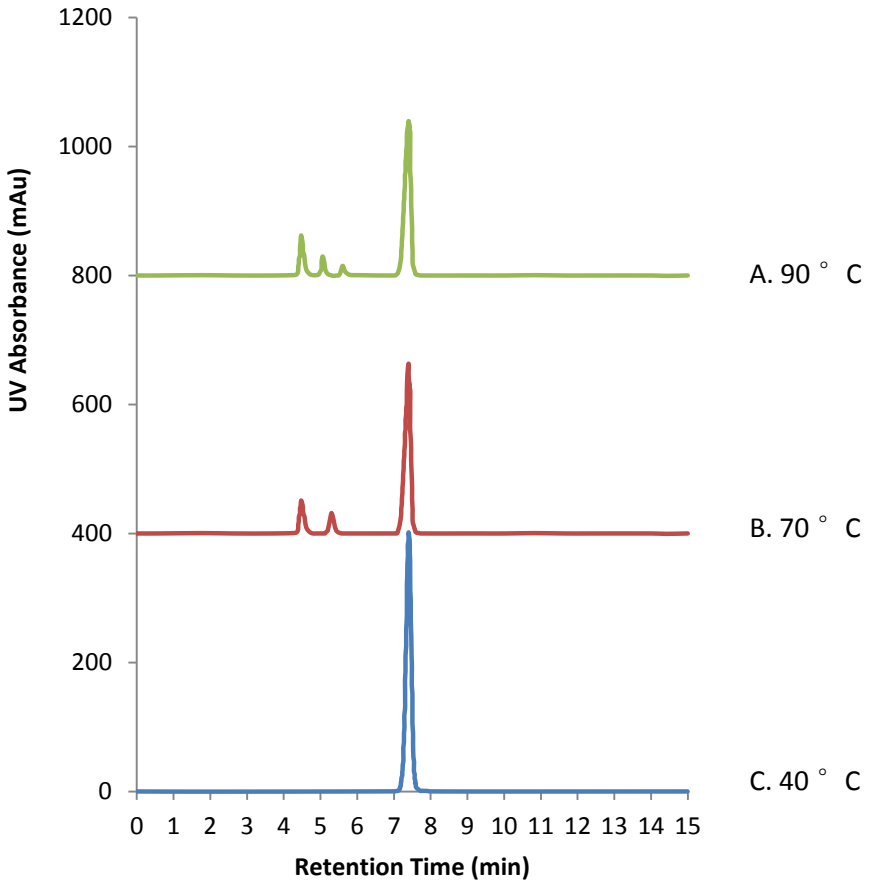

Figure 4. HPLC elution profile of melamine with D-galactose in phosphate buffer, pH 6.7 after the incubation of the two reactants for 1 hour at 90 °C (A), 70 °C (B), and 40 °C (C). Repeat chromatographic studies by HPLC revealed no significant differences in the elution profiles and the retention times of the different AGEs in the above reaction mixtures.

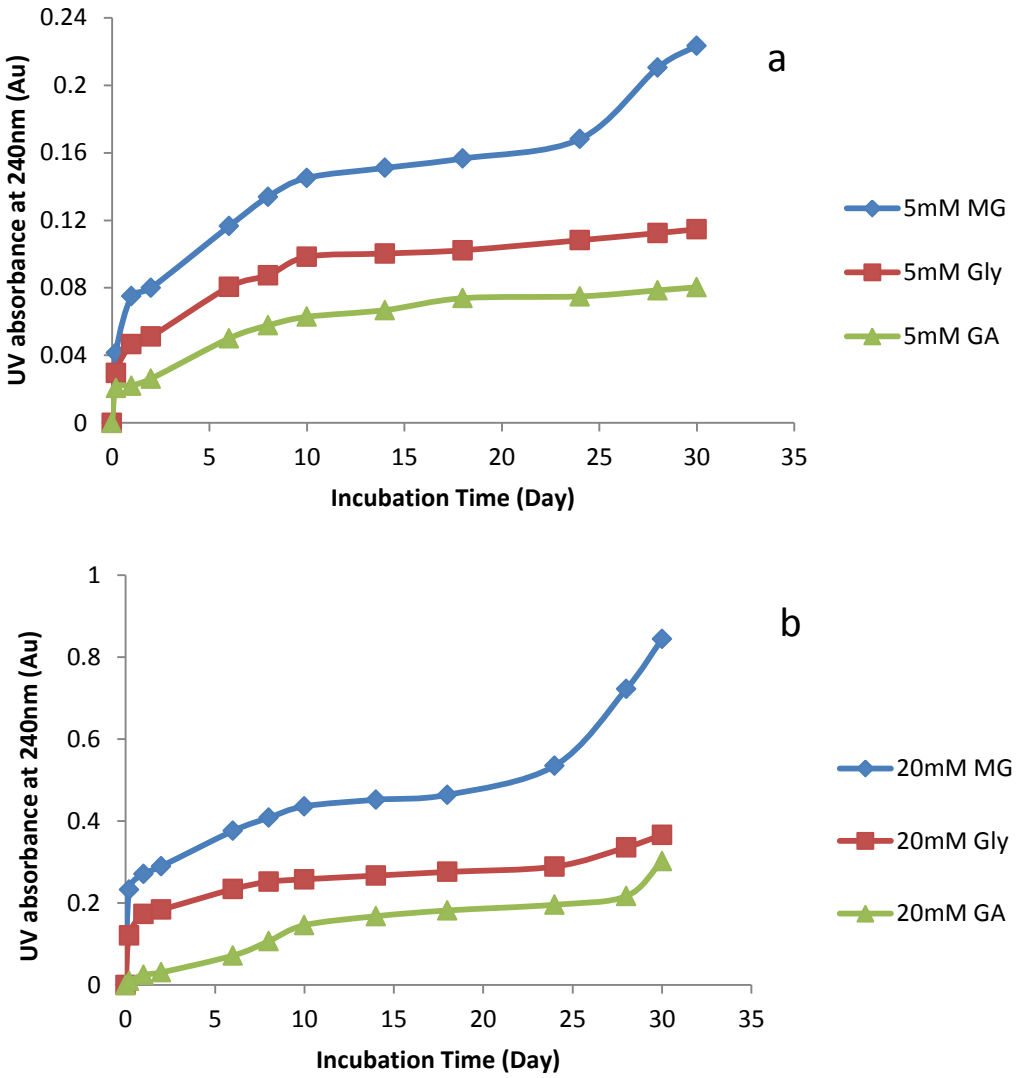

Figure 5 a and 5 b show the UV absorbance profiles of incubation mixtures containing varied amounts of methylglyoxal, glyoxal and DL-glyceraldehyde (5 mM in a and 20 mM in b) with set concentrations of melamine (2.5 mM) in phosphate buffer, pH 7.2 at 37 °C for 30 days. Blank solutions were incubated as above with either aldehyde alone (5 mM and 20 mM), or melamine alone (2.5 mM). All UV readings were subtracted from the blank readings.

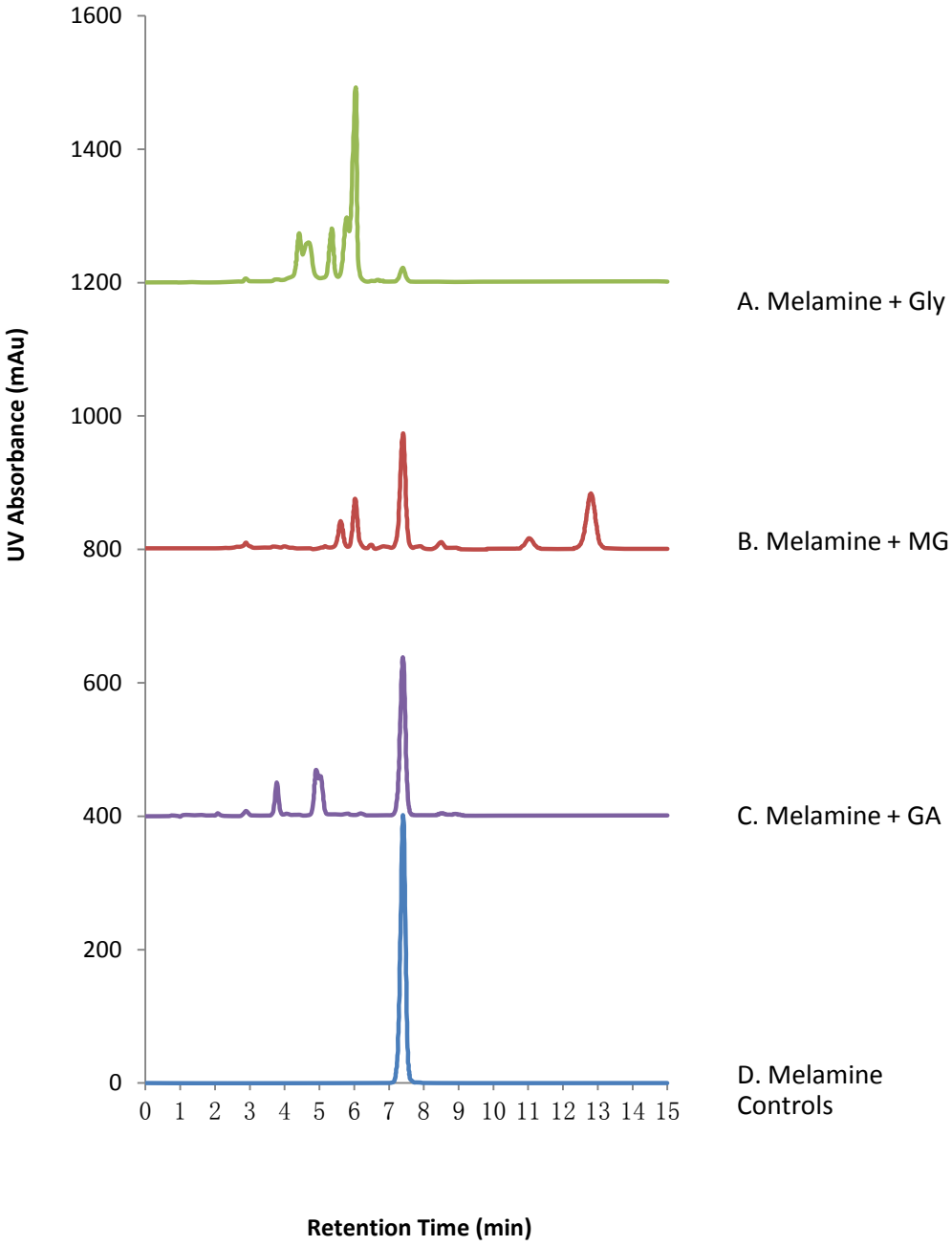

Figure 6. HPLC elution profiles of melamine (2.5 mM) with methylglyoxal (20 mM) [A], glyoxal (20 mM) [B] and DL-glyceraldehyde (20 mM) [C] after 30 days incubation at 37 °C. Figure 6D shows HPLC elution profile of melamine alone (2.5 mM) or melamine freshly incubated with aldehydes (20

mM each). All separations were performed on C_8 reverse phase HPLC column (5 μm×4.6 mm×150 mm) as described previously. Repeat chromatographic studies by HPLC revealed no significant differences in the elution profiles and the retention times of the AGE peaks.

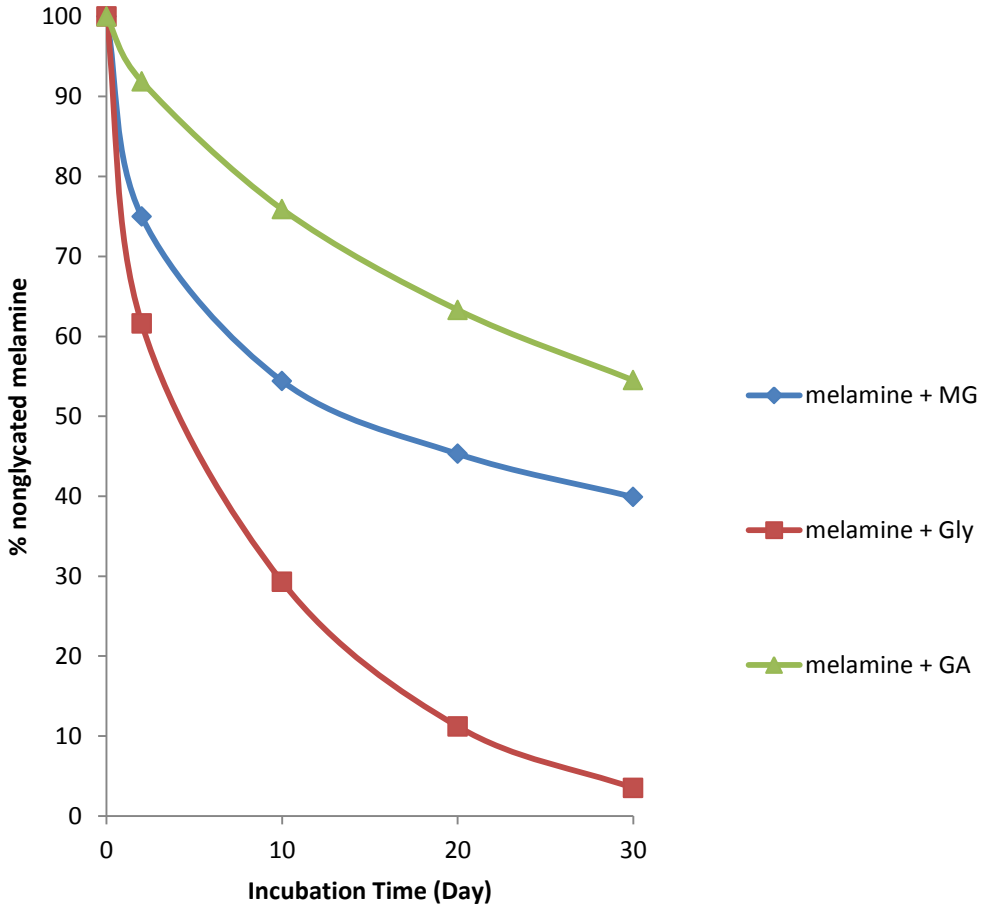

Figure 7. The order of reactivity of methylglyoxal, glyoxal and DL-glyceraldehyde with melamine. Glyoxal was the most reactive glycator of melamine followed by methylglyoxal then DL-glyceraldehyde. The percentages of nonglycated melamine were calculated on the basis of the ratio of HPLC band areas of nonglycated melamine to total band areas in each chromatograph. All values in the figure are the average of triplicate measurements. The variation of each set of triplicate readings is less than 1%.

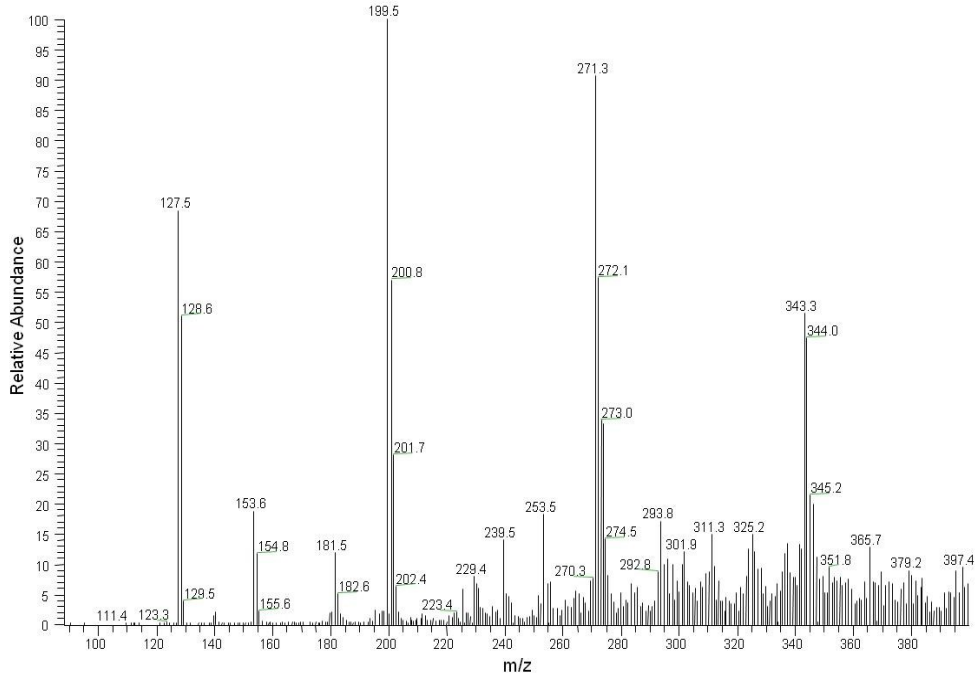

Figure 8. Mass spectral analysis of solutions of melamine [2.5 mM] incubated with methylglyoxal [20 mM] (A) at 37 °C for 30 days.

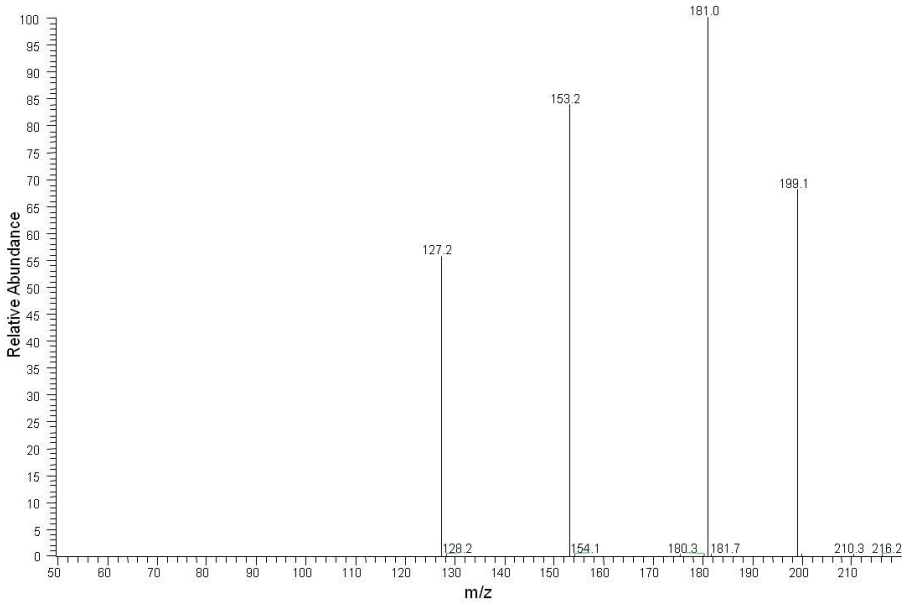

Figure 9a. CID mass spectra of mass spectrum profile in figure 8 recorded on the $(M+H)^+$ ion at m/z 199.

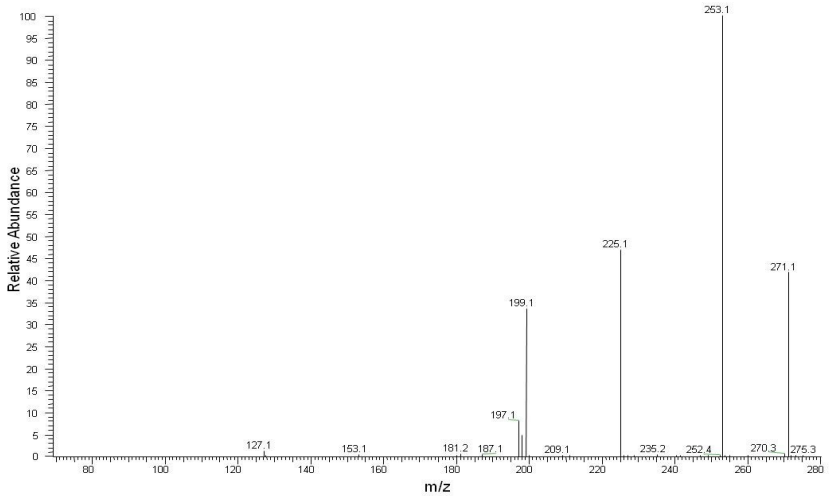

Figure 9b. CID mass spectra of mass spectrum profile in figure 8 recorded on the (M+H)+ ion at m/z 271

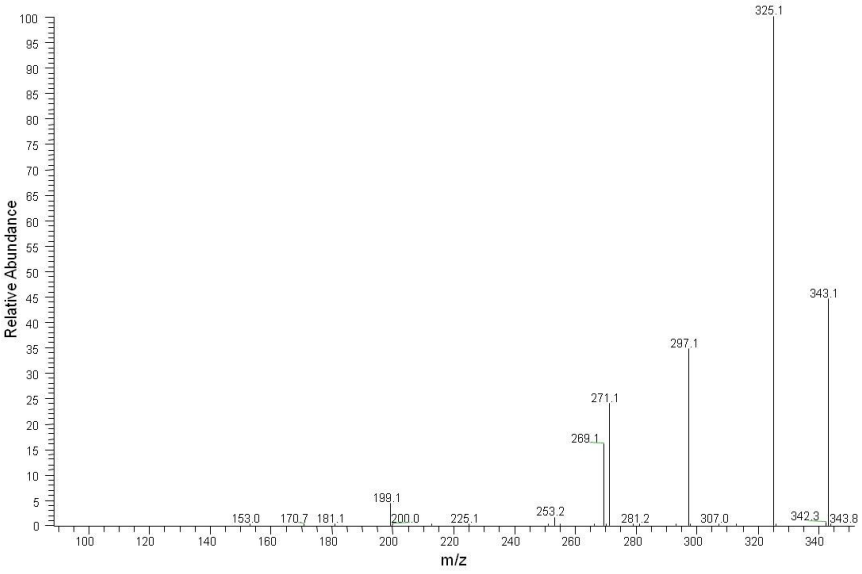

Figure 9c. CID mass spectra of mass spectrum profile in figure 8 recorded on the $(M+H)^+$ ion at m/z 343.

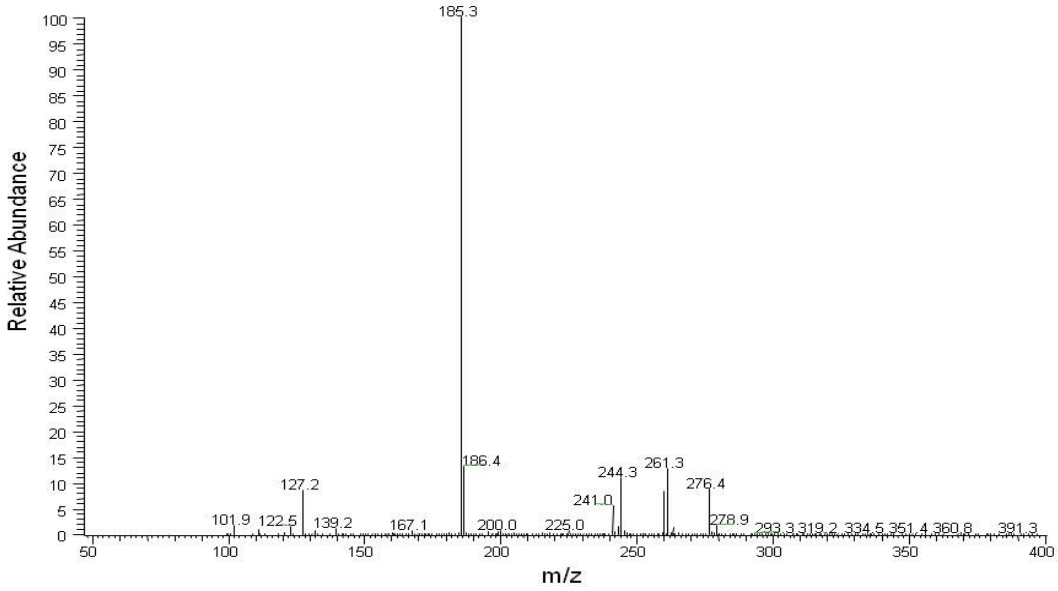

Figure 10. Mass spectral analysis of solutions of melamine [2.5 mM] incubated with glyoxal [20 mM] at 37 °C for 30 days.

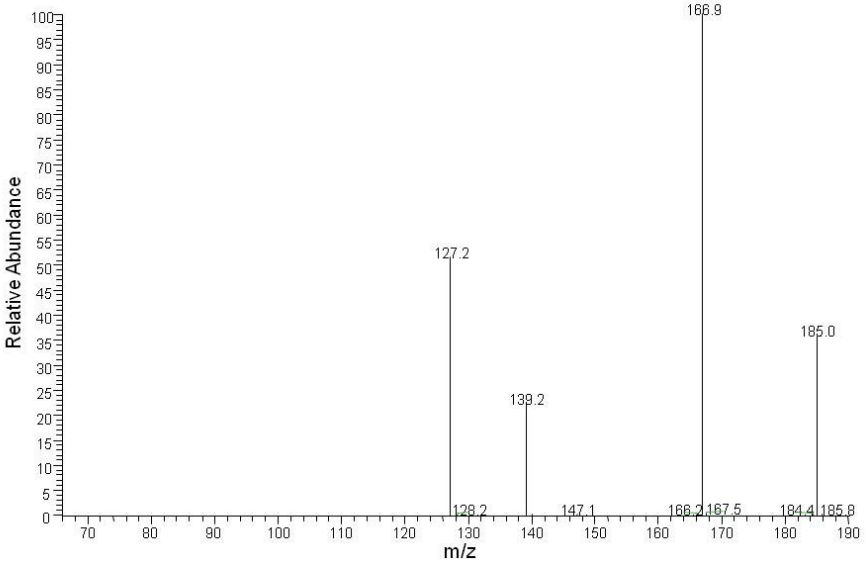

Figure 11a. CID mass spectra of mass spectrum profile in figure 10 recorded on the $(M+H)^+$ ion at m/z 185.

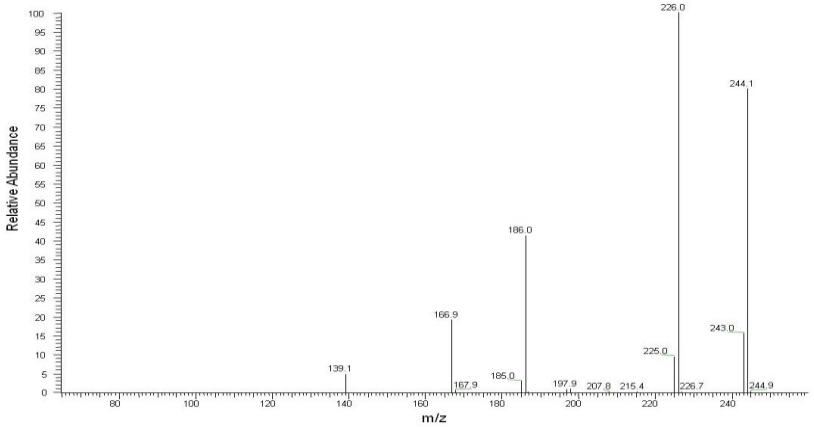

Figure 11b. CID mass spectra of mass spectrum profile in figure 10 recorded on the $(M+H)^+$ ion at m/z 244.

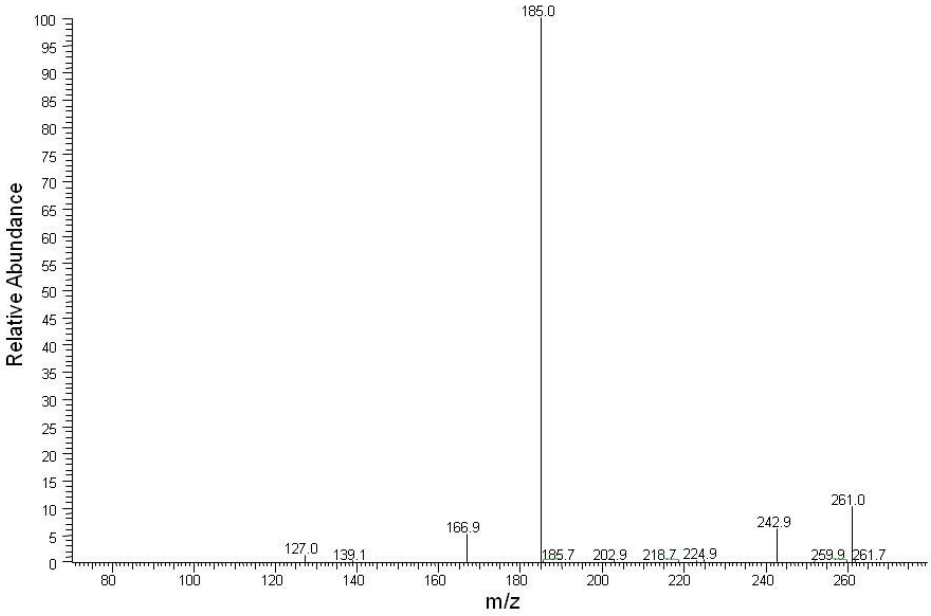

Figure 11c. CID mass spectra of mass spectrum profile in figure 10 recorded on the $(M+H)^+$ ion at m/z 261.

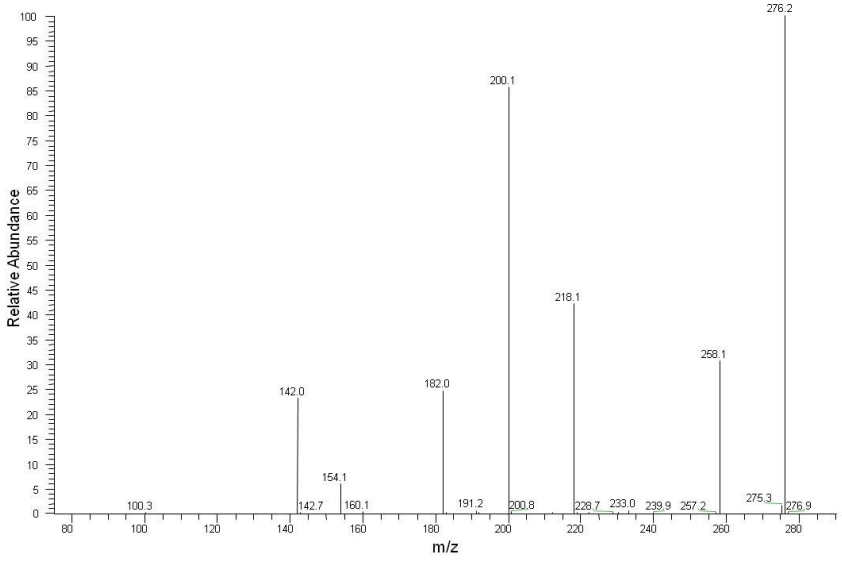

Figure 11d. CID mass spectra of mass spectrum profile in figure 10 recorded on the $(M+H)^+$ ion at m/z 276.

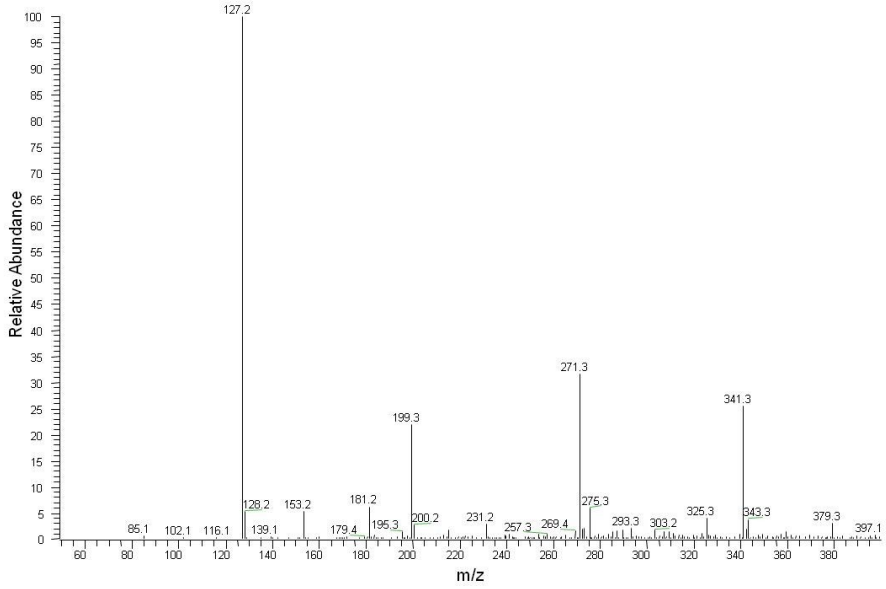

Figure 12. Mass spectral analysis of solutions of melamine [2.5 mM] incubated with DL-glyceraldehyde [20 mM] (C) at 37 °C for 30 days.

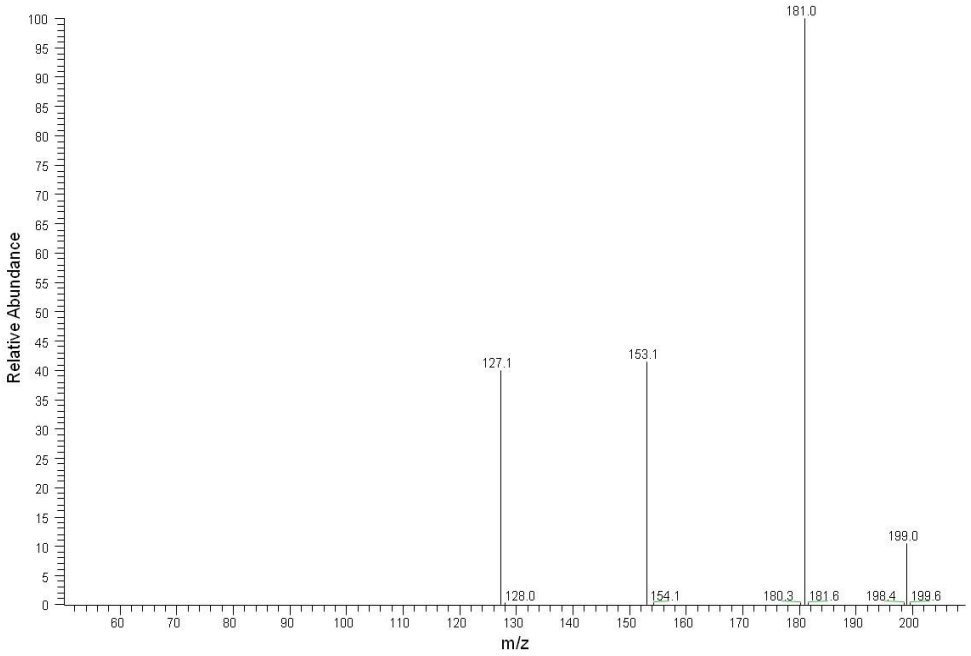

Figure 13a. CID mass spectra of the $(M+H)^+$ ion for DL-glyceraldehyde melamine product at m/z 199.

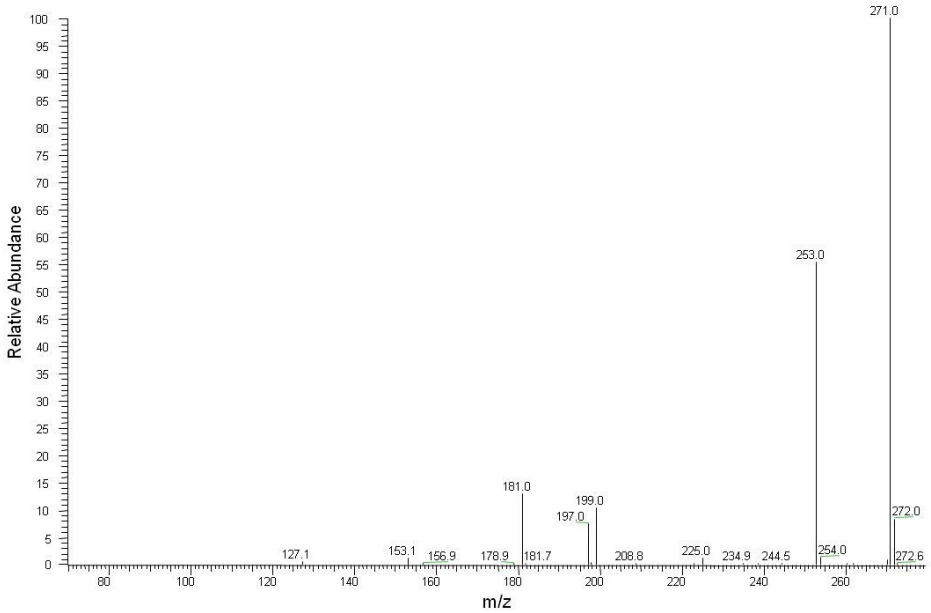

Figure 13b. CID mass spectra of the (M+H)+ ion for DL-glyceraldehyde melamine product at m/z 271.

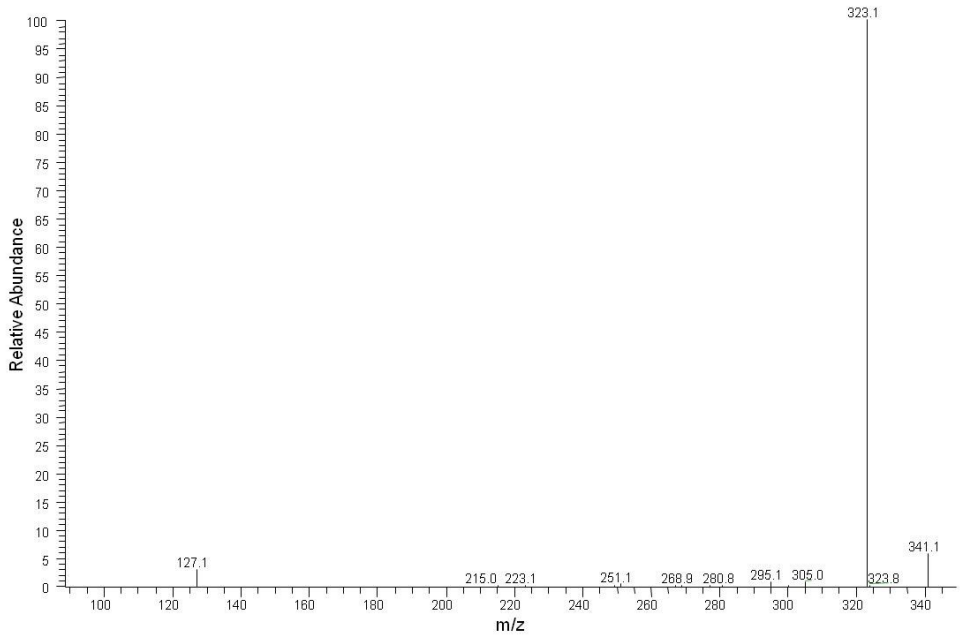

Figure 13c. CID mass spectra of the $(M+H)^+$ ion for DL-glyceraldehyde melamine product at m/z 341.

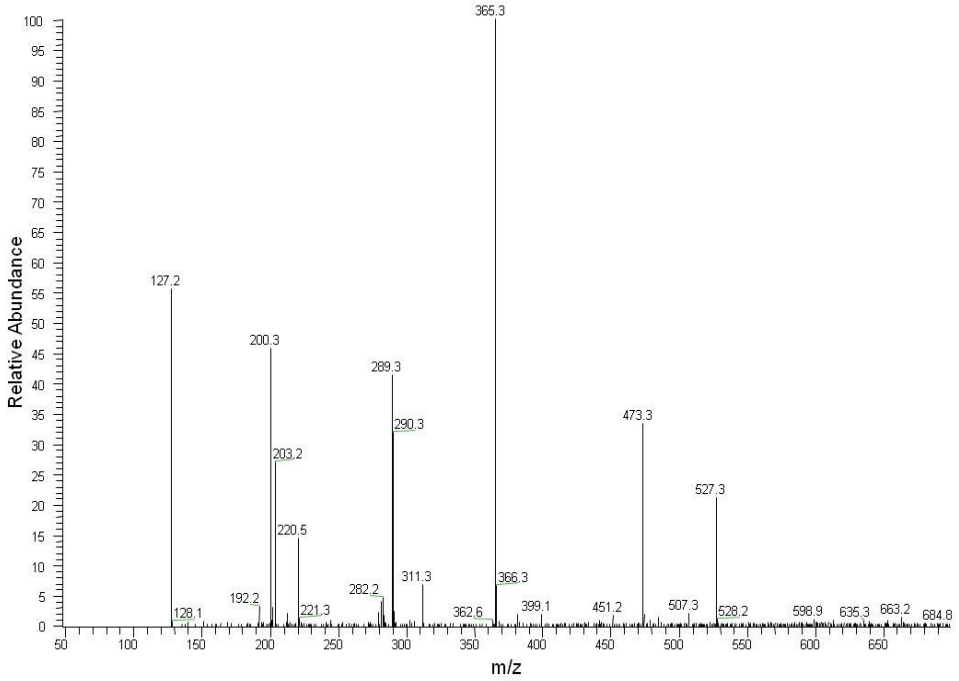

Figure 14. Mass spectral analysis of solutions of 2.5 mM melamine with 150 mM D-galactose at 80 °C incubated for 1 hour.

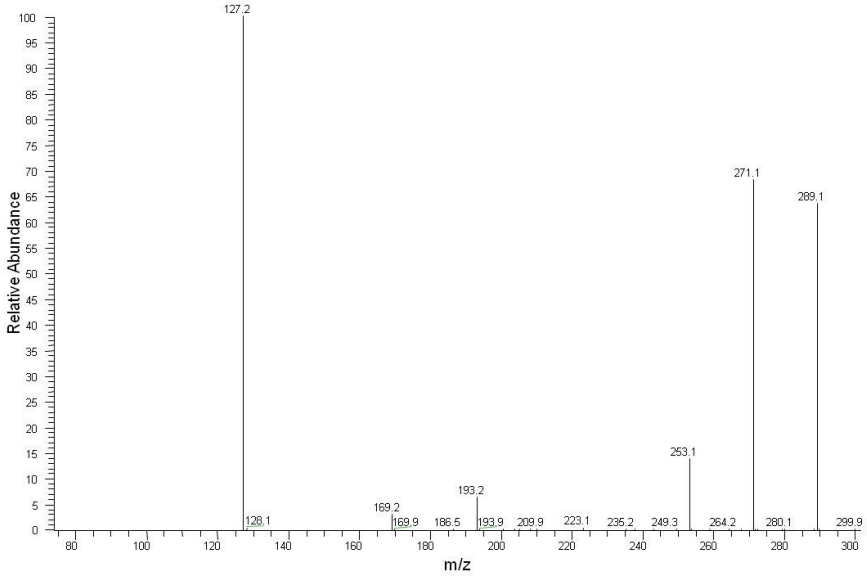

Figure 15a. CID mass spectra of the $(M+H)^+$ ion for D-galactose melamine product at m/z 289.

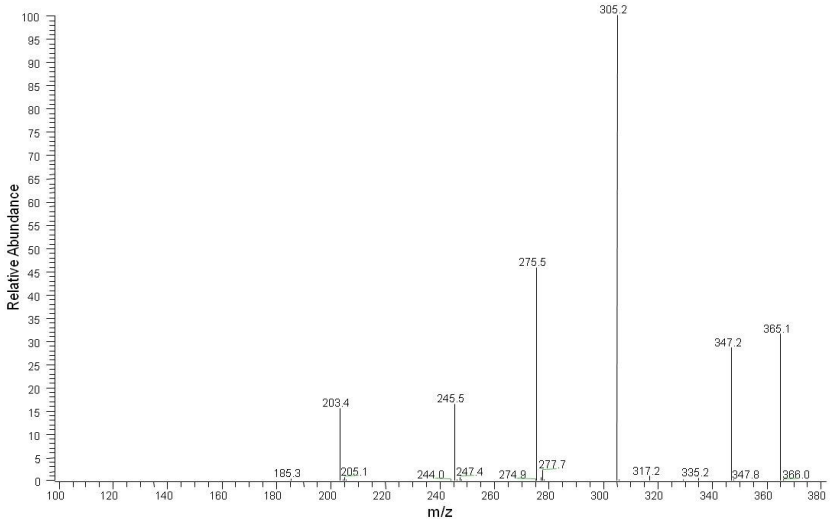

Figure 15b. CID mass spectra of the $(M+H)^+$ ion for D-galactose melamine product at m/z 365.

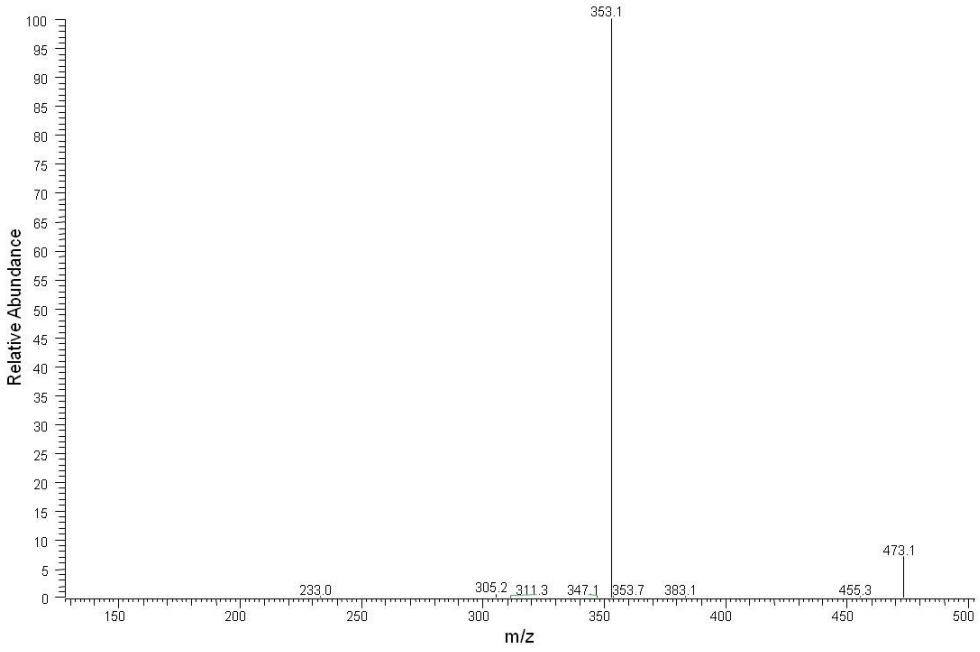

Figure 15c. CID mass spectra of the $(M+H)^+$ ion for D-galactose melamine product at m/z 473.

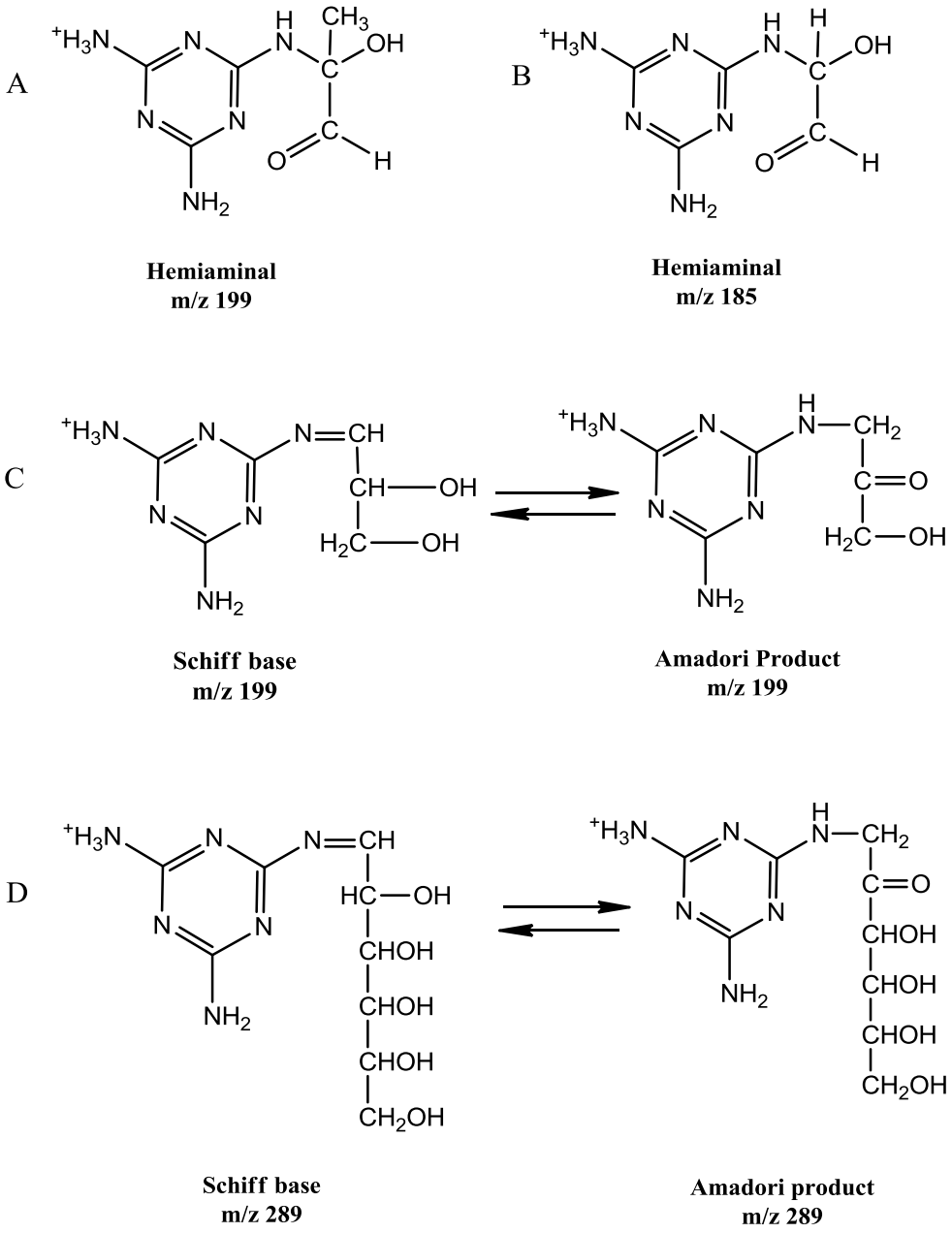

Figure 16. Elucidation of structures consistent with mass spectrometric data for primary products formed in incubation mixtures containing melamine with methyglyoxal (A), glyoxal (B), DL-glyceraldehyde (C), and D-galactose (D).

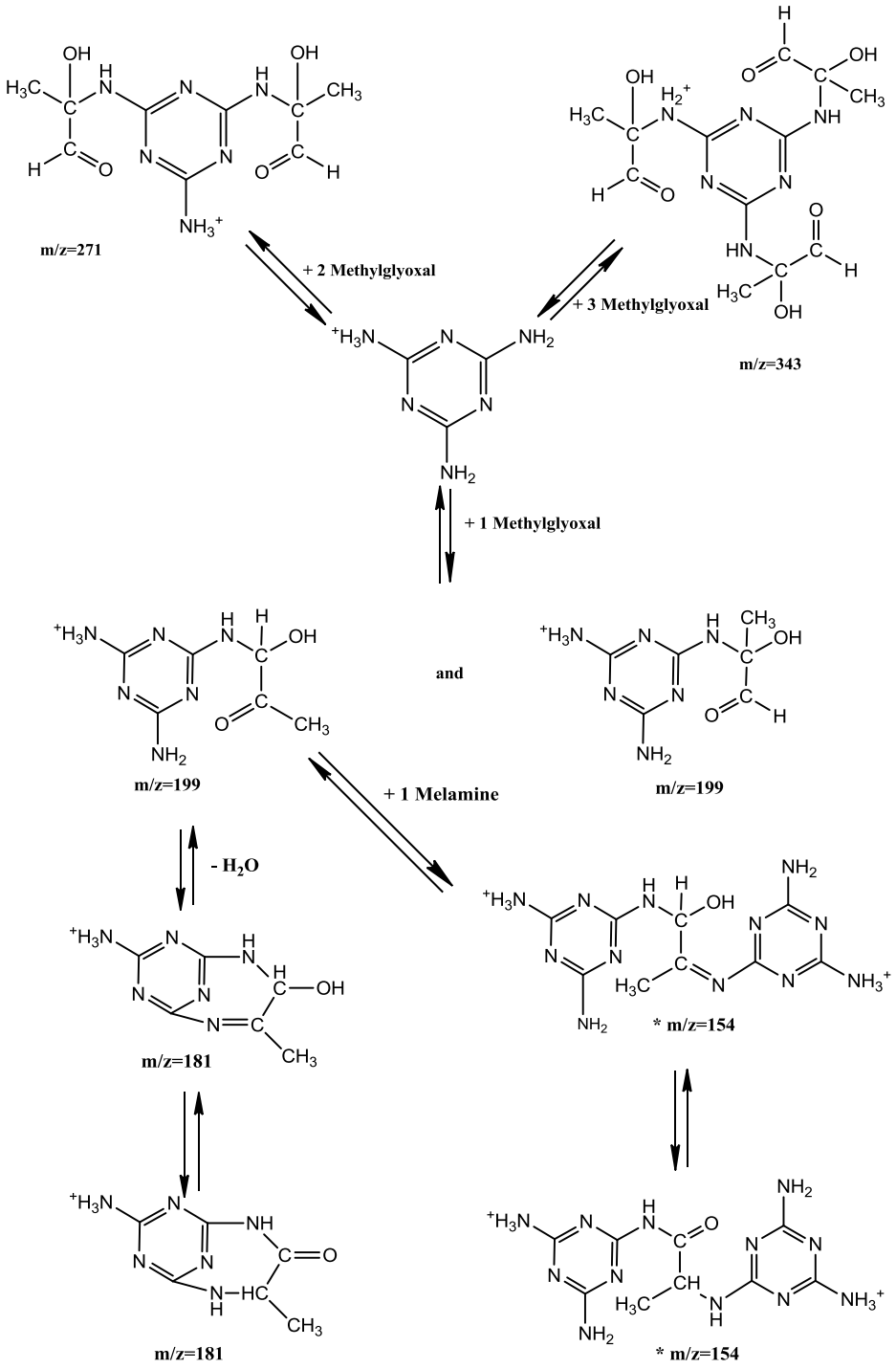

Figure 17. Postulated pathway for the formation of melamine AGEs with methylglyoxal.

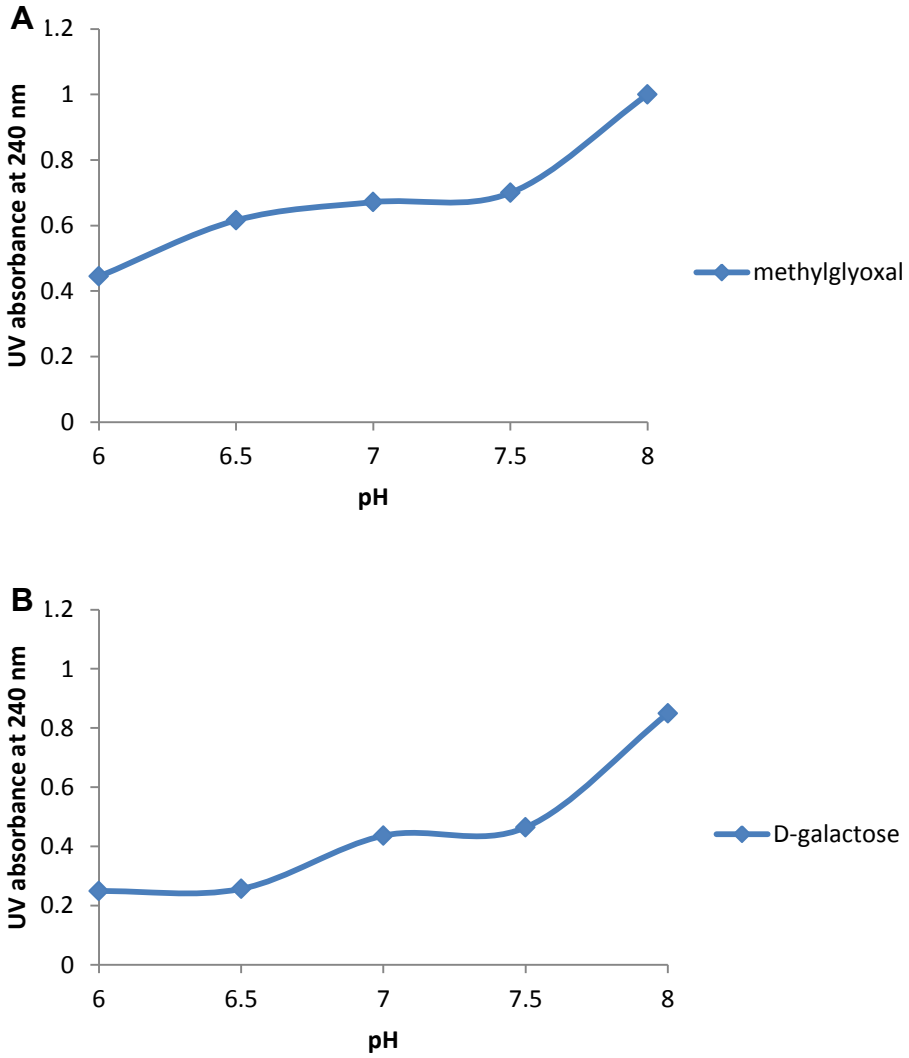

Figure 18. UV absorbance profiles of incubation mixtures of melamine (2.5 mM) with set concentration of methylglyoxal (20 mM) in phosphate buffer under pH 6.0, 6.5, 7.0, 7.5, 8.0 at 37 °C for 48 h (A), or with set concentration of D-galactose (150 mM) in phosphate buffer under pH 6.0, 6.5, 7.0, 7.5, 8.0 at 80 °C for 2 h (B). All readings were compared with the highest reading, which was set at 100%. All points represent the average of triplicate measurements, and every reading was found to be within 5% of its counterpart triplicate.

List of tables:

Table I

UV readings of incubation mixtures containing melamine (2.5 mM) and different aldehydes (5 mM and 20 mM)

Methylglyoxal	5 mM		20 mM	
	Actual UV Reading	% Relative Reading	Actual UV Reading	%Relative Reading
0 d	0.000±0.000	0.000	0.000±0.000	0.000
1 d	0.075±0.002	0.336	0.271±0.003	0.321
2 d	0.080±0.001	0.359	0.290±0.003	0.344
30 d	**†0.223±0.002**	**1.000**	**†0.844±0.002**	**1.000**
Glyoxal	**5 mM**		**20 mM**	
	Actual UV Reading	**% Relative Reading**	**Actual UV Reading**	**% Relative Reading**
0 d	0.000±0.000	0.000	0.000±0.000	0.000
1 d	0.046±0.001	0.206	0.173±0.003	0.205
2 d	0.051±0.003	0.229	0.184±0.003	0.218
30 d	0.116±0.001	0.520	0.366±0.004	0.434
DL-Glyceraldehyde	**5 mM**		**20 mM**	
	Actual UV Reading	**% Relative Reading**	**Actual UV Reading**	**% Relative Reading**
0 d	0.000±0.000	0.000	0.000±0.000	0.000
1 d	0.022±0.002	0.099	0.025±0.004	0.030
2 d	0.026±0.001	0.117	0.031±0.002	0.037
30 d	0.080±0.002	0.359	0.302±0.003	0.342

Reaction mixtures included methylglyoxal, glyoxal and DL-glyceraldehyde (5 mM or 20 mM) with melamine (2.5 mM) in phosphate buffer, pH 7.2 at 37 °C for 30 days. Blank solutions were incubated as above with either individual aldehydes alone, or melamine alone. All readings were subtracted from the readings of the blank solutions. % Relative readings were calculated based on the highest UV values obtained within each set of reaction mixtures (5 mM or 20 mM aldehyde) evaluated

† denotes the highest UV readings in each set of incubation mixtures.

Table II

Peak Retention Times and Percentages of AGE Band Areas Resulting from the Separation of Incubation Mixtures Containing Methylglyoxal, Glyoxal and DL-Glyceraldehyde with Melamine by HPLC

	Time (Day)	* % Band Area of Nonglycated Melamine (Rt=7.4 min)	HPLC Peak Retention Times of Melamine AGEs / % Band Areas of Melamine AGEs Relative to Total Band Areas									
			1	2	3	4	5	6	7	8	9	10
MG	0	100.0%										
	2	74.9%	8.4*min* / 12.0%	8.8*min* / 13.1%								
	10	54.4%	6.2*min* / 6.5%	6.7*min* / 6.1%	8.3*min* / 3.4%	8.7*min* / 16.0%	10.6*min* / 8.6%	12.1*min* / 4.9%				
	30	39.9%	2.9*min* / 2.3%	5.2*min* / 1.1%	5.6*min* / 9.8%	6.0*min* / 17.4%	6.5*min* / 1.5%	6.8*min* / 1.2%	7.9*min* / 1.1%	8.5*min* / 2.5%	11.0*min* / 3.8%	12.8*min* / 19.3%
Gly	0	100.0%										
	2	61.6%	6.0*min* / 38.4%									
	10	29.3%	4.4*min* / 4.0%	5.4*min* / 3.6%	6.1*min* / 63.1%							
	30	3.5%	2.9*min* / 1.1%	4.4*min* / 11.7%	4.7*min* / 9.5%	5.4*min* / 12.8%	5.8*min* / 15.4%	6.0*min* / 46.0%				
GA	0	100.0%										
	2	91.9%	3.8*min* / 3.6%	5.0*min* / 4.5%								
	10	75.9%	2.1*min* / 3.9%	3.8*min* / 4.7%	4.8*min* / 13.1%	5.0*min* / 2.3%						
	30	54.5%	2.9*min* / 1.9%	3.8*min* / 11.9%	4.9*min* / 16.3%	5.0*min* / 14.1%						

* Denotes the fractions of nonglycated melamine eluted at retention time of 7.4 min.

Manuscript 3

Prepared for Analytical Biochemistry
Anticipated submission date: January, 2013

Inhibitory Effect of Gold Nanoparticles on the Glycation of Bovine Serum Albumin by D-Ribose

Weixi Liu [1], Menashi A. Cohenford [2], Leslie Frost [3], Champika Seneviratne [1], Joel A. Dain [1*]

[1] Department of Chemistry, University of RI, Kingston, RI 02881

[2] Department of Integrated Science and Technology, Marshall University, Huntington, WV 25755

[3] Department of Chemistry, Marshall University, Huntington, WV 25755

E-mail address: wliu@chm.uri.edu (Weixi Liu).
E-mail address: cohenford@marshall.edu (Menashi A. Cohenford).
E-mail address: frost@marshall.edu (Frost Leslie)
E-mail address: pseneviratne@chm.uri.edu (Champika Seneviratne)
*Corresponding author: Phone: + 1-401-874-5942; fax: + 1-401-874-5072
E-mail address: jdain@chm.uri.edu (Joel A. Dain).

Abstract:

The formation of advanced glycation endproducts (AGEs) by non-enzymatic glycation of protein with reducing sugar is a major contributor to the pathology of diabetes, Alzheimer's disease and atherosclerosis. Previous study in our laboratory showed that 2 nm gold nanoparticles (GNPs) exhibit an inhibition effect on the formation of AGEs when serum albumin was glycated with DL-glyceraldehyde. The objective of this study was to evaluate the rate and extent of AGE formation of bovine serum albumin (BSA) in the presence of GNPs with varied sizes. A combination of UV spectrometry, HPLC and circular dichroism showed that only GNPs with size ranging from 2nm to 20nm inhibited the formation of BSA AGEs. The inhibition effect of GNPs was correlated to the overall surface area of nanoparticles in the solution. GNPs with higher surface areas were found to be better inhibitors of glycation, whereas those with low surface areas were less effective inhibitors. MALDI-TOF spectrum showed that in the presence of GNPs, BSA was less prone to be glycated by reducing sugar comparing to reaction mixtures absent of GNPs. The inhibitory effect of GNPs on non-enzymatic glycation reactions may be

due to the covalent bonding between gold atoms on the surface of GNP and ε amino groups of L-lysine residue on protein. As GNP is highly biocompatible and water soluble, an insight of its anti-glycation effect and its inhibition mechanism on the formation of AGEs might lead to a novel therapeutic application of GNP on reducing AGE related complications.

Key Words: gold nanoparticle; glycation; AGEs; BSA; D-ribose

1 Introduction

Glycation is a non-enzymatic reaction with reactants including a reducing sugar and a free amino containing molecule such as protein, lipid or nucleic acid. The reaction initiates with a nucleophilic attack of the free amino group on biomolecule to the carbonyl group of a reducing sugar, forming an unstable Schiff base structure. The Schiff base will then rearrange to a more stable ketoamine known as Amadori product. Under physiological condition, this Amadori product can undergo series of irreversible chemical reactions including self-degradation and condensation with other proteins, leading the formation of a heterogeneous group of compounds referred to as advanced glycation endproducts (AGEs) [1, 2]. The graduate accumulation of AGEs *in vivo* has been implicated as a major

contributor to various diabetic complications including renal failure, diabetic atherosclerosis and cataract formation, as well as other health disorders, such as Alzheimer's disease (AD) [3-5]. Abnormal built up of AGEs under hyperglycemia condition could trigger the generation of harmful inflammatory factors and reactive oxygen species, resulting in tissue damage. Long lived protein which has a low clearance rate tends to form crosslinking structures with certain type of AGEs and gradually lose its function *in vivo*.

Since the non-enzymatic glycation of proteins is tightly related to the pathology of long-term diseases, the inhibitors to prevent the formation of AGEs have been extensively investigated over years [6-8]. The reactants involved in the initial stage of glycation are a common target for anti-glycation drug design [9, 10]. This class of inhibitors act as sugar competitors by interacting with target glycation amino acid residues, most commonly lysine and arginine, and prevent their further modification by reducing sugars. Two notable potential anti-glycation agent fall into this class include acetylating aspirin and aldehyde pyridoxal-5'-phosphate.

Previous study in our laboratory showed that 2 nm gold nanoparticles (GNPs) exhibit an inhibitory effect on the formation of AGEs when Human Serum Albumin (HSA) was glycated by DL-glyceraldehyde [11]. GNP typically refers to gold colloid with a particle size ranging from one nanometer to several hundred nanometers. Due to its unique optical

property, very large surface-to volume ratio and easy modification, GNP has been applied in a broad range of fields including biomedicine, bio-imaging, material science and synthetic chemistry [12-14].

Proteins and amino acids are able to covalently bond to the gold atoms on the surface of nanoparticle through Au-S or Au-NH_2 bonds [15, 16]. The binding of biomolecules to GNP can stabilize the particle from conjugation and enhance its solubility in aqueous solution as well [17]. In the meanwhile, free amino groups in proteins or peptides, some of which are the seeding sites of GNP to these biomolecules, might also be reaction sites susceptible to glycation by reducing sugar. This suggests that the specific covalent bonding of GNP to these amino groups in protein might be able to protect these sites from glycation. Furthermore, GNP could possibly bind to the glycation intermediates of protein and prevent the formation of reactive dicarbonyl compounds. By trapping these AGE precursors, GNP could stabilize and fix the protein structure from further alteration and prevent the formation of AGEs.

The objective of this study was to evaluate the rate and extent of BSA glycation by D-ribose in the presence of spherical GNPs. A combination of UV spectrometry, HPLC, circular dichroism and MALDI were used to determine the formation of AGEs. This study emphasized also on the effect of different nanoparticle sizes on GNP's inhibitory efficiency. The correlation between particle size, total particle surface area in solution and GNP's

anti-glycation ability was evaluated by two separate experiments designated as experiment A and B. As GNP is highly biocompatible and water soluble, an insight of its anti-glycation effect and its inhibition mechanism on the formation of AGEs might lead to a novel therapeutic application of GNP on reducing AGE related complications.

5 Materials and methods

5.1 Chemicals and supplies

Fatty acid free albumin from bovine serum (BSA) and analytical grade D-ribose were purchased from Sigma-Aldrich Chemical Co. (St. Louis, MO, USA). Citrate reduced colloidal solution of spherical gold nanoparticles with variable sizes (2nm, 5nm and 20nm) were purchased form Ted Pella Inc. (Redding, CA, USA). Disposable UV-transparent cuvettes (12.5 mm X12.5 mm X 36 mm) and HPLC analytical grade solvents were obtained from Thermo Fisher Scientific (Rockford, IL, USA). ZipTip pipette tips with C_4 resin and 0.22 μm filter unit were purchased form EMD Millipore Co. (Billerica, MA, USA). Unless otherwise indicated, all other reagents of analytical grade were purchased from Sigma-Aldrich Chemical Co. (St. Louis, MO, USA).

5.2 Preparation of reaction mixtures

5.2.1 Stock solutions of BSA (105 mM) and D-ribose (100 mM) were prepared in 0.1 M phosphate buffer, pH 7.2. Gold colloids with different sizes of nanoparticles (2 nm, 5 nm, 20 nm, 50 nm, 100 nm

and 200 nm) were suspended in water and adjusted to a final Au mass concentration of 0.01 mg/ml each. Blank solutions included 35 mg/ml BSA alone, 20 mM D-ribose alone and 35 mg/ml BSA with different sizes of GNP without D-ribose. Controls included 35 mg/ml BSA incubated with 20 mM D-ribose at the absence of GNP. The concentration of BSA was adjusted to 35 mg/ml because this is the reported serum albumin concentration physiologically. The concentration of D-ribose was adjusted to 20 mM representing the blood sugar content under diabetic condition. D-ribose was chosen as the model glycated agent due to its greater reactivity comparing to D-glucose and its important role in several bio pathways related to carbohydrates metabolism.

5.2.2 Experiment A: Reaction mixtures contained 35 mg/ml BSA and 20 mM D-ribose with different sizes of GNP (2 nm, 5 nm and 20 nm) at set Au concentration of 0.005 mg/ml, resulting in different particle number and total particle surface area in each solution (Table I). All reaction mixtures and blanks were incubated in the dark at 37 °C in a shaking water bath for 21 days. After incubation, samples were placed at -20 °C until analyzed. Prior analysis, all samples were ultra-centrifuged at $1X10^4$ rpm for 30 min and the supernates were further purified by ZipTip pipette with C_4 resin.

5.2.3 Experiment B: Reaction mixtures contained 35 mg/ml BSA and 20 mM D-ribose with different sizes of GNP (2 nm, 5 nm and 20 nm) at different Au mass concentrations of 0.02 mg/ml, 0.01 mg/ml and 0.05mg/ml respectively. Such dilution resulted in an approximate identical total nanoparticle surface area in each solution containing different sizes of GNPs. All reaction mixtures and blanks were incubated in the dark at 37 °C in a shaking water bath for 21 days. After incubation, samples were placed at -20 °C until analyzed. Prior analysis, all samples were ultra-centrifuged at $1X10^4$ rpm for 30 min and the supernates were further purified by ZipTip pipette with C_4 resin.

5.3 UV and fluorescence spectroscopy

UV spectrum with wavelength ranging from 200 nm to 400 nm was determined on an UltroSpec 2100 instrument (Biochrom Ltd, Cambridge, UK). Fluorescence measurements were made at respective excitation and emission wavelengths of 340 nm and 420 nm using a Spectra Max M2 spectrometer (Molecular Devices, Sunnyvale, CA, USA). All samples were diluted 50 fold before analysis and all readings were obtained in thermostatically controlled cuvettes that were maintained at 25±1 °C. The above excitation and emission wavelengths were determined optimal for detecting BSA AGEs.

5.4 Circular dichroism

CD analysis were performed at a Jasco J-720 spectropolarimeter (Tokyo, Japan) using a quartz cuvette of 1 mm path length. The instrument was controlled by Jasco's Spectra Manager software. Before analysis, the concentration of BSA was adjusted to 0.5 mg/ml using 0.1 M phosphate buffer, pH 7.2. Signals were obtained in the far-ultraviolet region (190-250nm). A total of 10 consecutive scans with bandwidth of 1 nm, scan speed of 20 nm/min and response time of 2 s were averaged. The spectrums were then subtracted by corresponding blanks to eliminate any buffer effect.

5.5 High-performance liquid chromatography

Each HPLC run was performed in triplicate using a Hewlett Packard 1050 system (Waldbronn, Germany) equipped with a low-pressure gradient pump, a four-channel degasser, a sequential auto sampler, a high sensitivity diode-array detector (190–800 nm) and a programmable fluorescence detector (HP 1046A). The HPLC system was operated with the ChemStation System from Agilent Technologies (Santa Clara, CA, USA) with the same software used also for data analysis. AGE species were separated on a Shodex (New York, NY, USA) RSpak C_{18} reverse phase HPLC column (5 µm×4.6 mm×150 mm) with 415 Å pore size. Mobile phase A consisted of 0.1% trifluoroacetic acid (TFA) and 1% acetonitrile (ACN) in water and mobile phase B consisted of 0.1% TFA and 95% ACN in water. A linear gradient from 20% to 60% of mobile phase B was applied in 25 minutes at a constant flow rate of 1.0 ml/min. Prior to HPLC analysis, all solvents were degassed

and sonicated for 15 min. All samples were filtered with a 0.22 μm membrane, degassed and centrifuged.

5.6 Preparation and analysis of intact HSA by MALDI-TOF MS

All samples were purified with C_4 ZipTips and analyzed on a Bruker Autoflex MALDI–TOF (time-of-flight) mass spectrometer (Bruker Daltonics, Billerica, MA, USA). Prior to analysis, the protein samples (0.6 μl) were mixed with a 50% aqueous acetonitrile solution (0.6 μl) of saturated sinapinic acid containing 0.05% trifluoroacetic acid (TFA) as matrix, spotted onto a stainless steel sample plate, and allowed to air dry. Spectra were acquired in linear TOF mode with a 550 ns delay in the m/z range from 20,000 to 80,000. Each spectrum was the sum of 500 single laser shots randomized over 10 positions within the same spot (500/50). Analysis of data was performed using FlexAnalysis and ClinProTools (Bruker Daltonics).

3. Results

Figure 1 displays the respective UV spectral profiles of reaction mixtures in experiment A after 21 days incubation in dark at 37 °C. It should be noted that spherical GNPs with particle diameter larger than 20 nm (50 nm, 100 nm and 200 nm) aggregated with BSA after two to three days incubation, forming insoluble precipitants in phosphate buffer. Thus only 2 nm, 5 nm and 20 nm GNPs which retained their nanoparticle properties

without aggregating with BSA during incubation were evaluated in the following study.

Profiles in figure 1 from top to bottom are a) 35 mg/ml BSA incubated with 20 mM D-ribose at the absence of GNP, b) 35 mg/ml BSA glycated by 20 mM D-ribose at the presence of 20 nm GNP, c) 35 mg/ml BSA glycated by 20 mM D-ribose at the presence of 2 nm GNP, d) 35 mg/ml BSA glycated by 20 mM D-ribose at the presence of 5 nm GNP and e) 35 mg/ml BSA incubated in buffer alone. The UV spectrum scans ranged from 250 nm to 400 nm in each profile. Comparing to BSA blank, reaction mixture containing BSA and D-ribose showed dramatic increase in UV absorbance intensity after 21 days incubation, yielding a peak with the maximum absorbance at around 280 nm (profile a). Aromatic rings are known as the primary reason for the absorbance peak at 280 nm and the increased BSA UV intensity at 280 nm revealed the formation and accumulation of aromatic AGEs. As a result the increase in UV absorbance intensity at 280 nm could be used to evaluate the extent of BSA glycation. Comparing to reaction mixture containing BSA and D-ribose alone, BSA glycated in the presence of GNPs (profile b, c and d) showed significant reduction in UV intensity at 280 nm after 21 days incubation.

Though the absorbance measurements at 280 nm in profiles b, c and d all decreased noticeably comparing to control reaction in profile a, the extent of the reduction in each solution varied. Among three incubation mixtures of

different sizes of nanoparticles, reaction with 5 nm GNPs showed the lowest UV absorbance yielding a value of 0.151 at wavelength of 280 nm. In comparison, control group without the treatment of GNP had a much higher UV intensity at 280 nm valued 0.384. Followed by 5 nm GNP solution, sample with 2 nm GNP exhibited the second lowest UV reading (λ_{280}=0.180) while sample with 20 nm GNP showed the highest UV intensity among the three GNP containing mixtures (λ_{280}=0.269). Previous study in our lab demonstrated that increase in nanoparticle numbers in reaction solution was directly correlated to its inhibitory efficiency against glycation, probably due to the increased available binding area on the surface of GNP, which could mask protein's glycation sites. Adjusting Au mass concentration in profile b, c and d to the same mass value of 0.05 mg/ml resulted in a different particle number and total particle surface area in each solution. The value of total particle surface area in unit volume (ml) was obtained by multiplying the particle number in one unit volume (ml) with the single particle surface area (nm^2). According to table I, 5 nm GNP solution had the highest total particle surface area in solution, followed by 2 nm GNP and then 20 nm. Interestingly, this sequence corresponded to the order of their anti-glycation efficiency that 5 nm GNP showed the most reduction on the formation of AGEs while 20 nm the least.

To further evaluate the correlation between nanoparticle size, total particle surface area in solution and GNP's anti-glycation ability, we

conducted experiment B. In this separate study, we used the same blank and control samples as experiment A, while adjusted the Au mass concentration to 0.02 mg/ml, 0.01 mg/ml and 0.05 mg/ml for 2 nm GNP, 5 nm GNP and 20 nm GNP solutions respectively, resulting in a same particle surface area in all three GNP solutions. Figure 2 displays the UV absorbance spectrums of reaction mixtures in experiment B and profiles from top to bottom are: a) 35 mg/ml BSA incubated with 20 mM D-ribose at the absence of GNP, b) 35 mg/ml BSA glycated by 20 mM D-ribose at the presence of 20 nm GNP, c) 35 mg/ml BSA glycated by 20 mM D-ribose at the presence of 5 nm GNP, d) 35 mg/ml BSA glycated by 20 mM D-ribose at the presence of 2 nm GNP and e) 35 mg/ml BSA incubated in buffer alone. BSA glycated by D-ribose without the treatment of GNPs again yielded the highest UV intensity while BSA blank showed the lowest. However, 2 nm GNP and 5 nm GNP revealed a less inhibitory effect against glycation comparing to GNP solutions in experiment A, yielding UV spectral profiles that were nearly superimposable to that of 20 nm GNP. This suggested that all three GNP samples which had the same total nanoparticle surface areas exhibited similar ant-glycation abilities, regardless of the difference in their particle sizes and Au mass concentrations.

Advanced glycation of BSA not only produces aromatic AGEs that can be detected by UV absorbance, but also alters proteins secondary structure whose change can be monitored by circular dichroism in the far-UV spectral

region (190-250 nm). The secondary structure of BSA is composed of about 67% α-helix structure, so BSA conformation change was determine by monitoring the loss of α-helix structure in each sample. Figure 3 shows CD spectrum profiles for experiment A in the far-UV spectral region and figure 4 shows the CD data for samples in experiment B. The CD spectrum for intact BSA without the treatment of reducing sugar and GNPs featured a well-defined helical pattern, with characteristic double dip at 205 nm and 222 nm. BSA and D-ribose mixture incubated for 21 days showed drastic reduction of the featured helical pattern, indicating that BSA has lost α-helix structures during glycation due to the formation of AGEs and the consequent protein conformation change.

In experiment A (figure 3), profile b, c and d are designated to BSA glycated by D-ribose in the presence of 20 nm, 2 nm and 5 nm GNP solution respectively. Similar to earlier observations from UV spectrum scan, reaction mixture with 5 nm GNP retained most of the α-helical content of BSA, producing a spectrum profile most similar to the profile of natural BSA which has not been glycated by reducing sugar. BSA treated by 2 nm and 20 nm GNPs also revealed decreases in the loss of secondary structure comparing to control BSA which was glycated without GNP. CD spectrums for samples in experiment A revealed that reaction mixture with 5 nm retained the most helical structure followed by 2 nm sample then 20 nm. In contrast, CD profiles for experiment B seen in figure 4 showed that all three sizes of

nanoparticle exhibited similar anti-glycation ability, producing CD spectrum almost superimposable to each other.

Figure 5 and figure 6 display the respective HPLC elution profiles of reaction mixtures in experiment A incubated at 37 °C for 21 days. Both UV and fluorescence signals were monitored in the HPLC profile. Profile 5a shows the HPLC-UV elution data of solutions containing BSA alone (blank). BSA alone eluted as one prominent peak with a retention time (R_t) of 15.79 min. BSA glycated by D-ribose without the treatment of GNPs (profile 5b) yielded three AGE products by HPLC labeled as peak 1, 2 and 4. Of the bands corresponding to the AGE products, peak 1 and 2 were not well separated and eluted with a retention time of 2.25 min while peak three eluted at 5.21 min. Integration of the band areas (data shown in table II) revealed that without the treatment of GNPs, glycated BSA produced three AGEs adducts with the first two yielding a total peak area of 258.62 and the third of 12.39 respectively. In contrast, profiles of BSA glycated in the presence of GNPs (5c, 5d and 5e) revealed a disappearance of peak 4, indicating that less AGE species was formed in the presence of GNPs. Moreover, the peak areas of peak 1 and 2 in profiles 5c, 5d and 5e were noticeable reduced comparing to profile b, yielding a total AGE peak intensity of 88.78, 82.10 and 87.23 respectively. Peak 3 in profile b, c d and e indicated BSA with sugar addicts, yielding a broad HPLC band comparing to that of native BSA. The peak area of this bank also demonstrated the extent

of glycation since BSA with more sugar addicts would produce a broader band resulting in an increase in peak intensity. BSA glycated by D-ribose without GNP, again, yield a band with the highest peak area of 316.67 indicating the production of glycated BSA with most sugar addicts. BSA incubated with different sizes of GNPs all revealed a decrease in the peak area, and 5 nm GNP exhibited the most reduction in BSA glycation with peak intensity of 138.39, followed by 2 nm GNP (peak area= 151.95) and 5 nm GNP (peak area= 173.65).

To determine the number of sugar addicts on protein forming by glycation, we used MALDI-TOF to compare the mass shift of glycated BSA with native BSA. Figure 7 to 11 are MALDI spectrum of reaction mixtures in experiment A: native BSA (fig. 7), BSA incubated with D-ribose (fig. 8), BSA and D-ribose mixture with 2 nm GNP (fig. 9), BSA and D-ribose mixture with 5 nm GNP (fig. 10), BSA and D-ribose mixture with 20 nm GNP (fig. 11). In table III we summarized the peak m/z value in each MALDI profile and the mass shift comparing to native BSA. Since the increase in m/z value was mainly due to the addict of D-ribose molecules to the protein, the approximate number of D-ribose adducts on glycated BSA in each incubation mixture can be also calculated based on the shift in m/z value (shown in table III). A greater number of sugar addicts on protein revealed a higher extent of glycation, resulting in a more rapid and an enhanced formation of AGEs. A close scrutiny of the table confirmed the earlier

observations that the extent glycation of BSA was reduced by adding GNPs into the solution. Mixture containing BSA and D-ribose alone showed the highest shift in protein m/z value and 80 sugar molecules were estimated to bond with native protein after 21 days incubation. The number of sugar addicts was reduced considerably in reaction mixtures containing BSA and D-ribose with 2 nm, 5 nm or 20 nm GNPs. 5 nm GNP solution which exhibited the highest total nanoparticle surface area yielded the least shift in m/z value, followed by 2 nm GNPs and then 20 nm. This order, again corresponded to the order of total nanoparticle surface areas in each solution (5nm>2nm>20nm), confirming that GNP's anti-glycation ability is directly correlated to the total nanoparticle surface area in each solution. GNP solution with enhanced total surface area exhibited a higher inhibitory effect against the formation of AGEs. This anti-glycation property of AGEs was reduced by decreasing the nanoparticle numbers in solution which resulted in a decrease of total particle surface area.

4. Discussion

The non-enzymatic glycation of protein by reducing sugars causes the irreversible formation of AGEs, a heterogeneous group of compounds accumulating *in vivo* over times. The built up of AGEs has been implicated to be related to the pathology of several long term diseases including diabetes and AD. Thus the search for anti-glycation agents is an important clinical issue since an increasing amount of AGE modified proteins have

been detected during the development of such diseases. Unfortunately, though several potential inhibitors against the formation of AGEs have been discovered and proposed, no promising anti-glycation drug has been applied clinically. Since glycation is a complicated process involving multiple targets and bio-pathways, the invention of inhibitors against such biological event is challenging. In this study, we evaluated the effect of gold nanoparticles on the formation of AGEs using BSA glycated by D-ribose as model reaction. The anti-glycation efficiency of GNPs with different particle diameters ranging from 2 nm to 200 nm was also compared.

Our studies showed that spherical GNPs with particle diameter larger than 20 nm (50 nm, 100 nm and 200 nm) aggregated with BSA after two to three days incubation, forming insoluble precipitants in phosphate buffer. However, 2 nm, 5 nm and 20 nm GNPs retained their nanoparticle properties without aggregating with BSA during incubation. Moreover, BSA-ribose reaction mixture treated with 2 nm, 5nm or 20 nm GNP all showed a reduced glycation level comparing to BSA incubated with D-ribose alone. UV spectrum revealed that under the treatment of GNPs, less aromatic AGEs were formed during the incubation of BSA with D-ribose. This result was confirmed by HPLC elution profiles that less AGE peaks and lower peak intensities were detected in reaction mixtures containing GNPs. It was also shown that GNP retained the secondary structure of BSA and prevented the

conformational change of protein, a finding which was demonstrated by CD spectrum.

The other important finding of this study was the correlation between GNP's anti-glycation efficiency and the total nanoparticle surface area in the solution. GNP's inhibitory effect against the formation of AGEs could be enhanced by increasing the total GNP particle surface areas in solution. This can be achieved by increasing the total nanoparticle concentration or increasing the nanoparticle sizes. It should be noted that larger size GNP or saturated GNP solution tends to conjugate with protein and precipitates out. Thus it is important to keep the particle size and concentration within a range which GNPs still retain their nanoparticle properties without aggregating with protein during glycation. In our study, we found that 5 nm GNPs with an Au mass concentration of 0.05 mg/ml exhibited the most anti-glycation ability while stayed homogenously during the entire incubation process.

The mechanism of GNP's inhibitory effect against the formation of AGEs is still under investigation. We proposed that GNPs competitively bind to the potent glycation sites on BSA, preventing their further modification by glycation. There is a strong implication that amino acid residues are able to covalently bond to the gold atoms on the surface of nanoparticle through Au-S or Au-NH_2 bonds. Such binding not only stabilizes nanoparticle from conjugation, but also protects free amino groups such as lysine from glycation. Furthermore, GNP could possibly bind to the glycation

intermediates of protein and prevent the formation of reactive dicarbonyl compounds.

In the specific case of our study, GNP with a higher surface area exhibited better inhibitory ability against glycation, probably due to the increase in available binding area on GNP surface to protein's potential glycation sites. As GNP is highly biocompatible and water soluble, an insight of its anti-glycation effect and its inhibition mechanism on the formation of AGEs might lead to a novel therapeutic application of GNP on reducing AGE related complications.

Acknowledgment

This research was made possible by the use of Research and Bioinformatics Core Facilities supported jointly by NCRR/NIH Grant # P20 RR016457 and the Network institutions.

Reference:

1. DeGroot J (2004) The AGE of the matrix: chemistry, consequence and cure. Curr Opin Pharmacol 4:301-305
2. Neglia CI, Cohen HJ, Garber AR, Ellis PD, Thorpe SR, Baynes JW (1983) 13C NMR investigation of nonenzymatic glucosylationof protein: Model studies using RNase A. J Biol Chem 258:14279-14283
3. Furth AJ (1997) Glycated proteins in diabetes. Br J Biomed Sci 54:192–200
4. Ulrich P, Cerami A (2001) Protein glycation, diabetes, and aging. Recent Prog Horm Res 56:1-21.
5. Thornalley PJ (2002) Glycation in diabetic neuropathy: characteristics, consequences, causes, and therapeutic options. Int Rev Neurobiol 50:37-57
6. Vasan S, Foiles P, Founds H (2003) Therapeutic potential of breakers of advanced glycation end product-protein crosslinks. Arch Biochem Biophys 419(1): 89-96
7. Peng X, Ma J, Chen F, Wang M (2011) Naturally occurring inhibitors against the formation of advanced glycation end-products. Food Funct 2: 289-301
8. Peyroux J, Sternberg M (2006) Advanced glycation endproducts (AGEs): Pharmacological inhibition in diabetes. Pathol Biol 54(7):405-19

9. Reiser KM (1998) Non-enzymatic glycation of collagen in aging and diabetes.Proc Soc Exp Biol Med 218:23–37
10. Harding JJ (1985) Non-enzymatic covalent posttranslational modification of proteins in vivo. Adv Protein Chem 37:247–334
11. Seneviratne S, Narayanan R, Liu W, Dain J (2012) The in vitro inhibition effect of 2 nm gold nanoparticles on non-enzymatic glycation of human serum albumin. Biochem Biophys Res Commun 422:447-454
12. Singha S, Bhattacharya J, Datta H, Dasgupta A (2009) Anti-glycation activity of gold nanoparticles. Nanomedicine 5:21-29
13. Hahn A, Singh A, Sharma P, Brown S, Moudgil B (2010) Nanoparticles as contrast agents for in-vivo bioimaging: current status and future perspectives. Anal Bioanal Chem 399:3-27
14. Arvizo R, Rana S, Miranda O, Bhattacharya R, Rotello V, Mukherjee P (2011) Mechanism of anti-angiogenic property of gold nanoparticles: role of nanoparticle size and surface charge. Nanomedicine 7:580-587
15. GhoshMoulick R, Bhattacharya J, Mitra C, Basak S, Dasgupta A (2007) Protein seeding of gold nanoparticles and mechanism of glycation sensing. Nanomedicine 3:208-214
16. Aggarwal P, Hall J, McLeland C, Dobrovolskaia M, McNeil S (2009) Nanoparticle interaction with plasma proteins as it relates to particle biodistribution, biocompatibility and therapeutic efficacy. Adv Drug Deliver Rev 61:428-437

17. Porta F, Speranza G, Krpetic Z, Santo V, Francescato P, Scari G (2007) Gold Nanoparticles capped by peptides. Mat Sci and Eng B 140:187-194

List of figures:

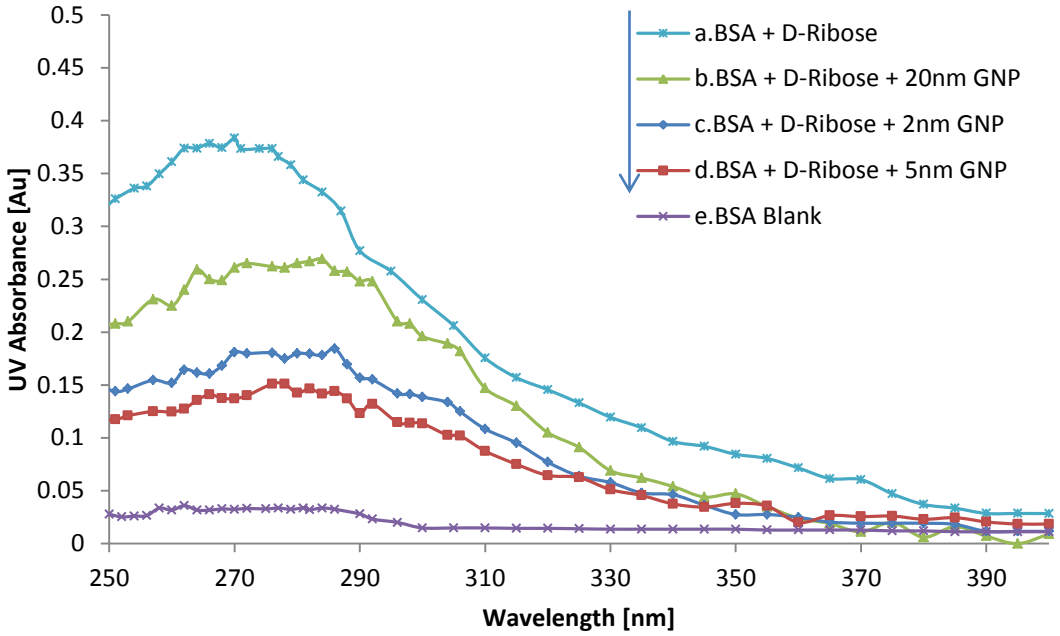

Figure 1. UV absorbance spectrum of reaction mixtures in experiment A. Each group contained 35 mg/ml BSA and 20 mM D-ribose incubated with and without different sizes of GNP (2 nm, 5 nm and 20 nm) at 37 °C for 21 days. The Au mass concentration was adjusted to 0.05 mg/ml in solutions containing GNP resulting in different total nanoparticle surface area (refer to table I). The spectrum is ranging from 250 nm to 400 nm with glycation products absorbed most at 280 nm. All data points represent the averages of three replicate measurements.

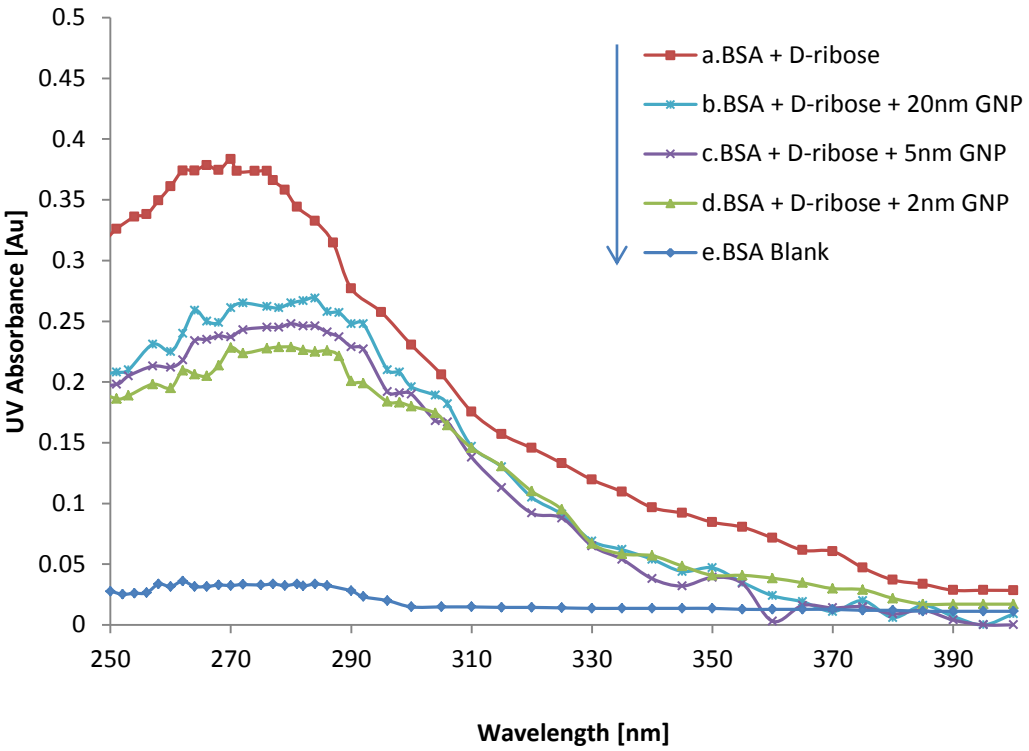

Figure 2. UV absorbance spectrum of reaction mixtures in experiment B. Each group contained 35 mg/ml BSA and 20 mM D-ribose incubated with or without different sizes of GNP (2 nm, 5 nm and 20 nm) at 37 °C for 21 days. The total nanoparticle surface area in each solution was adjusted to the same value (refer to table I). The spectrum is ranging from 250 nm to 400 nm with glycation products absorbed most at 280 nm. All data points represent the averages of three replicate measurements.

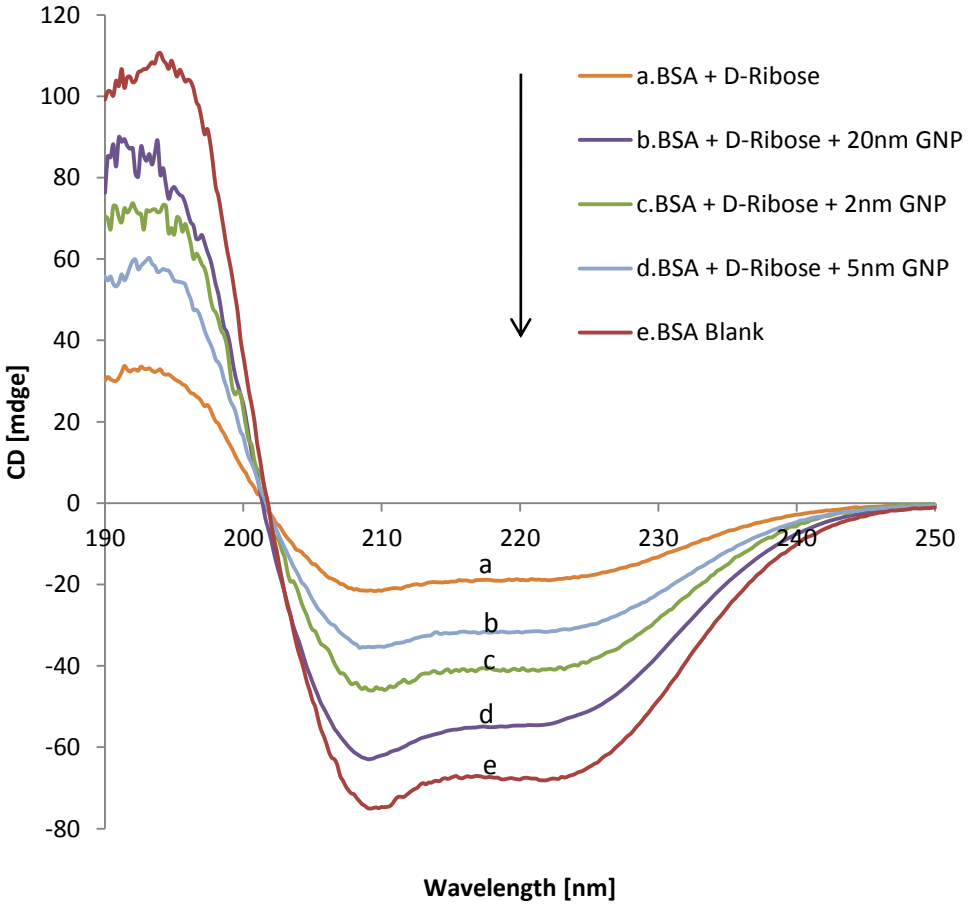

Figure 3. CD profiles of reaction mixtures in experiment A: (A) 35 mg/ml BSA and 20 mM D-ribose without GNP, (B) 35 mg/ml BSA and 20 mM D-ribose with 20 nm GNP, (C) 35 mg/ml BSA and 20 mM D-ribose with 2 nm GNP, (D) 35 mg/ml BSA and 20 mM D-ribose with 5 nm GNP and (E) 35 mg/ml BSA alone at 37 °C for 21 days. BSA concentration was diluted to 0.5 mg/ml with deionized water before analysis. Repeat scan revealed no significant difference in the spectra.

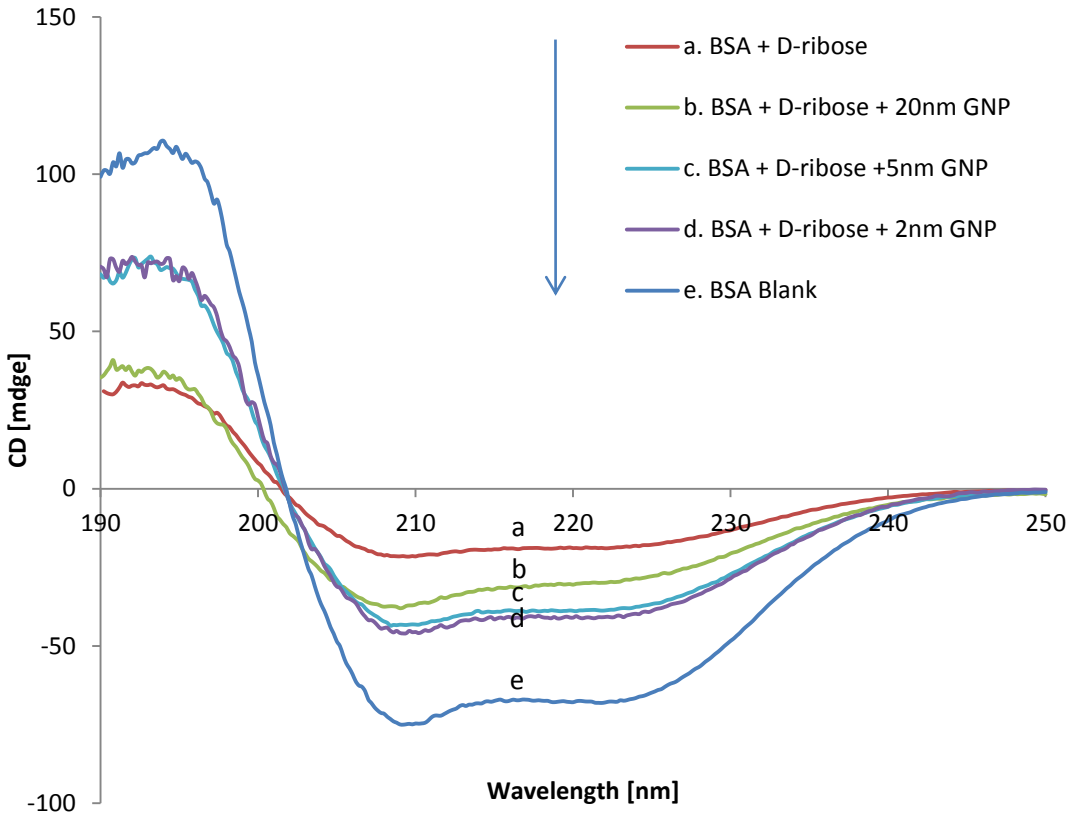

Figure 4. CD profiles of reaction mixtures in experiment B: (A) 35 mg/ml BSA and 20 mM D-ribose without GNP, (B) 35 mg/ml BSA and 20 mM D-ribose with 20 nm GNP, (C) 35 mg/ml BSA and 20 mM D-ribose with 5 nm GNP, (D) 35 mg/ml BSA and 20 mM D-ribose with 2 nm GNP and (E) 35 mg/ml BSA alone at 37 °C for 21 days. BSA concentration was diluted to 0.5 mg/ml with deionized water before analysis. Repeat scan revealed no significant difference in the spectra.

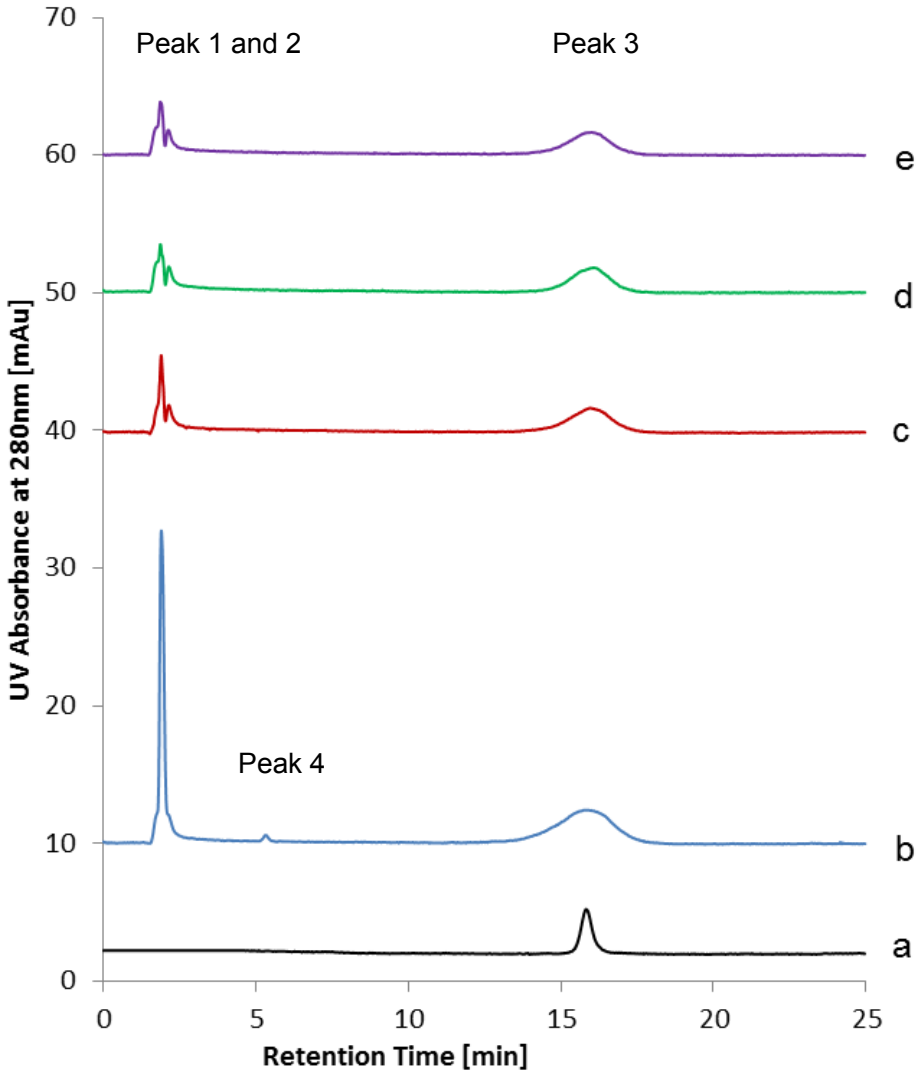

Figure 5. HPLC-UV elution profile for reactions in experiment A. 35 mg/ml BSA alone served as blank solution (a). 35 mg/ml BSA incubated with 20 mM D-ribose without GNP served as control solution (b). Profiles for BSA glycated at the presence of different sizes of GNP are shown in c (20 nm), d (5 nm) and e (2 nm). All reaction mixtures were incubated in dark at 37 °C for 21 days.

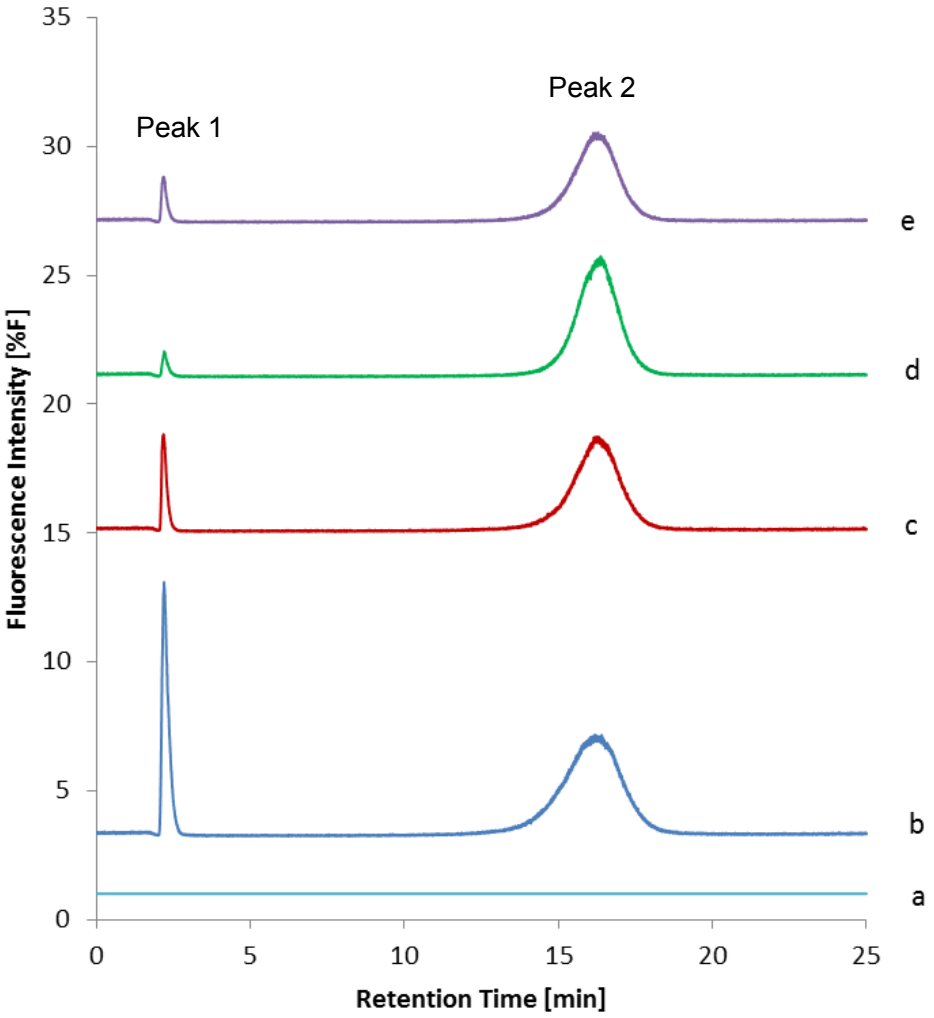

Figure 6. HPLC-fluorescence elution profile for reaction mixtures in experiment A. 35 mg/ml BSA alone served as blank solution (a). 35 mg/ml BSA incubated with 20 mM D-ribose without GNP served as control solution (b). Profiles for BSA glycated at the presence of different sizes of GNP are shown in c (20 nm), d (5 nm) and e (2 nm). All reaction mixtures were incubated in dark at 37 °C for 21 days.

.

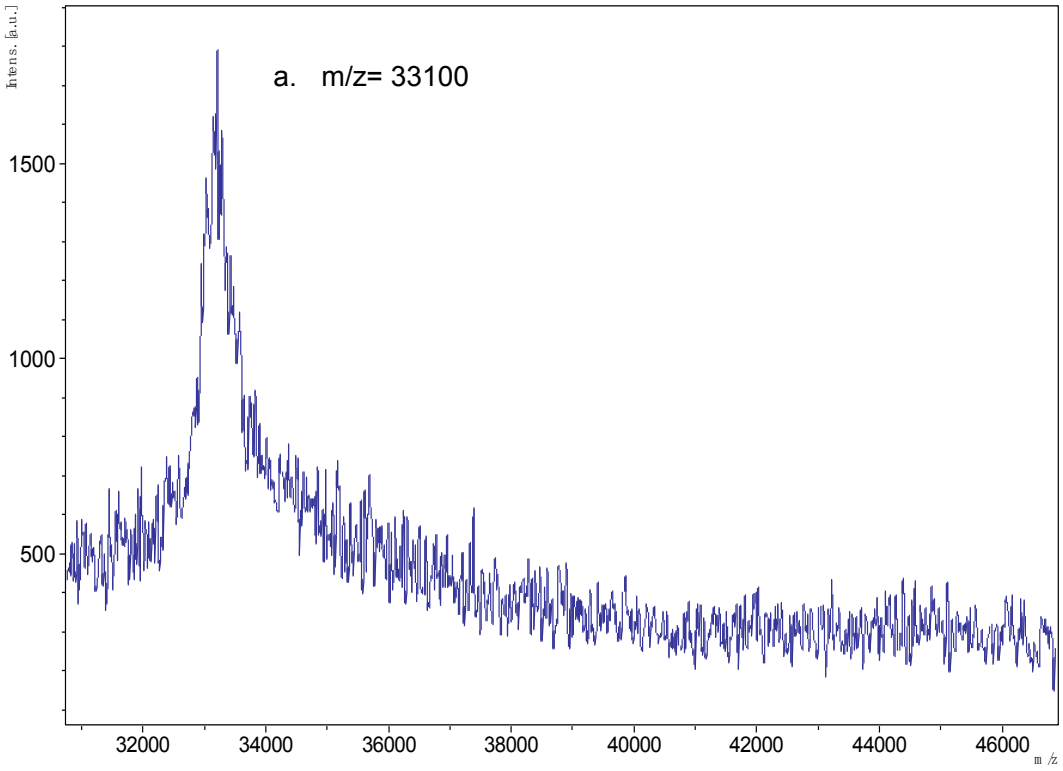

Figure 7. MALDI-TOF profile of reaction mixtures containing 35 mg/ml BSA incubated in dark at 37 °C for 21 days. The spectrum peak indicates to double charge intact BSA. The maximum peak m/z value was found at 33100.

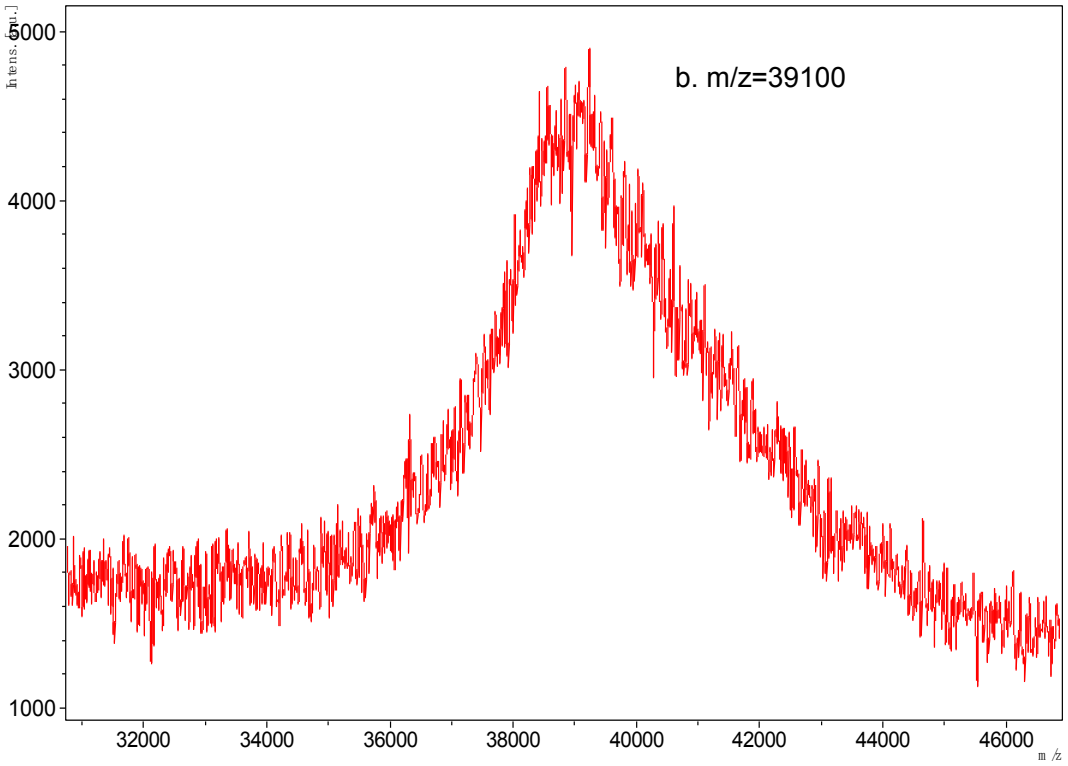

Figure 8. MALDI-TOF profile of reaction mixture in experiment A which contained 35 mg/ml BSA glycated by 20 mM D-ribose in dark at 37 °C for 21 days. The spectrum peak indicates to double charge glycated BSA. The maximum peak m/z value was found at 39100.

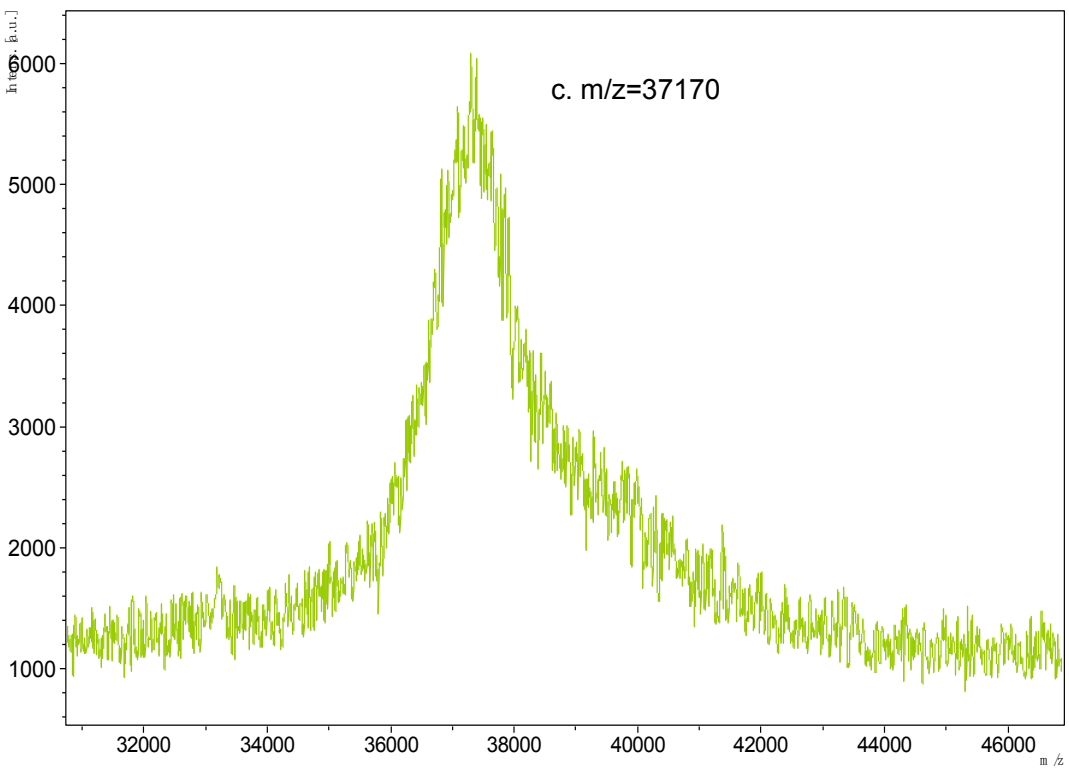

Figure 9. MALDI-TOF profile of reaction mixture in experiment A which contained 35 mg/ml BSA glycated by 20 mM D-ribose at the presence of 2 nm GNP with Au mass concentration of 0.05 mg/ml. The reaction took place in dark at 37 °C for 21 days. The spectrum peak indicates to double charge glycated BSA. The maximum peak m/z value was found at 37170.

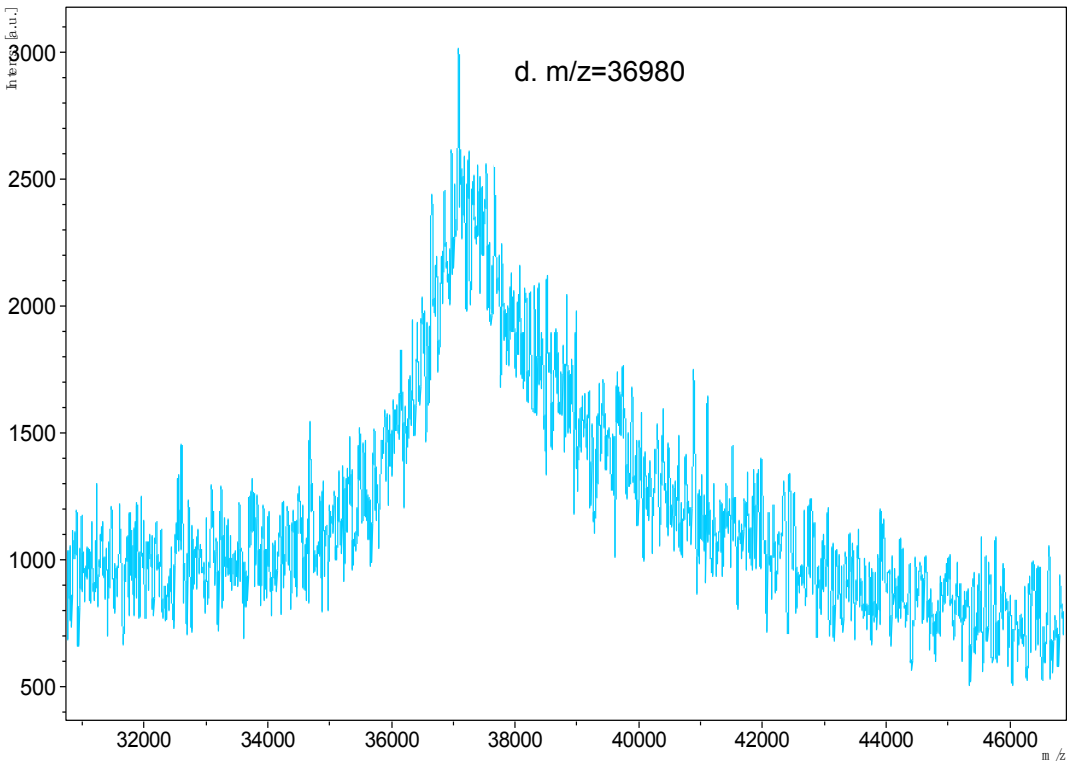

Figure 10. MALDI-TOF profile of reaction mixture in experiment A which contained 35 mg/ml BSA glycated by 20 mM D-ribose at the presence of 5 nm GNP with Au mass concentration of 0.05 mg/ml. The reaction took place in dark at 37 °C for 21 days. The spectrum peak indicates to double charge glycated BSA. The maximum peak m/z value was found at 36980.

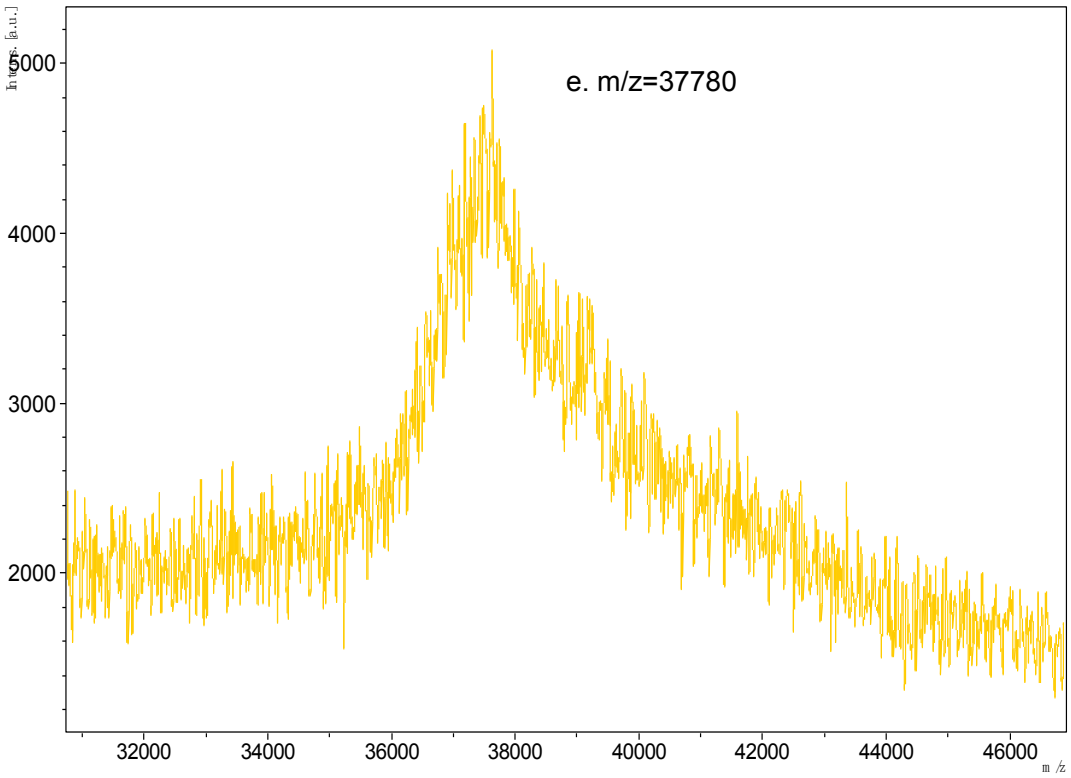

Figure 11. MALDI-TOF profile of reaction mixture in experiment A which contained 35 mg/ml BSA glycated by 20 mM D-ribose at the presence of 20 nm GNP with Au mass concentration of 0.05 mg/ml. The reaction took place in dark at 37 °C for 21 days. The spectrum peak indicates to double charge glycated BSA. The maximum peak m/z value was found at 37780.

Tables:

Table I.
Particle Size and Surface Area of 2nm, 5nm, 20nm Gold Colloid Water Solution in Experiment A and B

	Particle Size (nm)	Particle/ml	Au Mass Concentration (mg/ml)	Single Particle Surface Area (nm^2)	Total Particle Surface Area/ml (nm^2/ml)
A	2 nm	1.5×10^{14}	0.05	50	7.54×10^{15}
	5 nm	5.0×10^{13}	0.05	314	15.7×10^{15}
	20 nm	7.0×10^{11}	0.05	5024	3.52×10^{15}
B	2 nm	7.0×10^{13}	0.02	50	3.52×10^{15}
	5 nm	1.0×10^{13}	0.01	314	3.52×10^{15}
	20 nm	7.0×10^{11}	0.05	5024	3.52×10^{15}

Table II.
HPLC Peak Areas of BSA AGEs generated under incubation condition with or without different sizes of GNP in experiment A

	UV Absorbance at 280nm		Fluorescence Intensity (Excitation: 340nm Emission: 420nm)	
BSA+D-Ribose with 2nm GNP	Peak1 and 2 **87.227**	Peak 3 **151.948**	Peak 1 **22.099**	Peak2 **374.429**
BSA+D-Ribose with 5nm GNP	Peak1 and 2 **82.097**	Peak 3 **138.390**	Peak 1 **12.347**	Peak 2 **346.101**
BSA+D-Ribose with 20nm GNP	Peak1 and 2 **88.782**	Peak 3 **173.654**	Peak 1 **44.230**	Peak 2 **435.874**
BSA+D-Ribose without GNP	Peak1 and 2 **258.626**	Peak 3 **316.672**	Peak 1 **144.484**	Peak 2 **502.327**

Table III.
Mass Shift of BSA glycated by D-ribose with or without the presence of GNP in experiment A

	Peak m/z value (double charge)	Glycated BSA shifted m/z (double charge)	Approximate number of D-ribose adducts
BSA Blank	33100	0	0
BSA +D-Ribose	39100	6000	80
BSA+D-Ribose+ 2nm GNP	37170	4070	54
BSA+D-Ribose+ 5nm GNP	36980	3800	50
BSA+D-Ribose+ 20nm GNP	37780	4680	62

Manuscript 4

Prepared for Analytical Biochemistry
Anticipated submission date: February, 2013

Ultraviolet C radiation enhances glycation of human serum albumin and the formation of CML *in vitro*

Weixi Liu [1], Menashi A. Cohenford [2], Leslie Frost [3], Joel A. Dain [1*]

[1] Department of Chemistry, University of RI, Kingston, RI 02881
[2] Department of Integrated Science and Technology, Marshall University, Huntington, WV 25755
[3] Department of Chemistry, Marshall University, Huntington, WV 25755

E-mail address: wliu@chm.uri.edu (Weixi Liu).
E-mail address: cohenford@marshall.edu (Menashi A. Cohenford).
E-mail address: frost@marshall.edu (Frost Leslie)
*Corresponding author: Phone: + 1-401-874-5942; fax: + 1-401-874-5072
E-mail address: jdain@chm.uri.edu (Joel A. Dain).

Abstract:

Non-enzymatic glycation of human serum albumin (HSA) is a major contributor to the pathology of diabetes. The final products of this reaction are a polymorphic group of compounds collectively referred to as Advanced Glycation Endproducts (AGEs). Exposure to ultraviolet C (UVC) irradiation is known to perturb protein structure and generate reactive oxygen species (ROS) such as hydrogen peroxides, which might eventually accelerate protein glycation and enhance the formation of AGEs. The objective of this study was to evaluate the effect of UVC irradiation on the glycation level of human serum albumin and the formation of carboxymethyl lysine (CML), a well characterized AGE which is used as a biomarker of oxidatively damaged tissues *in vivo*. A combination of several analytical methods including UV spectrometry, HPLC and MALDI-TOF were used to study the glycation level of HSA at 37 °C under neutral pH in the presence of D-glucose *in vitro*. Compared to the untreated HSA, UVC exposed HSA showed a more rapid increase in absorbance intensity at 280 nm over time, as well as enhanced peak areas of AGEs in the HPLC elution profile. In MALDI-TOF spectrum, more D-glucose adducts were found on UVC treated HSA, generating a higher mass shift of protein. We also quantified the amount of CML using enzyme-linked immunosorbent assay technique with a monoclonal antibody which recognizes CML. Comparing to control samples in the dark, reactions exposure to UVC radiation produced about double

amount of CML within 48 hours of incubation. In conclusion, exposure to UVC radiation accelerates the glycation level of HSA and promotes the formation of AGEs, which may be stimulated by the generation of ROS by UV radiation. This study warrants further investigation as there have been few reports on the correlation between the UV radiation of proteins and their enhanced glycation by a reducing sugar.

Key words: HSA, CML, glycation, UVC, ROS

1. Introduction

Human serum albumin (HSA) constitutes almost half of the protein content in the plasma of normal healthy individuals [1]. As one of the major circulating protein in blood, HSA is the most abundant protein and utilizes a wide variety of physiological functions due to the flexibility of its structure [2]. First of all, albumin has a comparatively low molecular weight of 66 KDa comparing to other globulins in the plasma system. This property makes the protein a key element in maintaining the osmotic pressure needed for proper distribution of body fluids between intravascular compartments and body tissues [3]. HSA also functions as a carrier protein for small size metabolites such as hydrophobic steroid hormones, ions and fatty acids. The binding sites which allow the affinity for these metabolites are distributed widely on all three domains of the protein. As a result, albumin is also involved in the pharmacokinetics of many therapeutic drugs that can be bound to the protein [4, 5]. In addition, HSA represents the predominant antioxidant in plasma, a body compartment continuously exposed to high oxidative stress [6, 7]. Previous study has shown that more than 70% of the free radical-trapping activity of serum was due to HSA [6].

In normal conditions, HSA has a long half-life time of about 21 days and a high plasmatic concentration between 35 to 50 mg/ml. Being constantly exposed to numerous metabolites, albumin is highly sensitive to the structural modification by these molecules. In particularly, non-enzymatic

glycation is among the major mechanisms which contribute to the alteration of HSA's functions. Glycation is a non-enzymatic process that involves a series of steps initiated with a condensation reaction between the aldehyde group of a reducing sugar and the free amino group of a protein, resulting in the formation of an unstable aldimine, also known as the Schiff base. This intermediate then undergoes Amadori rearrangement and converts to a more stable ketoamine structure referred to as Amadori products. Late stage of glycation involves irreversible modification of these early stage glycation intermediates such as dehydration, cyclization, oxidation, and rearrangement to form a polymorphic group of compounds called advanced glycation endproducts (AGEs) [8-10]. The accumulation of AGEs plays a significant role in the pathogenesis of diabetic complications.

Glycated albumin accounts for about 80% of the circulating glycated protein [11]. *In vivo*, the proportion of glycated albumin in healthy persons is in the range of between 1% and 10% [2]. In the case of diabetes mellitus, the proportion of glycation HSA may increase two to three fold and even reach to 90% for severe diabetic patients with poor diabetic control [12, 13]. Glycation-induced modifications have a determinant impact on HSA's biological functional properties such as its antioxidant property and metabolites binding capacity. In addition, glycation is accompanied by the production of AGEs, which triggers the release of pro-inflammatory molecules and free radicals, inducing oxidative cellular dysfunction.

The glycation level of HSA can be up-graded by several factors including genetic deficiency, high calories diet and environmental factors. UV light is electromagnetic radiation with a wavelength in the range of 100 nm to 400 nm. UV radiation is classified into three types or bands—UVA (400-315 nm), UVB (315-280 nm), and UVC (280-100 nm). Exposure to ultraviolet (UV) irradiation is known to perturb protein structure and generate reactive oxygen species (ROS) [14, 15]. Solar UVC is absorbed by ozone in the stratosphere and the biological effect on human beings from natural sources is limited. However, with increasing use of man-made UVC radiation such as germicidal application and light therapy for wound healing, there is a growing concern about the biological effect of UVC. Previously study has shown that UVC irradiation could disturb structural stability of HSA and cause conformational rearrangement and aggregation of the protein [16]. The production of ROS was also found to be stimulated by UVC irradiation *in vivo* [17].

ROS play a significant role in the mechanism of protein glycation. The free radicals are not only the product of glycation, but can also accelerate the reaction rate and enhance the formation of AGEs. This suggests that UVC radiation might eventually promote protein glycation by disturbing structural stability of HSA and producing ROS. The objective of this study was to evaluate the effect of UVC irradiation on the glycation level of human serum albumin when D-glucose was used as model glycator. The formation of

carboxymethyl lysine (CML), a well characterized AGE which is used as a biomarker of oxidatively damaged tissues was also measured. A combination of several analytical methods including UV spectrometry, HPLC, ELISA and MALDI-TOF were used to study the glycation level of HSA at 37 °C under neutral pH in the presence of D-glucose *in vitro*.

6 Materials and methods

6.1 Chemicals and supplies

Fatty acid free albumin from human serum (HSA) and analytical grade D-glucose were purchased from Sigma-Aldrich Chemical Co. (St. Louis, MO, USA). Disposable UV-transparent cuvettes (12.5 mm X12.5 mm X 36 mm) and HPLC analytical grade solvents were obtained from Thermo Fisher Scientific (Rockford, IL, USA). Ziptip pipette tips with C_4 resin and 0.22 µm filter unit were purchased form EMD Millipore Co. (Billerica, MA, USA). Photometric Enzyme-Linked Immunosorbent Assay (ELISA) kit for the quantitative determination of Carboxymethyl Lysine (CML) was purchased from Neo Bio Lab (Cambridge, MA, USA). Unless otherwise indicated, all other reagents of analytical grade were purchased from Sigma-Aldrich Chemical Co. (St. Louis, MO, USA).

6.2 Sample preparation and UVC exposition

Stock solutions of HSA (105 mg/ml) and D-glucose (100 mM) were prepared in 0.1 M phosphate buffer, pH 7.2. Blank solutions included 35

mg/ml HSA alone or 20 mM D-glucose alone. Controls included 35 mg/ml BSA incubated with 20 mM D-glucose incubated in dark without any exposure to UVC radiation. The concentration of HSA was adjusted to 35 mg/ml because this is the reported serum albumin concentration in health human individuals. The concentration of D-glucose was adjusted to 20 mM, the concentration reported to be the blood sugar content under diabetic condition. Two sets of studies were conducted designated as experiment A and experiment B.

In experiment A, 35 mg/ml HSA incubated with 20 mM D-glucose in 0.1 M phosphate buffer at 37 °C, pH 7.2 for up to 14 days. Reaction mixture incubated in dark without any exposure to UVC radiation was serving as control solution. Experiment group was exposed to UVC light with a peak wavelength at 254 nm. The UVC radiation was produced by a 30 watts low-pressure vapor discharge lamp.

In experiment B, HSA was exposed to UVC light for 24 hours before the glycation agent was added into the solution. In control group, 35 mg/ml HSA was incubated in dark at 37 °C for 24 hours and then mixed with 20 mM D-glucose. In comparison, experiment solution was prepared by first exposing 35 mg/ml HSA under UVC light with a peak wavelength at 254 nm for 24 hours, then mixing with 20 mM D-glucose. Both control and experiment samples were then incubate in dark at 37 °C for up to 96 hours. After incubation, all reaction mixtures were placed at -20 °C until analyzed.

Prior analysis, all samples were unfrozen, ultra-centrifuged at $5X10^3$ rpm for 15 min and the supernates were further purified by ZipTip pipette with C4 resin.

2.3 UV spectroscopy

UV readings were obtained at a wavelength of 280 nm with an UltroSpec 2100 instrument (Biochrom Ltd, Cambridge, UK). The above wavelength was determined optimal for detecting HSA AGEs by spectrum scan ranging from 200 nm to 400 nm. All samples were diluted 20 fold before analysis and all readings were obtained in thermostatically controlled cuvettes that were maintained at 25±1 °C. All values are the average of triplicate measurements.

2.4 High-performance liquid chromatography

Each HPLC run was performed in triplicate using a Hewlett Packard 1050 system (Waldbronn, Germany) equipped with a low-pressure gradient pump, a four-channel degasser, a sequential auto sampler, a high sensitivity diode-array detector (190–800 nm) and a programmable fluorescence detector (HP 1046A). The HPLC system was operated with the ChemStation System from Agilent Technologies (Santa Clara, CA, USA) with the same software used also for data analysis. AGE species were separated on a Shodex (New York, NY, USA) RSpak C_{18} reverse phase HPLC column (5 µm×4.6 mm×150 mm) with 415 Å pore size. Mobile phase A consisted of 0.1% trifluoroacetic acid (TFA) in water and mobile phase B consisted of 0.1%

TFA in ACN. A linear gradient from 20% to 60% of mobile phase B was applied in 20 minutes at a constant flow rate of 1.0 ml/min. Prior to HPLC analysis, all solvents were degassed and sonicated for 15 min. All samples were filtered with a 0.22 μm membrane, degassed and centrifuged.

2.5 ELISA with anti-CML AGE antibodies

ELISA assay was performed according to the standard procedure provided by Neo Bio lab form where the ELISA assay kit (Catalog Number: PC0780) was obtained. Each sample was first diluted 10 times to 100 μl and then added to the labeled wells in the supplied microtiter plate. Then 50 μl of conjugate solution was added in each well and the plate was covered and incubated for 1 hour at 37 °C. Each well was washed for 5 times with 300-400 μl wash solution followed by the addition of 50 μl substrate A to each well and then 50 μl substrate B. The plate was again covered and put into incubation for 15 minutes at room temperature. Finally, 50 ul of stop solution was added to each well and the optical density (O.D.) for each sample was immediately determined at 450 nm using a Spectra Max M2 spectrometer (Molecular Devices, Sunnyvale, CA). Each experiment solution was run in duplicate and the values were averaged.

2.6 Preparation and analysis of intact HSA by MALDI-TOF MS

All samples were purified with C_4 ZipTips and analyzed on a Bruker Autoflex MALDI–TOF (time-of-flight) mass spectrometer (Bruker Daltonics, Billerica, MA, USA). Prior to analysis, the protein samples (0.6 μl) were

mixed with a 50% aqueous acetonitrile solution (0.6 µl) of saturated sinapinic acid containing 0.05% trifluoroacetic acid (TFA) as matrix, spotted onto a stainless steel sample plate, and allowed to air dry. Spectra were acquired in linear TOF mode with a 550 ns delay in the m/z range from 20,000 to 80,000. Each spectrum was the sum of 500 single laser shots randomized over 10 positions within the same spot (500/50). Analysis of data was performed using FlexAnalysis and ClinProTools (Bruker Daltonics).

3 Results

3.1 Detection of aromatic AGEs by UV spectrometry

Tables I shows the UV absorption readings of incubation mixtures containing 35 mg/ml HSA with 20 mM D-glucose (hereinafter referred to as “HSA-glc”) in both experiment A and B. In experiment A, samples were collected at different time points (0, 1, 2, 4 and 7 days of incubation respectively). In both control sample which was incubated in dark and experimental sample which was exposed to constant UVC radiation, HSA was found to form AGEs and the highest levels of glycation were achieved when HSA reacted with D-glucose for 7 days. It should be noted that a severe protein crosslinking was observed in UV exposed sample after 7 days incubation. HSA denatured and precipitated out of phosphate buffer due to protein conjugation. As a result, only samples collected within the first 7 days of reaction were analyzed afterwards. A considerable difference in

UV intensities between control sample and UVC treated sample revealed that exposure to UVC radiation enhanced the glycation level of HSA. The formation of aromatic AGEs which exhibited a UV absorbance at 280 nm was boosted by UVC treatment, producing a UV intensity value (λ_{280}=1.172) almost double as the untreated HSA-glc mixture (λ_{280}=0.623) after 7 days incubation. No increases were observed in the UV absorbance of blanks containing HSA alone. Similarly, no increases in the UV absorbance of control tubes containing freshly added HSA with D-glucose were noted. In experiment B, HSA was pre-incubated under the exposure of UVC radiation before D-glucose was added to the solution. A close scrutiny of the UV values in table I revealed that comparing to control, the rate and extent of glycation in UVC treated sample were much higher even at the initially stage of the reaction after 24 hours incubation, yielding an intensity value (λ_{280}=1.322) almost four times higher than the untreated solution (λ_{280}=0.091). Similar to experiment A, HSA started to form cross-linked structures and precipitated out of the mixture after 96 hours incubation. As a result, only samples collected within the first 96 hours of reaction in experiment B were analyzed afterwards. The UV readings obtained at 280 nm revealed two important findings: 1) UVC radiation enhanced the formation of aromatic AGEs of HSA, which was found to be responsible for the increased UV intensity at 280 nm; 2) HSA exposed to UVC radiation was more prone to be glycated by reducing sugar. This finding suggested that

UVC treatment might cause conformational restructuring of HSA, making the protein more susceptible to glycation.

3.2 Quantification of AGEs by HPLC

The extent of HSA glycation under the treatment of UVC radiation in both experiment A and B was determined by HPLC. Figure 1 shows the HPLC elution profile of blank solution of HSA alone and control solutions of HSA freshly added to D-glucose. Protein alone eluted as one prominent peak with a retention time (R_t) of 14.02 min. Under the same separation conditions, freshly mixed solutions of HSA with D-glucose also yielded one discrete peak coincident in location with that of HSA (R_t=14.02 min). This control showed that immediate mixing of the sugar with HSA had no effect on the elution profile of HSA itself; nor did it immediately cause the formation of AGEs.

Figure 2 and figure 3 show the HPLC elution profiles of HSA-glc mixture incubated in dark (figure 2) or incubated under the exposure to UVC radiation (figure 3) for 2 days in experiment A. A series of new peaks that emerged represent the formation of several AGE species in both solutions. According to the peak area intensities of these glycation products numbered peak 1 (R_t=1.87 min), peak 2 (R_t=3.15 min) and peak 3 (5.10 min), experimental sample under UVC radiation yielded AGE peaks with higher band areas comparing to that of control solution incubated in dark (data shown in Table II). Meanwhile, the peak area of band eluted at 14.02 min

which represented unglycated HSA had a lower value than HSA peak in control mixture; indicating HSA had been modified by D-glucose more intensively to form AGEs when treated by UVC. HPLC Elution profiles of HSA-glc mixture incubated for 7 days were shown in figure 4 (control solution incubated in dark) and figure 5 (experimental solution incubated under UVC radiation). Again, three AGE species were observed in both profiles. However, the amount of unglycated HSA was drastically decreased comparing to that of control, yielding a peak intensity of only 715.3. In the meanwhile, the peak area of AGE eluted as peak number 1 in UV treated sample was much higher than that of the solution incubated in dark, revealing a higher glycation level.

Figure 8 and 9 show the HPLC elution profiles of reaction mixtures in experiment B after 48 hours incubation. Incubations of UVC-treated HSA with D-glucose yielded four additional peaks numbered 1, 2, 3, and 4 with retention times of 1.71 min, 1.87 min, 3.14 min and 5.08 min respectively (seen in figure 9). Whereas profile of untreated HSA incubated with D-glucose for 48 hours indicated the formation of only three AGE species formed, a result indicated that more AGE species were formed when HSA was pre-treated with UVC radiation for 24 hours. Moreover, the peak intensity of AGE species in UVC treated solution was higher than the value of untreated control sample, verifying that exposure to UVC radiation made HSA more susceptible to glycation by reducing sugar.

3.3 The detection of CML by ELISA

CML is an AGE resulted from oxidative stress and chemical glycation. CML adducts was found accumulated with aging and over produced in several diabetic related complications. CML-modified proteins are recognized by the receptor RAGE which is expressed on a variety of cells. This process could initiate the expression of ROS and induce oxidative stress. The formations of CML in HSA-glc mixtures in both experiment A and B were evaluated by ELISA assy. Higher levels of CML leaded to increased CML-antibody conjugate binding and greater OD signal at 450 nm. Figure 10 shows the OD intensities of reaction mixtures in experiment A including a) 35 mg blank HSA, b) HSA-glc incubated in dark and c) HSA-glc incubated under UVC radiation. The increased in OD value over time revealed the formation of CML in both mixture b and c over time. No OD absorbance at 450 nm was observed when HSA was incubated along without any glycation agent. Comparing to sample incubated in dark, UVC treated solution produced a much higher amount of CML and the highest CML level was observed in HSA-glc mixture incubated under UVC radiation for 7 days. In experiment B, HSA pre-treated by UVC radiation yielded more CML comparing to untreated HSA (showing in figure 11). The difference in CML levels between control solution and UVC exposed sample started to be observed at the very early stage of glycation after only 12 hours of incubation. After 48 hours, UVC treated HSA produced about double amount of CML

comparing to control solution, an observation confirming our earlier conclusion base on UV spectrometry and HPLC elution profile.

3.4 Measurement of HSA mass shift by MALDI-TOF

To determine the number of sugar addicts on HSA forming by glycation, we used MALDI-TOF to quantify the mass shift of glycated HSA comparing to unglycated BSA. Since the increase in m/z value was mainly due to the addict of D-glucose molecules to the protein, the approximate number of sugar adducts on glycated HSA in each incubation mixture can be calculated based on the shift in m/z value (shown in table III). A greater number of sugar addicts on protein revealed a higher extent of glycation, resulting in an enhanced formation of AGEs. It should be noted that each MALDI spectra shown in figure 12 to figure 18 reflected the double charged albumin molecule which gave a better spectrum peak in each profile. As a result, the actual mass value for glycated HSA should be doubled by the m/z value obtained in MALDI spectrum.

A close scrutiny of the table confirmed the earlier observations that the extent of HSA was enhanced by exposing sample to UVC radiation. Solution containing HSA alone showed m/z value of 33000 Da in double charged form, resulting in a protein mass of 66000 Da which is closed to the reported HSA molecule weight. Based on the mass shift, the glycation levels of reaction mixtures in experiment A were not very considerable after 2 days incubation. In solution incubated in dark, one D-glucose addict was found on

HSA after 2 days reaction and two sugar molecules were found to addict on HSA in UVC treated sample. The difference was enhanced by prolonging the incubation time to 7 days. In samples incubated for 7 days, we noticed a mass shift of 740 in solution exposed to UVC radiation, which equals to 8 D-glucose addicts, whereas only 3 sugar molecules were found to addict on HSA in mixture incubated in dark. This observation again corresponded to our early conclusion that UVC irradiation enhanced the degree of glycation.

Moreover, HSA pre-incubated under UVC radiation for 24 hours in experiment B yielded mass shift of 290 after 48 hours incubation, which equals to 3 D-glucose addicts on HSA. Interestingly, this number is closed to the mass shift produced by HSA-glc mixture incubated in dark for 7 days, which suggested that the exposure to UVC not only enhanced the glycation level, but also increased the reaction rate.

4. Conclusion

The non-enzymatic glycation of HSA has been found to play a major role in human physiology. The reactive carbonyl groups of reducing sugars condensed with the amino groups of certain amino acid residues such as lysine and arginine on HSA and form Amadori products that can rearrange to form AGEs after a variety of chemical reactions. Accumulation of AGEs has been reported to account for many of the chronic complications including diabetes and Alzheimer’s disease.

Recently, there has been an increasing interest on the physiological effect of UVC radiation since they are readily absorbed by DNA and are highly genotoxic [19]. The biological effects of ultraviolet radiation (UV) include DNA damage, mutagenesis, cellular aging, and carcinogenesis. These effects are in part mediated by reactive oxygen species (ROS), the production of which is stimulated by UV irradiation of cells and tissues [16, 18]. Since the production of ROS also enhanced the glycation level in biological system, current study made an effort to evaluate the influence of UVC radiation on the formation of AGEs when physiological concentration of HSA was glycated by D-glucose *in-vitro*.

A combination of several analytical methods including UV spectrometry, HPLC and MALDI-TOF revealed that UVC radiation enhanced the glycation level of HSA even at the early stage of the reaction. Moreover, the glycation rate was also boosted when the reaction took place under UVC exposure. HSA started to form noticeable cross-link structures after a few days treatment with UVC, denaturized, and precipitated out from the reaction system. HSA pre-incubated under UVC radiation was more susceptible to glycation by reducing sugar comparing to untreated HSA. Although the detailed mechanism of this phenomenon is still under elucidation, it might be related to the alteration in HSA's conformational structure when the protein is exposed to UVC radiation.

In this study we also quantified the production of CML from HSA glycation using ELISA immune assay. The major source of CML during protein glycation is oxidative degradation of Amadori intermediate and ROS was found to accelerate the formation of CML. We observed a considerable increase in CML production when the protein was glycated under UVC radiation; a finding suggested that UVC radiation promoted the formation of ROS, which could then stimulate oxidative degradation of Amadori addicts to form AGEs.

At present, there is little information on the biological effect of short UV wavelength, and there is practically no data on glycation of HSA under the influence of UVC radiation. UVC radiation was found to enhance the glycation rate and promote the formation of HSA AGEs. The high energy UV radiation was also suspected to perturb protein structure; making protein more susceptible to glycation. As a result, more attention on the safe usage of UVC light should be addressed because the negative biological effect of high energy, short wavelength UV may not only be related to their genotoxic but may also be caused by their ability to enhanced protein glycation.

Acknowledgment

This research was made possible by the use of Research and Bioinformatics Core Facilities supported jointly by NCRR/NIH Grant # P20 RR016457 and the Network institutions.

Reference:

[1] T.W. Evans, Albumin as a drug‐biological effects of albumin unrelated to oncotic pressure, Aliment Pharmacol. Ther. 16 (2002) 6-11.

[2] T.J. Peters, All about Albumin-Biochemistry, Genetics, and Medical Applications. Academic Press, San Diego, 1996.

[3] G. Scatchard, A.C. Batchelder, A. Brown, Chemical, clinical, and immunological studies on the products of human plasma fractionation, J. Clin. Invest. 23 (1944) 458-464.

[4] T.A.Waldmann, Albumin Structure, Function and Uses. Pergamon Press, New York, 1977, 255-273 p.

[5] M. Wood, Plasma drug binding: implications for anesthesiologists, Anesth. Analg. 65 (1986) 786-804.

[6] E. Bourdon, D. Blache, The importance of proteins in defense against oxidation, Antioxid. Redox Signal 3 (2001) 293-311.

[7] B. Halliwell, Albumin - an important extracellular antioxidant? Biochem. Pharmacol. 37 (1988) 569-571.

[8] A.J. Furth, Glycated proteins in diabetes, Br. J. Biomed. Sci. 54 (1997) 192–200.

[9] P.J. Thornalley, Measurement of protein glycation, glycated peptides, and glycation free adducts, Periton. Dialysis Int. 25 (2005) 522-533.

[10] C. Seneviratne, G.W. Dombi, W. Liu, J.A. Dain, In vitro glycation of human serum albumin by dihydroxyacetone and dihydroxyacetone phosphate, Biochem. Bioph. Res. Co. 417 (2012) 817-823.

[11] R.L. Garlick, J.S. Mazer, The principal site of nonenzymatic glycosylation of human serum albumin in vivo. J. Biol. Chem. 258 (1983) 6142–6146.

[12] E. Bourdon, N. Loreau, D. Blache, Glucose and free radicals impair the anti-oxidant properties of serum albumin, FASEB J. 13 (1999) 233-244.

[14] R. Kisugi, T. Kouzuma, T. Yamamoto, S. Akizuki, H. Miyamoto, Y. Someya, Yokoyama, I. Abe, N. Hirai, A. Ohnishi, Structural and glycation site

changes of albumin in diabetic patient with very high glycated albumin, Clin. Chim. Acta 382 (2007) 59-64.

[15] J. Longstreth, F.R. de Gruijl, M.L. Kripke, S. Abseck, F. Arnold, H.I. Slaper, G. Velders, Y. Takizawa, J.C. van der Leun, Health risks, J. Photochem. Photobiol. 46 (1999) 20–39.

[16] J. Clydesdale, G.W. Dandie, H.K. Muller, Ultraviolet light induced injury: immunological and inflammatory effects, Immunol. Cell. Biol. 79 (2001) 547–568.

[17] A. Michnik, K. Michalik, Z. Drzazga, Effect of UVC radiation on conformational restructuring of human serum albumin, J. Photochem. Photobiol. B: Biol. 90 (2008) 170–178.

[18] S. Wu, L. Tong, Differential signaling circuits in regulation of ultraviolet c light-induced early- and late-phase activation of NF-λB, J. Photochem. Photobiol. 86 (2010) 995–999.

[19] C. Kielbassa, L. Roza, B. Epe, Wavelength dependence of oxidative DNA damage induced by UV and visible light, Carcinogenesis 18 (1997) 811–816.

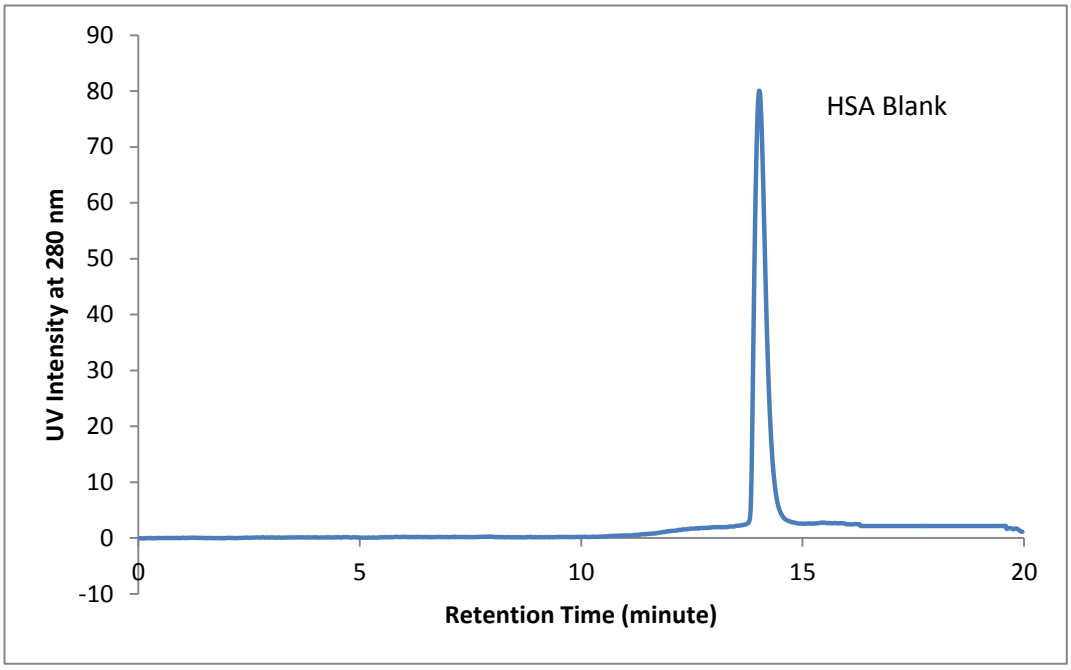

Figure 1. HPLC-UV elution profile of 35 mg/ml HSA alone in 0.1 M phosphate buffer, pH 7.2 serving as blank solution. HSA eluted at 14.02 minute, producing a single peak with a total peak area of 1402.6.

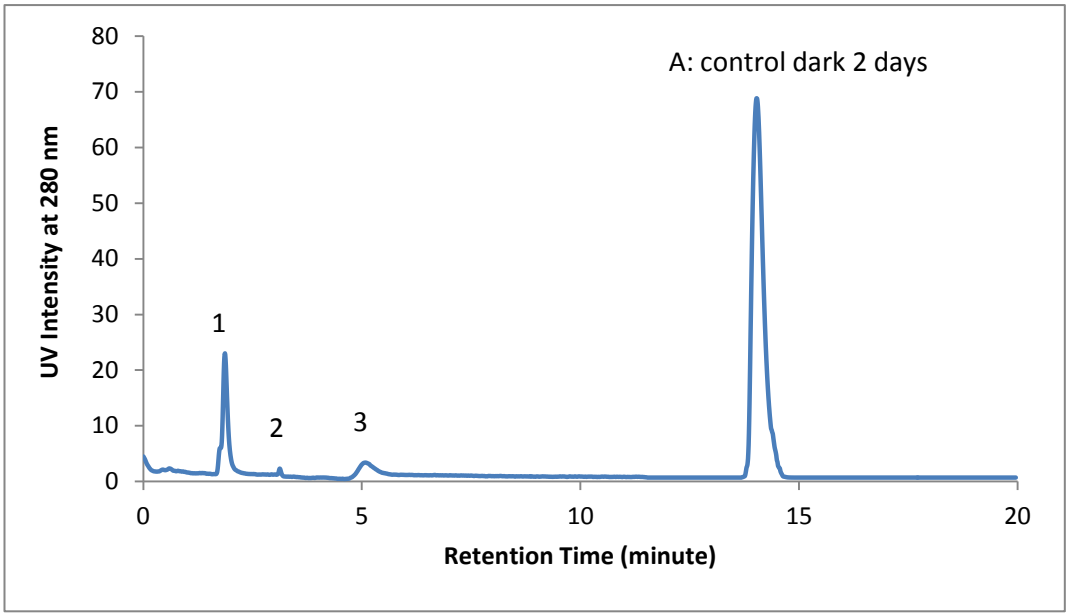

Figure 2. HPLC-UV elution profile of control reaction mixture containing 35 mg/ml HSA and 20 mM D-glucose in experiment A. The sample was incubated in 0.1 M phosphate buffer, pH 7.2 in dark for 2 days before analysis.

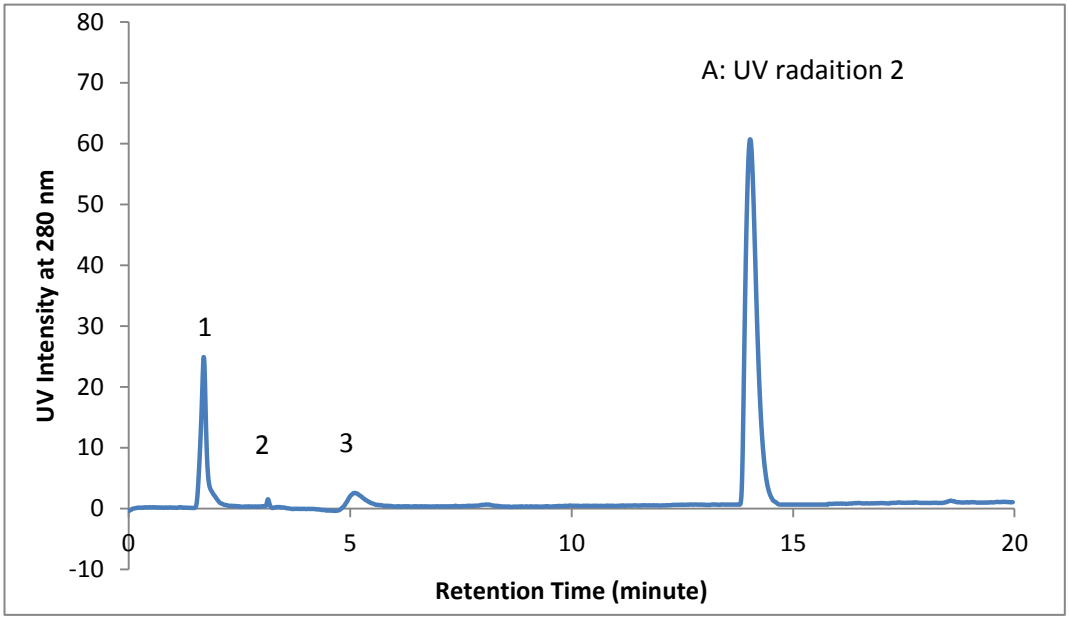

Figure 3. HPLC-UV elution profile of experimental reaction mixture containing 35 mg/ml HSA and 20 mM D-glucose in experiment A. The sample was incubated in 0.1 M phosphate buffer, pH 7.2 under UVC radiation for 2 days before analysis.

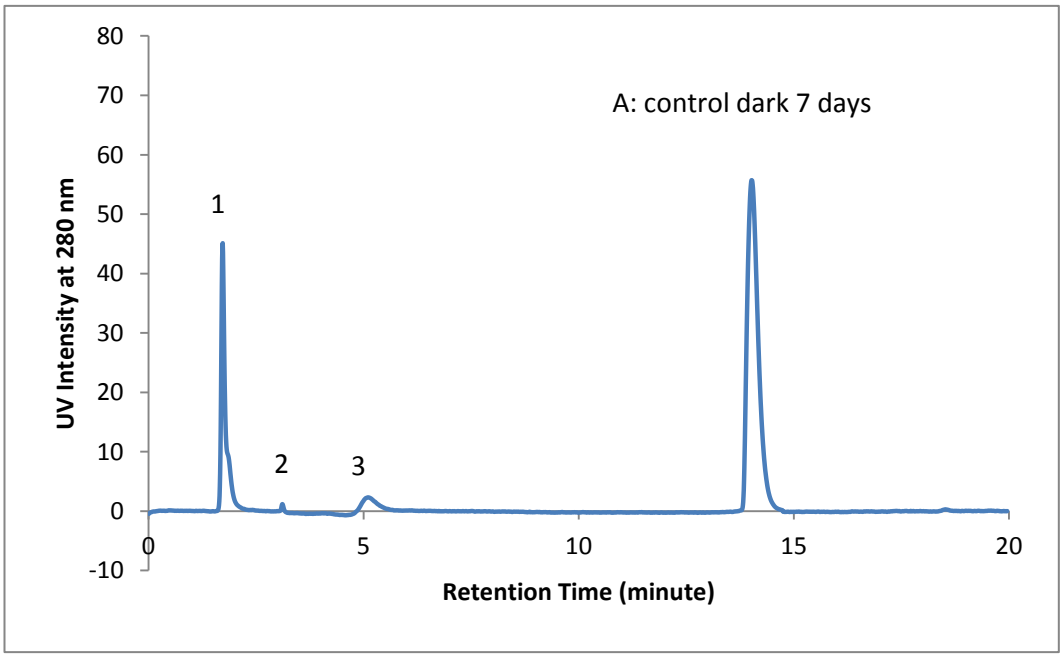

Figure 4. HPLC-UV elution profile of control reaction mixture containing 35 mg/ml HSA and 20 mM D-glucose in experiment A. The sample was incubated in 0.1 M phosphate buffer, pH 7.2 in dark for 7 days before analysis.

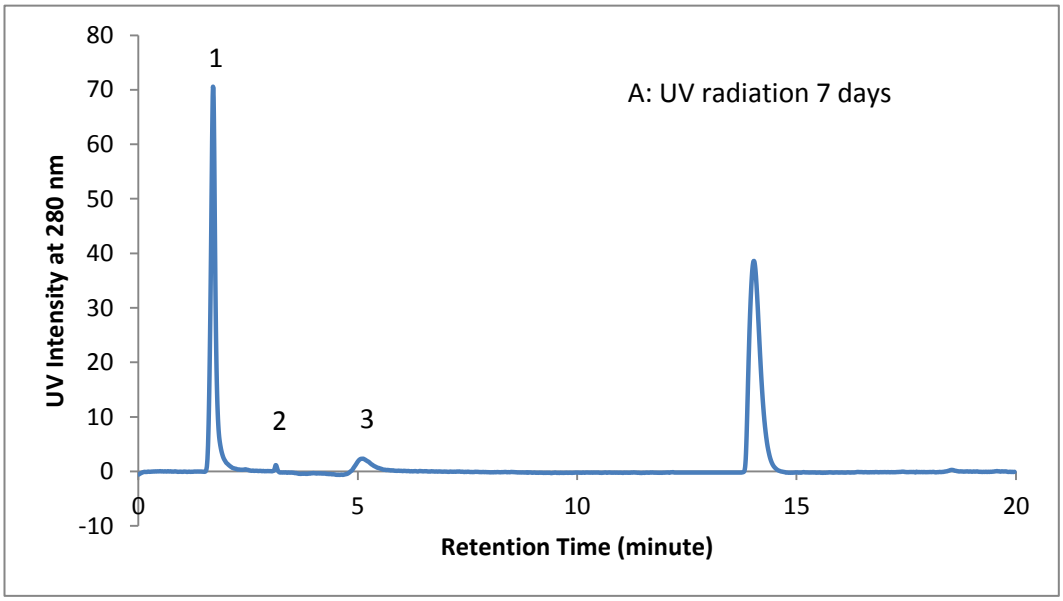

Figure 5. HPLC-UV elution profile of experimental reaction mixture containing 35 mg/ml HSA and 20 mM D-glucose in experiment A. The sample has been incubated in 0.1 M phosphate buffer, pH 7.2 under UVC radiation for 7 days before analysis.

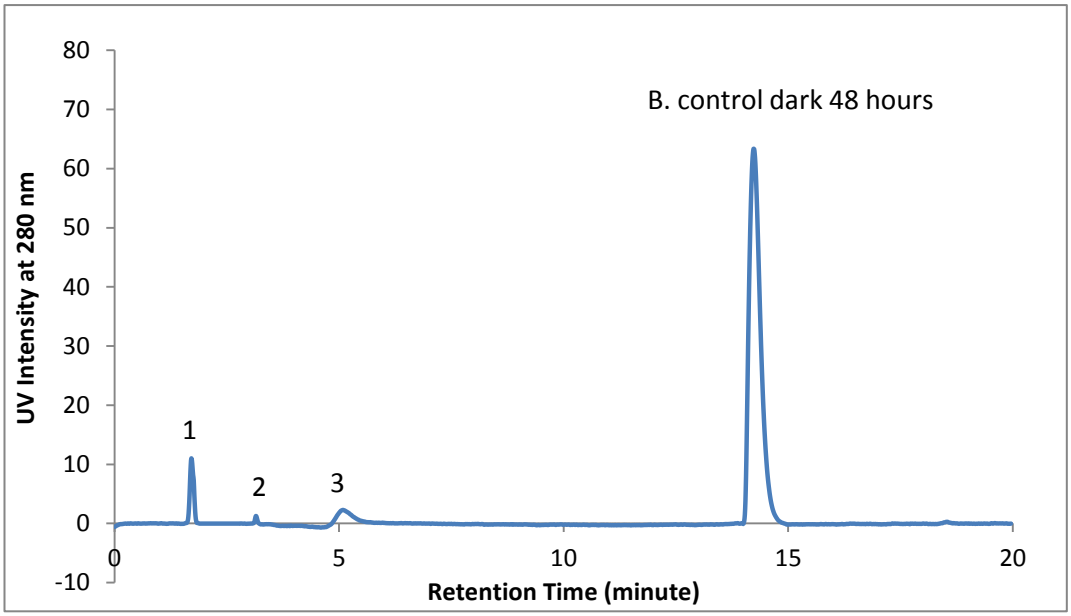

Figure 6. HPLC-UV elution profile of control reaction mixture containing 35 mg/ml HSA and 20 mM D-glucose in experiment B. HSA was pre-incubated in dark for 24 hours before D-glucose was added. The sample was then incubated in 0.1 M phosphate buffer, pH 7.2 in dark for 48 hours before analysis.

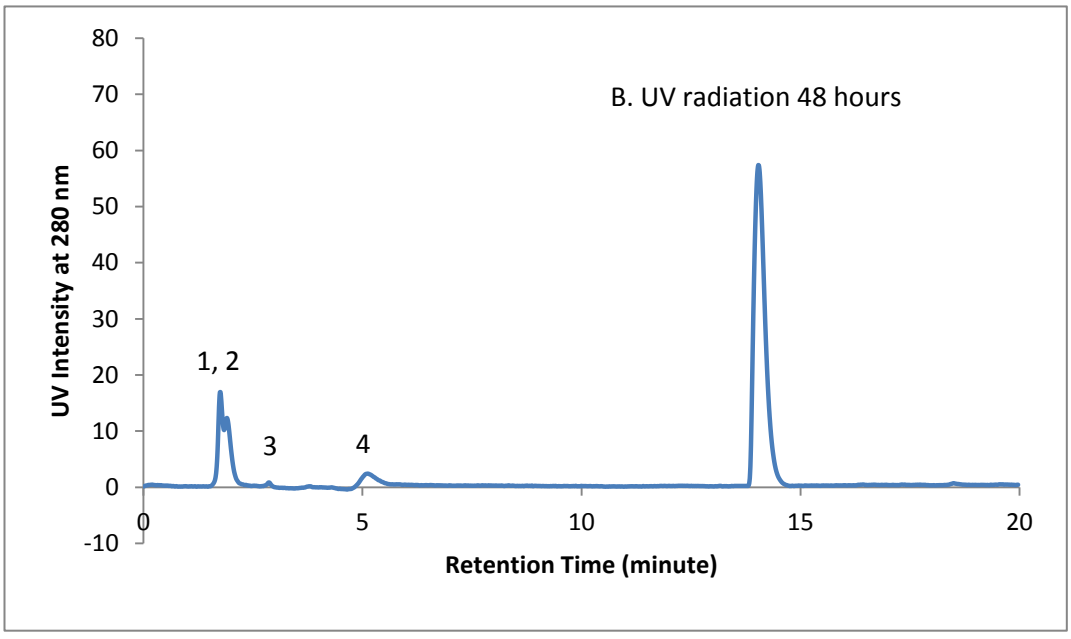

Figure 7. HPLC-UV elution profile of experimental reaction mixture containing 35 mg/ml HSA and 20 mM D-glucose in experiment B. HSA was pre-incubated under UVC exposure for 24 hours before D-glucose was added. The sample was then incubated in 0.1 M phosphate buffer, pH 7.2 in dark for 2 days before analysis.

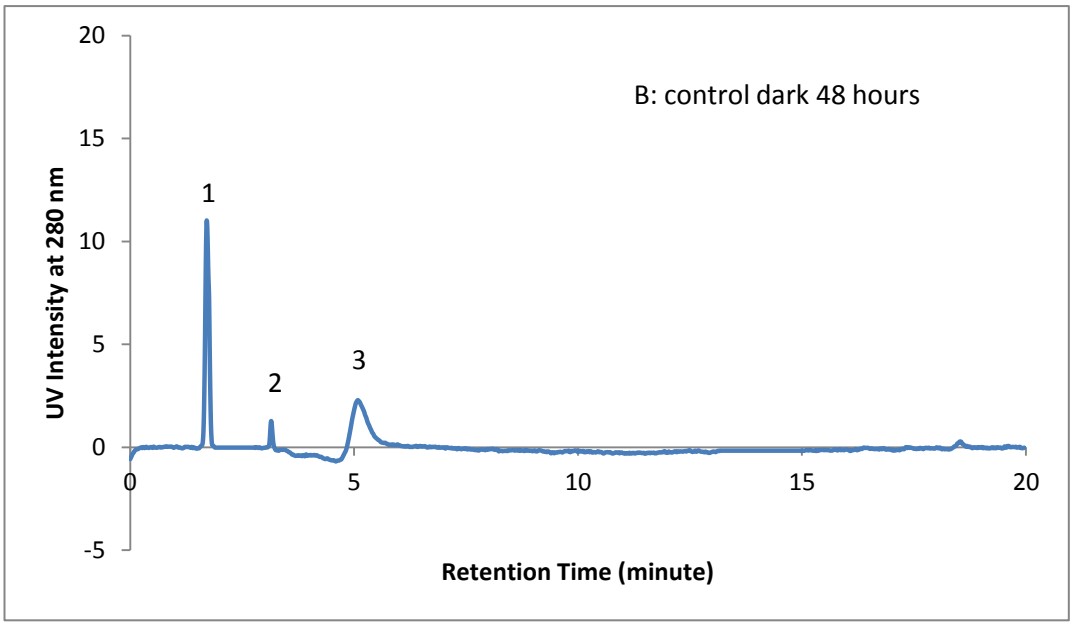

Figure 8. Modified HPLC-UV elution profile of spectrum shown in figure 6. Unglycated HSA with a retention time of 14.02 minute was eliminated in the spectrum to improve the view of AGE signals.

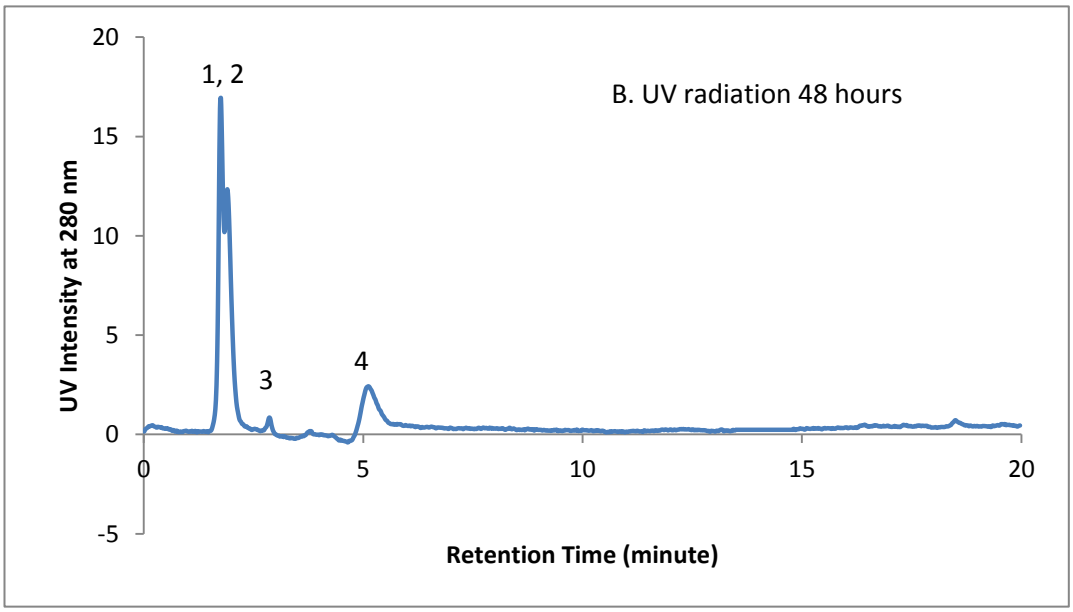

Figure 9. Modified HPLC-UV elution profile of spectrum shown in figure 7. Unglycated HSA with a retention time of 14.02 minute was eliminated in the spectrum to improve the view of AGE signals.

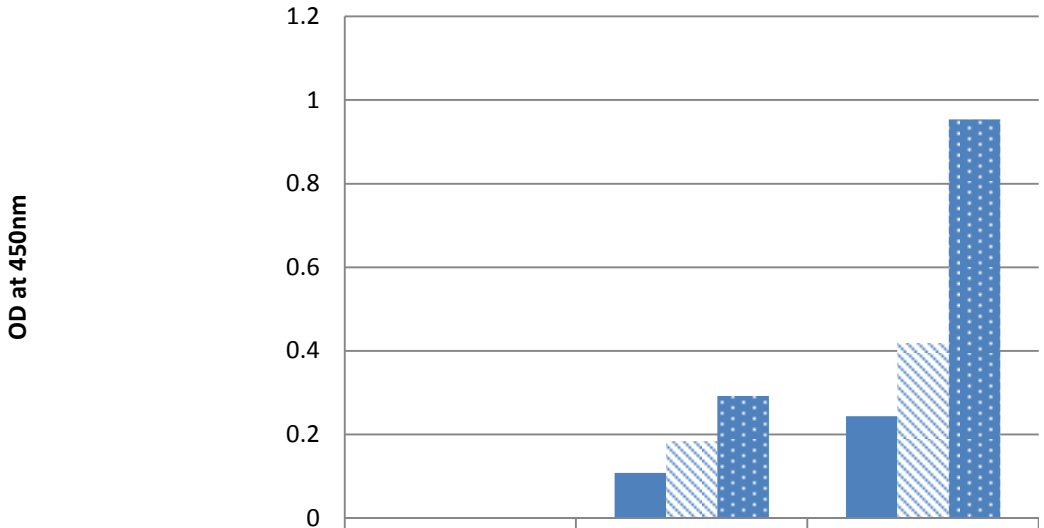

	1d	2d	7d
Blank HSA	0	0.108	0.244
HSA + Glucose in dark	0	0.184	0.418
HSA + Glucose under UVC	0	0.292	0.954

Figure 10. Comparison of the production of CML in each reaction mixture in experiment A with incubation times of 0, 2 and 7 days. The amount of CML was detected with antibodies to glucose-modified HSA using ELISA assay. The increase in OD value indicated the accumulation of CML over time. Each experiment solution was run in duplicate and the values were averaged.

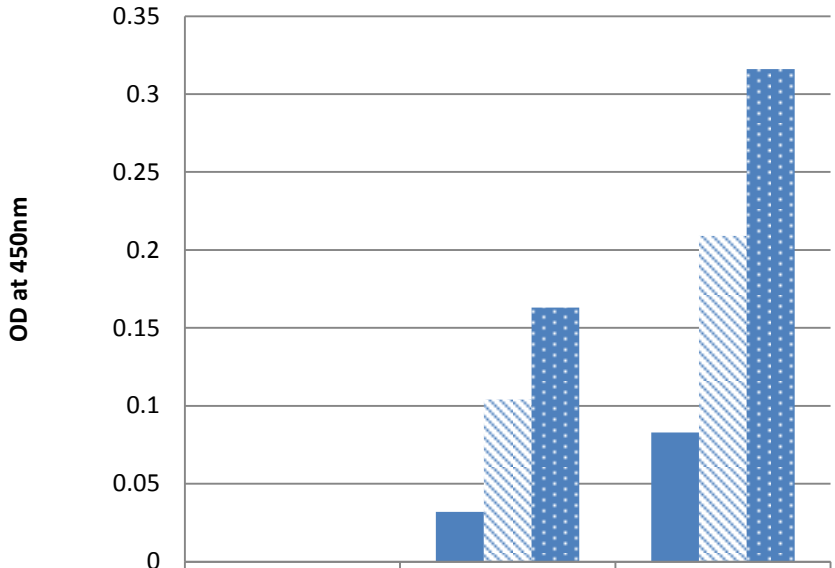

	12h	24h	48h
Blank HSA	0	0.032	0.083
Untreated HSA + Glucose	0	0.104	0.209
UVC treated HSA + Glucose	0	0.163	0.316

Figure 11. Comparison of the production of CML in each reaction mixture in experiment B with incubation times of 12, 24 and 48 hours. The amount of CML was detected with antibodies to glucose-modified HSA using ELISA assay. The increase in OD value indicated the accumulation of CML over time. Each experiment solution was run in duplicate and the values were averaged.

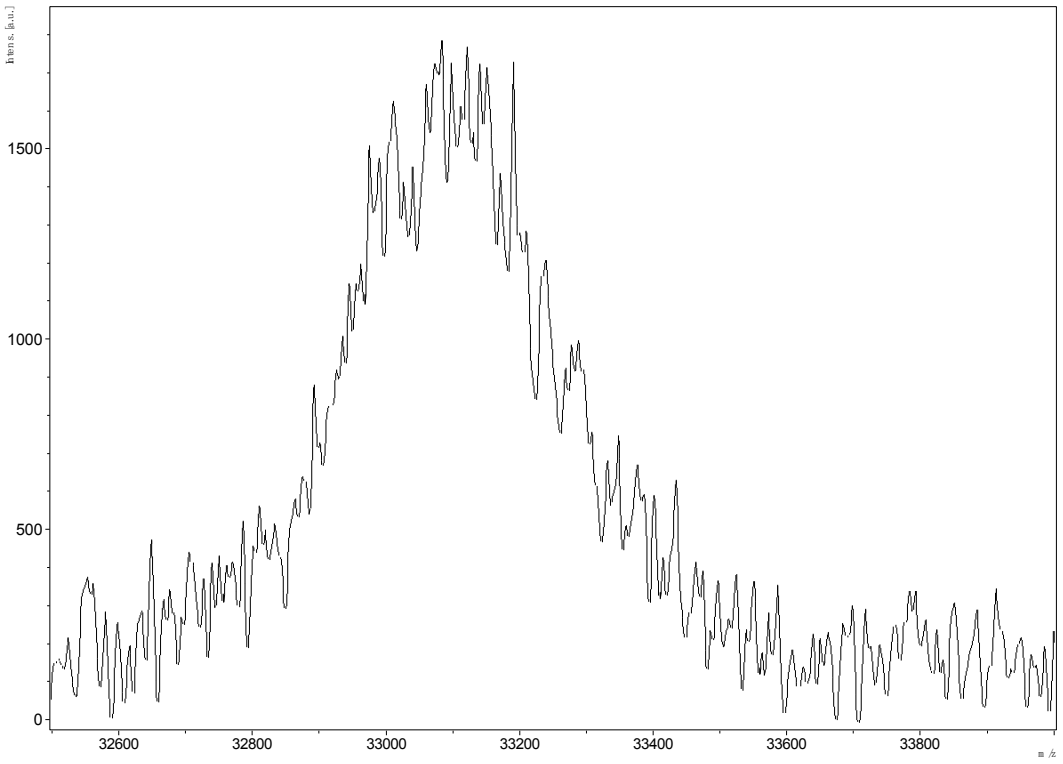

Figure 12. MALDI-TOF profile of reaction mixtures containing 35 mg/ml HSA incubated in dark at 37 °C for 7 days. The spectrum peak indicates to double charge intact HSA. The maximum peak m/z value was found at 33000.

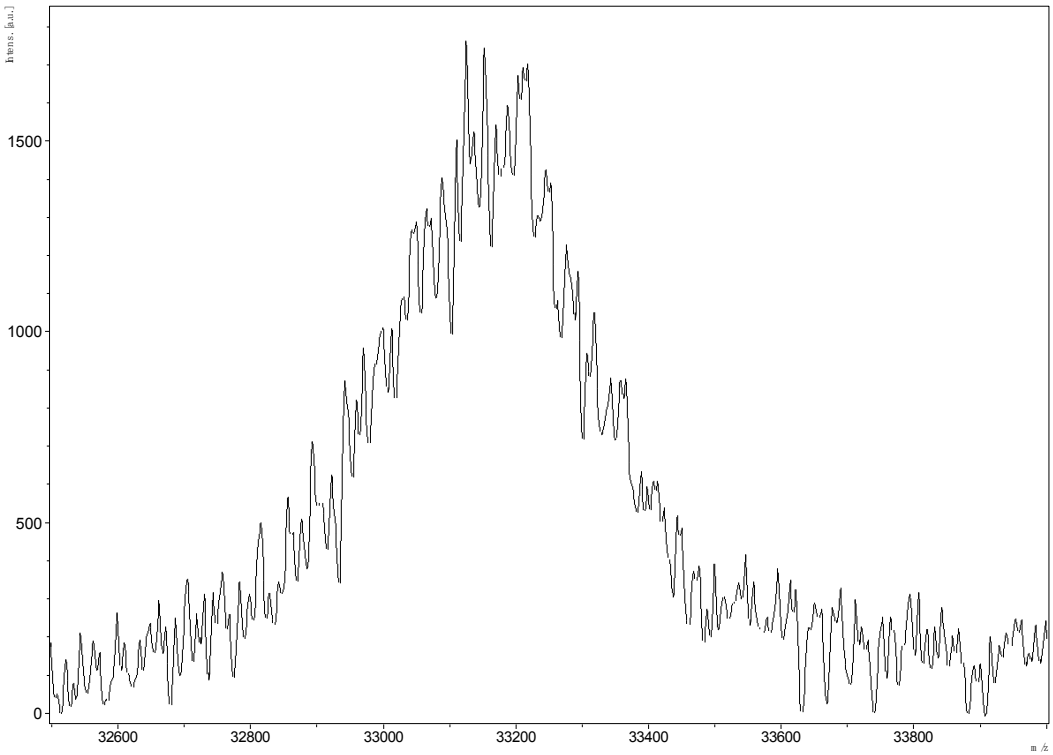

Figure 13. MALDI-TOF profile of reaction mixtures containing 35 mg/ml HSA and 20 mM D-glucose incubated in dark at 37 °C for 2 days (experiment A). The spectrum peak indicates to double charged glycated HSA. The maximum peak m/z value was found at 33080.

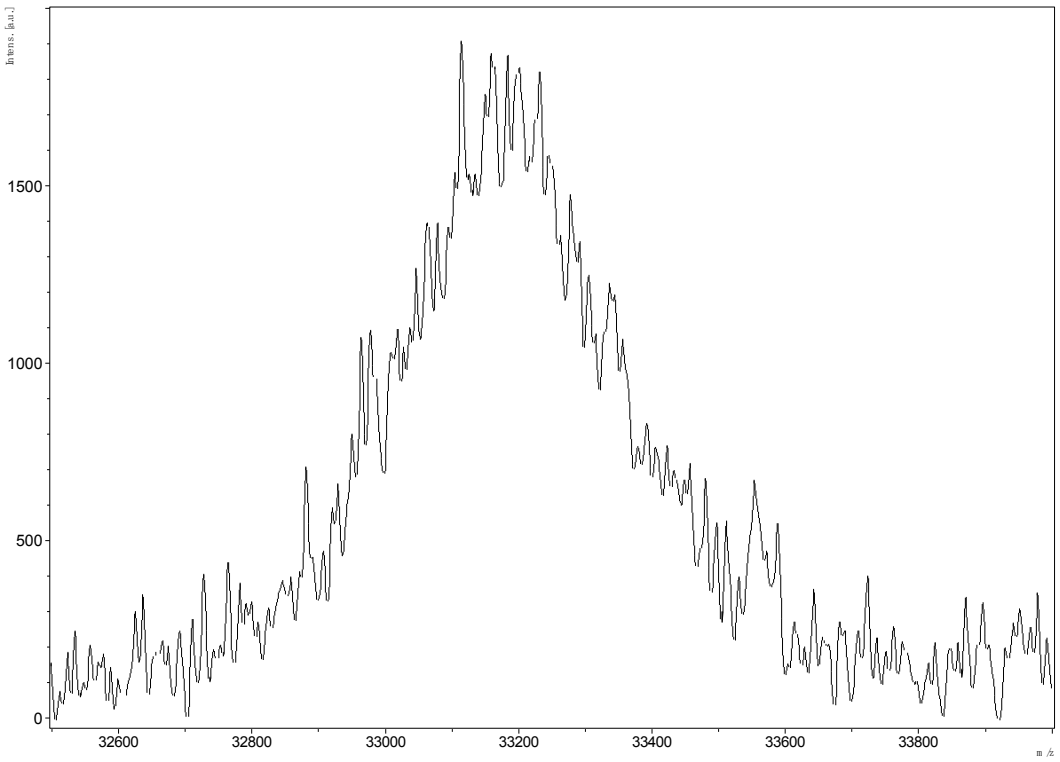

Figure 14. MALDI-TOF profile of reaction mixtures containing 35 mg/ml HSA and 20 mM D-glucose incubated under UVC radiation at 37 °C for 2 days (experiment A). The spectrum peak indicates to double charged glycated HSA. The maximum peak m/z value was found at 33180.

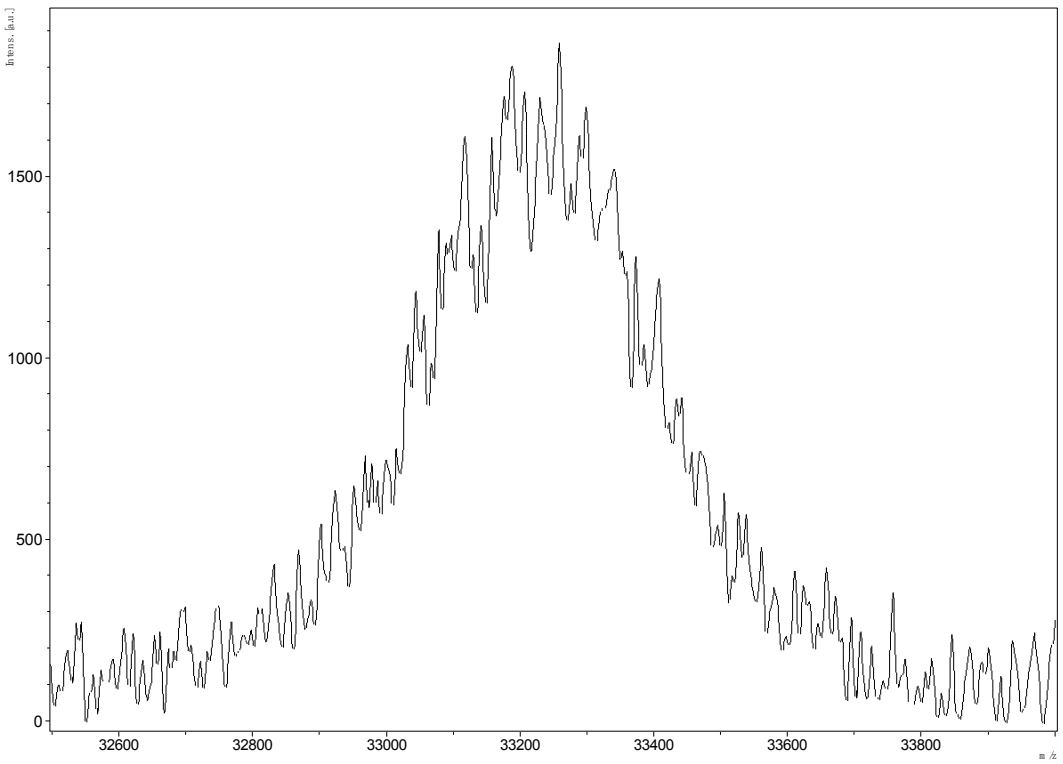

Figure 15. MALDI-TOF profile of reaction mixtures containing 35 mg/ml HSA and 20 mM D-glucose incubated in dark at 37 °C for 7 days (experiment A). The spectrum peak indicates to double charged glycated HSA. The maximum peak m/z value was found at 33280.

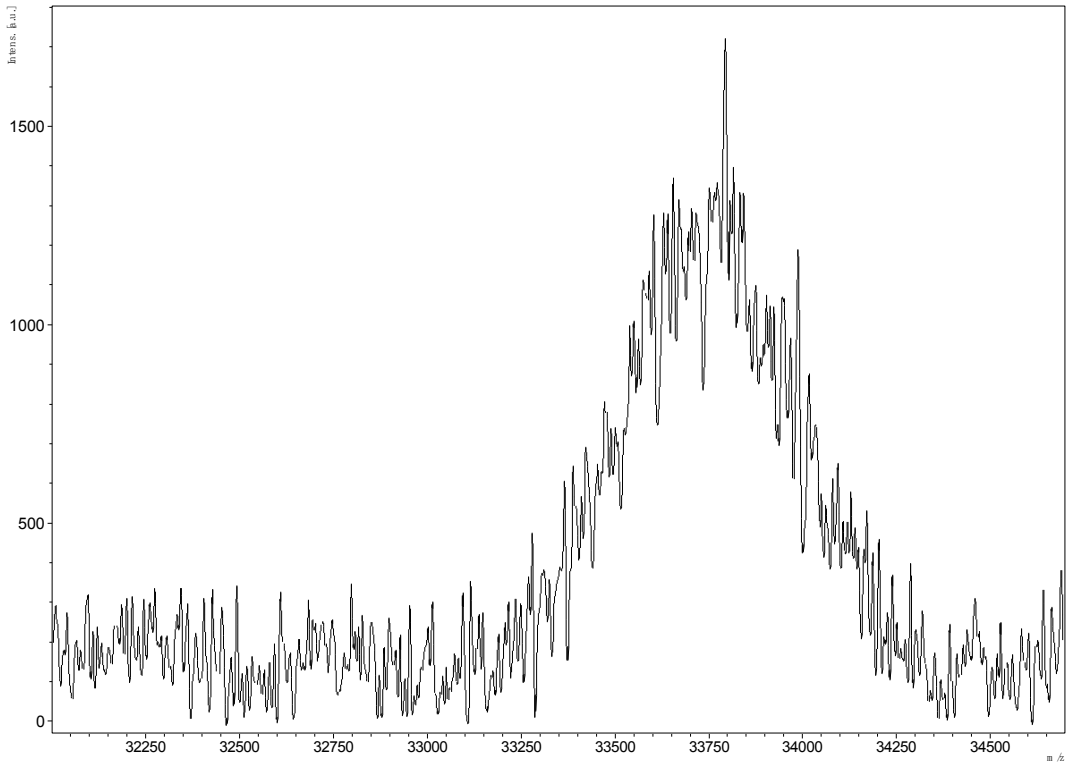

Figure 16. MALDI-TOF profile of reaction mixtures containing 35 mg/ml HSA and 20 mM D-glucose incubated under UVC radiation at 37 °C for 7 days (experiment A). The spectrum peak indicates to double charged glycated HSA. The maximum peak m/z value was found at 33740.

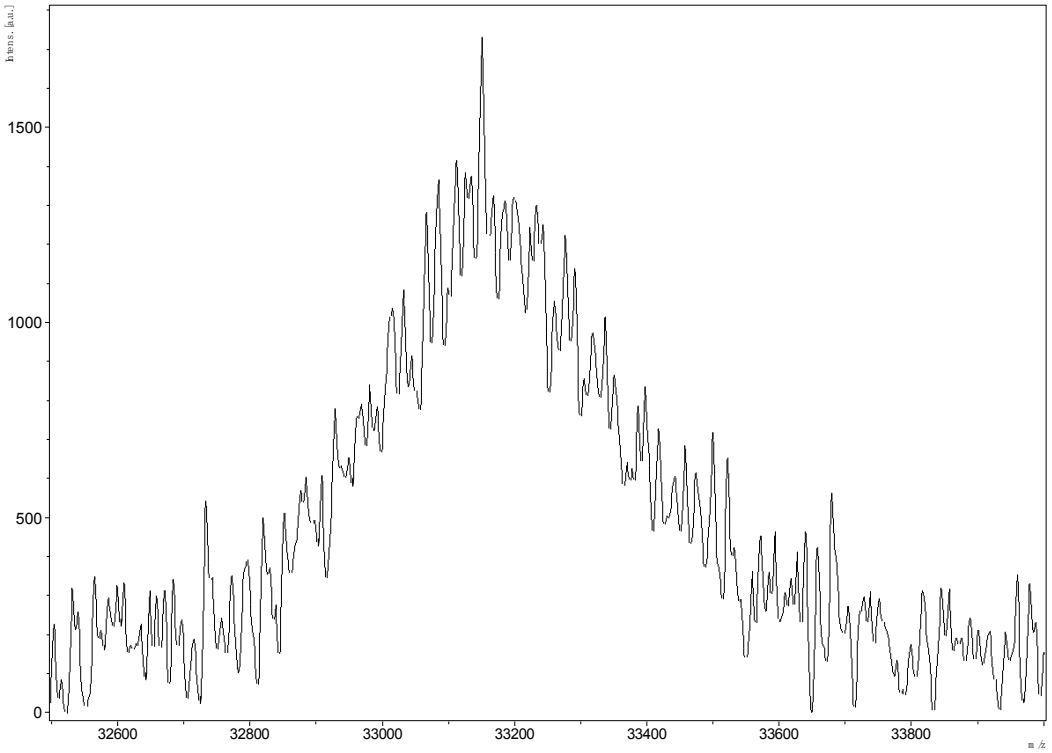

Figure 17. MALDI-TOF profile of reaction mixtures containing 35 mg/ml HSA and 20 mM D-glucose (experiment B). HSA was pre-incubated in dark for 24 hours before D-glucose was added. The sample was then incubated in 0.1 M phosphate buffer, pH 7.2 in dark for 2 days before analysis. The spectrum peak indicates to double charged glycated HSA. The maximum peak m/z value was found at 33100.

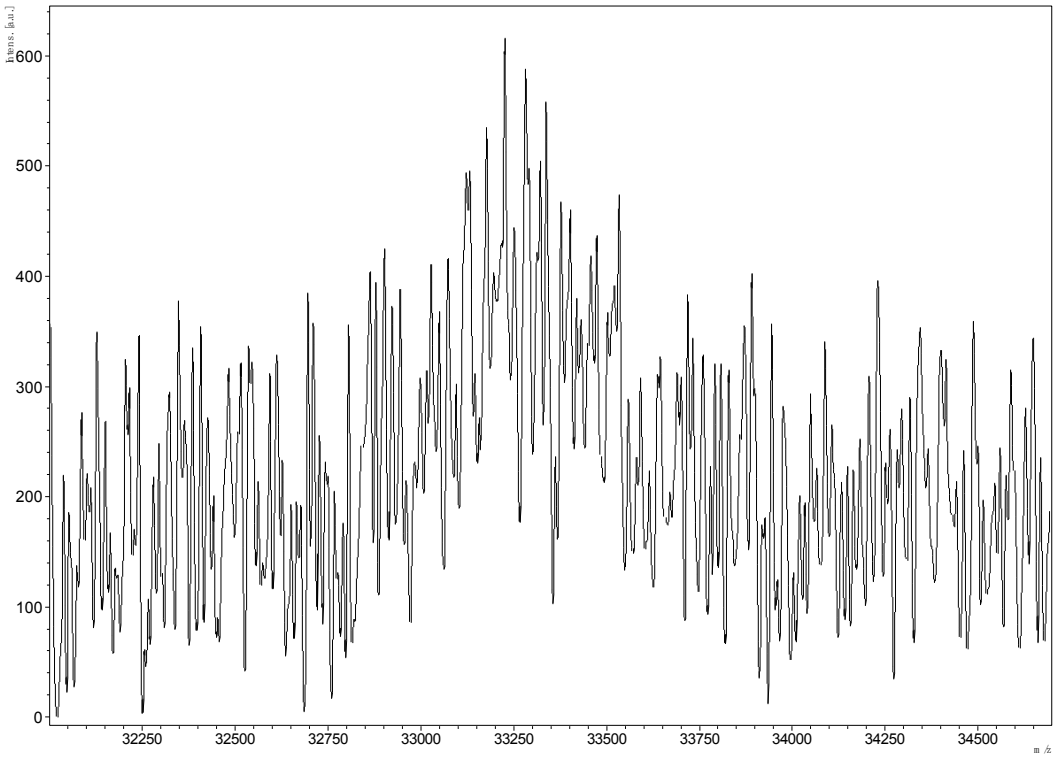

Figure 18. MALDI-TOF profile of reaction mixtures containing 35 mg/ml HSA and 20 mM D-glucose (experiment B). HSA was pre-incubated under UVC radiation for 24 hours before D-glucose was added. The sample was then incubated in 0.1 M phosphate buffer, pH 7.2 in dark for 2 days before analysis. The spectrum peak indicates to double charged glycated HSA. The maximum peak m/z value was found at 33290.

Table I

UV readings of reaction mixtures containing 35 mg/ml HSA and 20 mM D-glucose incubated in dark or under UVC radiation

Incubation Time	Experiment A		Experiment B	
	Dark	UV Exposure	Dark	UV Exposure
0 d	0.000±0.01	0.000±0.001	0.000±0.002	0.000±0.001
1 d	0.075±0.003	0.275±0.004	0.091±0.002	0.322±0.004
2 d	0.287±0.005	0.459±0.002	0.290±0.003	0.507±0.005
4 d	0.336±0.001	0.713±0.002	0.389±0.003	0.728±0.006
7 d	0.523±0.006	1.172±0.004	N/A	N/A

Table II.

HPLC Peak Areas of unglycated HSA and HSA AGEs generated with or without the exposure to UVC radiation in experiment A (7 days) and B (48 hours)

	Experiment A		Experiment B	
dark (Control)	AGE peak 1	314.7	AGE peak 1	65.5
	AGE peak 2	12.1	AGE peak 2	121.1
	AGE peak 3	72.7	AGE peak 3	50.6
	Unglycated HSA	937.9	Unglycated HSA	1168.6
UVC radiation (Experimental)	AGE peak 1	541.6	AGE peak 1 and 2	128.9
	AGE peak 2	15.3	AGE peak 3	125.8
	AGE peak 3	78.4	AGE peak 4	63.0
	Unglycated HSA	715.3	Unglycated HSA	1051.9

Table III.

Mass Shift of HSA glycated by D-glucose in dark or under the exposure of UVC radiation in experiment A and B

Incubation Condition	Peak m/z value (double charge)	Glycated BSA shifted m/z (double charge)	Approximate number of D-glucose (m/z=180) adducts
Experiment A			
HSA Blank	33000	0	0
HSA + D-glucose in dark (2 days)	33080	80	1
HSA + D-glucose under UVC (2 days)	33180	180	2
HSA + D-glucose in dark (7 days)	33280	280	3
HSA + D-glucose under UVC (7 days)	33740	740	8
Experiment B			
HSA Blank	33000	0	0
HSA + D-glucose in dark (48 hours)	33100	100	1
HSA + D-glucose under UVC (48 hours)	33290	290	3